KINETICS AND THERMODYNAMICS OF *N*-ALKANE THIN FILM EPITAXIAL GROWTH

A Thesis Submitted to the College of

Graduate Studies and Research

In Partial Fulfillment of the Requirements

For the Degree of Doctor of Philosophy

In the Department of Chemistry

University of Saskatchewan

Saskatoon

By

MITRA MASNADI KHIABANI

Permission to Use

In presenting this thesis in partial fulfilment of the requirements for a Postgraduate degree from the University of Saskatchewan, I agree that the Libraries of this University may make it freely available for inspection. I further agree that permission for copying of this thesis in any manner, in whole or in part, for scholarly purposes may be granted by Professor Stephen G. Urquhart who supervised my thesis work or, in their absence, by the Head of the Department or the Dean of the College in which my thesis work was done. It is understood that any copying or publication or use of this thesis or parts thereof for financial gain shall not be allowed without my written permission. It is also understood that due recognition shall be given to me and to the University of Saskatchewan in any scholarly use which may be made of any material in my thesis.

Requests for permission to copy or to make other use of material in this thesis in whole or part should be addressed to:

Head of the Department of Chemistry

University of Saskatchewan

Saskatoon, Saskatchewan

Canada S7N 5C9

Abstract

Controlling molecular orientation is of great importance in organic thin films due to the fact that the fundamental properties of functional nanomaterials depend on molecular orientation at the nanoscale. However, controlling molecular orientation cannot be achieved without having an extensive understanding about the controlling factors in the organic film growth processes. Most previous studies have been devoted to monolayer structures. The structure of multilayer films has not been well investigated. This study was performed using a phenomenological approach, in which the morphology and orientation of *n*-alkane thin films were studied as a function of substrate identity, interface treatment, substrate temperature and deposition rate. The experimental techniques that were used include IR-spectroscopy, polarized optical microscopy, and near-edge X-ray absorption fine structure (NEXAFS) spectroscopy and X-ray microscopy. The kinetic and thermodynamic factors that govern the orientation of organic thin films were extracted from the experimental results, and generalized to make a framework by which the morphology and orientation of organic films can be predicted.

Epitaxial growth was specifically considered as a method to pattern organic thin films. In epitaxial growth, the oriented crystals of an organic film grow on a crystalline substrate such that the structure of the substrate is copied by the deposit crystals. For epitaxy it is required that the lattice planes of two crystals are parallel and similar in the lattice points spacing.

A minor part of this dissertation is devoted to epitaxy in an inorganic system. One of the favorable consequences of epitaxial growth in inorganic systems is lattice strain that alters the electronic properties of semiconductor devices. A synchrotron based experimental method has been developed to quantitatively measure the degree of strain in $Si_{1-x}Ge_x$ alloy films grown epitaxially on the Si(100) substrate.

Acknowledgments

First and foremost, I would like to express the deepest appreciation to my supervisor, Professor Stephen G. Urquhart, who has always inspired me with the spirit of adventure in my research. He also patiently taught me valuable lessons in academic writing. I would like to thank my advisory committee members, Professors Richard Bowles, Matthew Paige and Michael Bradley, who guided me through the past several years. I wish to thank the SM, PGM, SGM, and SXRMB beam lines scientists at the Canadian Light Source. I am particularly grateful to Dr. Jian Wang for his training and support on the use of the STXM microscope. I appreciate Professor Ian Burgess for generously providing access to the infrared spectroscopy facility.

A special acknowledgment goes to the Department of Chemistry staff: Dr. Valerie MacKenzie as my TA manager, Leah Hildbrandt for her endless support in my academic paperwork, Garth Parry and Devin Beaudoin at the Electronics shop, Cathy Surtees and Dwight Reynaud at the Chemistry store, Jason Maley at the Saskatchewan Structural Science Centre for his assistance in the STM and Raman training.

I am sincerely thankful for my precious friends Dr. Pouyan Zahedi, Razieh and Rezvan Ostadali, Adel Panahi, Hesam Younesi, Souzan Pouralibaba, Mohammad Hashemian, Kianoosh Poorkazem and Nora Breit to be supportive in every way. They have cherished with me every great moment and supported me whenever I needed it. Many thanks to Dr. Wei Cao, Amara Zuhaib and Sahan Perera and my other office mates in Professor Urquhart's group who made a warm and friendly atmosphere in our lab.

Finally, I express my deepest gratitude to my parents, Ghafour Masnadi and Faezeh Narimani for being the source of love and energy during my life. I thank my two lovely sisters, Maryam Masnadi and Parisa Masnadi, for supporting and encouraging me with their best wishes.

Table of Contents

List of Figures

Chapter 1

Chapter 2

Chapter 3

Chapter 4

Chapter 5

Chapter 6

Chapter 7

Chapter 8

Chapter 9

Chapter 10

List of Tables

List of Abbreviations

AFM	Atomic Force Microscopy
CLS	Canadian Light Source
C28	*n*-$C_{28}H_{58}$, Octacosane
C36	*n*-$C_{36}H_{74}$, Hexatriacontane
C40	*n*- $C_{40}H_{82}$, Tetracontane
C44	*n*-$C_{44}H_{90}$, Tetratetracontane
C50	*n*-$C_{50}H_{102}$, Pentacontane
C60	*n*-$C_{60}H_{122}$, Hexacontane
8CB	4-octyl-4-cyanobiphenyl
HOPG	Highly Oriented Pyrolytic Graphite
EMR	Electromagnetic Radiation
EPU	Elliptically Polarized Undulator
FM	Frank – van der Merwe
IP	Ionization Potential
LC	Liquid Crystal
LD	Linear Dichroism
MBE	Molecular Beam Epitaxy
MO	Molecular Orbital
NEXAFS	Near Edge X-ray Absorption Fine Structure

OD	Optical Density
OSA	Order Sorting Aperture
POM	Polarized Optical Microscope
PVD	Physical Vapor Deposition
RT	Room Temperature
SAMs	Self Assembled Monolayers
SK	Stranski – Krastanov
STM	Scanning Tunneling Microscope
STXM	Scanning Transmission X-ray Microscope
TDM	Transition Dipole Moment
VM	Volmer – Weber
X-PEEM	X-ray Photoemission Electron Microscope

CHAPTER 1: INTRODUCTION

Control of molecular orientation in the organic thin films can potentially be achieved if the determining growth parameters are well understood. Previously in a fundamental study started by Juxia Fu,[62] linear dichroism in near edge X-ray absorption fine structure (NEXAFS) spectroscopy has been probed as an experimental technique that provides identification of molecular orientation with nanoscale spatial resolution. This technique has been applied to characterize *n*-alkane thin films grown on NaCl(001) and these results have motivated further investigations. In this project, the morphology and orientation of *n*-alkane films will be studied by polarized optical microscopy and linear dichroism in NEXAFS spectroscopy respectively. The combination of these two complementary techniques makes it possible to relate the morphology variation to the molecular orientation. Optical microscopy provides quick view of fine structures and subtle variations in the morphology of the organic thin films with changing the growth conditions while X-ray linear dichroism can be used to determine the corresponding molecular orientation. The primary goal of this project is to investigate the thermodynamic and kinetic factors that drive the morphology and molecular orientation of *n*-alkane thin films in microscopic domains. The experimental variables are (a) substrate and interface nature, (b) *n*-alkane chain length, and (c) growth conditions such as substrate temperature and deposition rate.

The importance of molecular alignment in organic thin films will be presented in §1.1. Common orientations observed for *n*-alkane thin films will be described in § 1.2. Epitaxial growth of organic thin films will be introduced in §1.3 as a method to control molecular orientation. In §1.4 different modes of growth in epitaxial growth will be discussed. The preparation method for *n*-alkane thin films employed in this study, physical-vapour deposition, will be explained in §1.5. Indirect epitaxy across a metallic thin film will be explained in §1.6. In

the next section, §1.7, inorganic epitaxy and its favorable consequences will be explained for the defined system of a $Si_{1-x}Ge_x$ alloy film on Si(100) surface. Linear dichroism in NEXAFS spectroscopy will be reviewed as a molecular alignment detection method in §1.8 and §1.9. The research objectives related to the main project (organic epitaxy) will be described in details in §1.10. Finally, a summary of materials that will be covered in Chapters 2 to 10 will be presented in §1.11.

1.1 Orientation in organic thin films and its importance

The structure of the deposit–substrate interface in organic films at the nanometer scale plays an important role in phenomena such as crystal growth, lubrication, wetting and surface chemical reactions. It is essential to understand the determining factors that drive the structure of thin films. The ordered arrangement of an organic monolayer is a key step to build molecular devices such as self-assembled monolayers on metallic or semiconductor substrates.[1,2] Surface electronic and optical properties of organic thin films can be tuned through an understanding of the relationship between structural characteristics and surface properties such as photoconductivity, linear and non-linear optical properties, and dye sensitization efficiency, as these are related to structural order, molecular orientation and morphology.[3] However, the growth regimes that are well understood for monolayer devices cannot be simply extended to multilayer systems. Competitive forces (deposit-deposit interaction versus deposit-substrate interaction) should be considered as the thickness of the organic deposit increases from a monolayer to a "bulk" multilayer. Alkanes are the basic components in many organic molecules and play an essential role in molecular orientation and packing in organic films such as liquid crystals, Langmuir-Blodgett films and self-assembled monolayers.[4] Therefore, the growth of *n*-alkane films is a feature of this work.

1.2 Molecular orientation of *n*-alkane thin films

Since *n*-alkanes are physisorbed on a variety of substrates with their carbon backbone in all-*trans* conformation, they will be assumed to have linear conformation unless otherwise noted. As can be seen in Figure 1.1 *n*-alkane molecules can be aligned in the lateral and normal orientations with their carbon backbone parallel and perpendicular to the surface respectively.[5] Some derivatives of *n*-alkane molecules can be aligned with the angle α (0°< α <90°) with respect to the surface, such as alkane thiols adsorbed on a gold surface.[6]

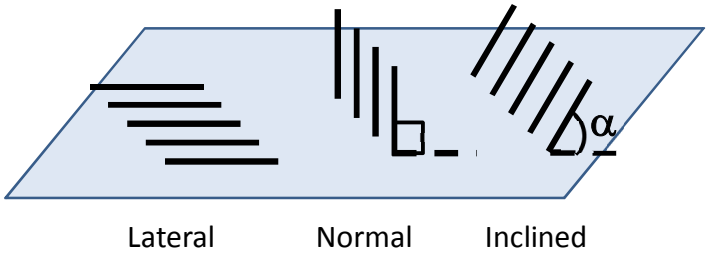

Figure 1.1 Molecular orientations of linear molecules adsorbed on a surface.

Kubono and Akiyama[7] proposed that at initial stages of film growth, there is an equilibrium between lateral and normal-oriented nuclei and their relative number follows a Boltzmann distribution based on an activation process as follows:

$$\frac{N_N}{N_L} = \exp(-\frac{E_N - E_L}{kT}) \qquad (1.1)$$

N_N and N_L are the number of nuclei with molecules in normal and lateral orientations respectively. E_N and E_L are the potential energies for the normal and lateral nuclei. k is the Boltzmann′s constant and T is the substrate temperature. This equation implies that the lateral orientation is always energetically favored at any temperature due to strong interaction between

the substrate and deposit molecules (Figure 1.2). However, it will be discussed that the potential energy is not the only determining factor in the orientation of deposit.

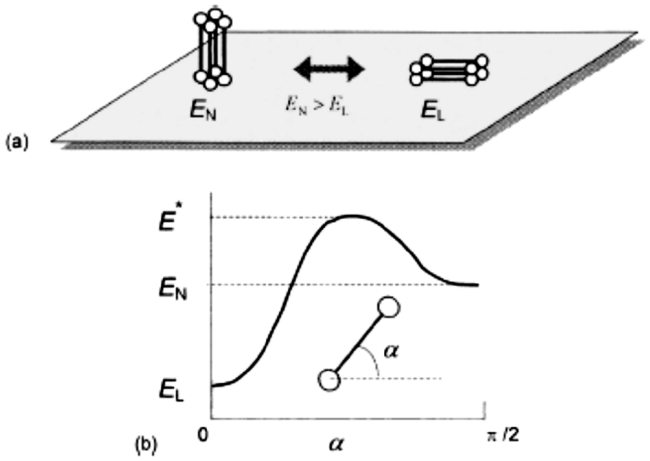

Figure 1.2 a.) Equilibrium between lateral and normal orientations with the potential energies of E_L and E_N; b.) potential energy versus molecular tilt angle with respect to the surface. Figure reprinted from Ref. 7 with permission.

The contribution of entropy change in the diagram shown in Figure 1.2 can be neglected as discussed in more detail below. At initial stages of nucleation, each cluster has a degree of freedom for rotation around the axis normal to the substrate surface. Therefore, for the *n*-alkane deposited on a substrate with n-fold axis normal to the surface, the normal and lateral-oriented nuclei should have infinite and n-fold degrees of freedom for rotation respectively. Hence, the normal orientation should have higher entropy than the lateral.[7] But generally the role of entropy is neglected by taking the assumption that the substrate has an isotropic surface and at the initial stages of nucleation the number of energetically equivalent states for the lateral and normal orientations are the same. Therefore, entropy is assumed orientation independent unless otherwise stated.[7]

In the kinetic model of organic film orientation, supersaturation, *S*, is related to the chemical potential change of the deposit-substrate interface with respect to the bulk deposit, $S \propto exp(\Delta\mu)$, and is used as a growth parameter that determines the orientation of organic films.[8,9] Matsuzaki et al.[8] reported that supersaturation is associated with the substrate temperature and/or deposition rate. Lateral nucleation is favored at high supersaturation (low substrate temperatures and/or high deposition rate). At high supersaturation, a quasi-liquid layer is formed on the surface of the substrate and the overlayer crystal grows by the molecules supplied from liquid instead of vapour directly onto (hk0) surface of substrate to form laterally oriented clusters.[7] But the kinetics of growth plays an important role in determining the growth pathway (lateral or normal) and can make the normal orientation preferred at low supersaturation (high substrate temperature and/or low deposition rate). This can be rationalized by considering that at the high substrate temperature (or low deposition rate) the re-evaporation rate of lateral nuclei is higher due to larger area in contact with the surface. This makes the lateral nuclei to be less stable than normal nuclei at low supersaturation. Therefore, the balance of molecule capture and re-evaporation determines the preferential orientation of organic thin films.[7]

In the study that was performed by Kubono and Akiyama,[5] the thermodynamics of lateral and normal nucleation was considered in terms of the free energy change. They calculated the minimum (critical) energy required for lateral and normal nucleation (ΔG^*). The basic equation that they used for the free energy of nucleus formation was a function of chemical potential change ($\Delta\mu$), and surface free energy per area (σ) as follows:[5]

$$\Delta G = -n\Delta\mu + \oint_A \sigma \, dA \qquad (1.2)$$

where n is the number of molecules in the nucleus, and dA is a small area on the surface. Their calculations show a critical value for chemical potential change ($\Delta\mu_{th}$), below which critical free energy for normal nucleation (ΔG_N^*) is lower than that for lateral nucleation (ΔG_L^*) (Figure 1.3a) and consequently the rate of normal orientation is higher than lateral orientation (Figure 1.3b). The rate of nucleation for each orientation (J) can be written as:

$$J = C\ exp(-\frac{\Delta G^*}{kT}) \tag{1.3}$$

In which C is pre-exponent factor, k is Boltzmann constant and T is temperature.[5]

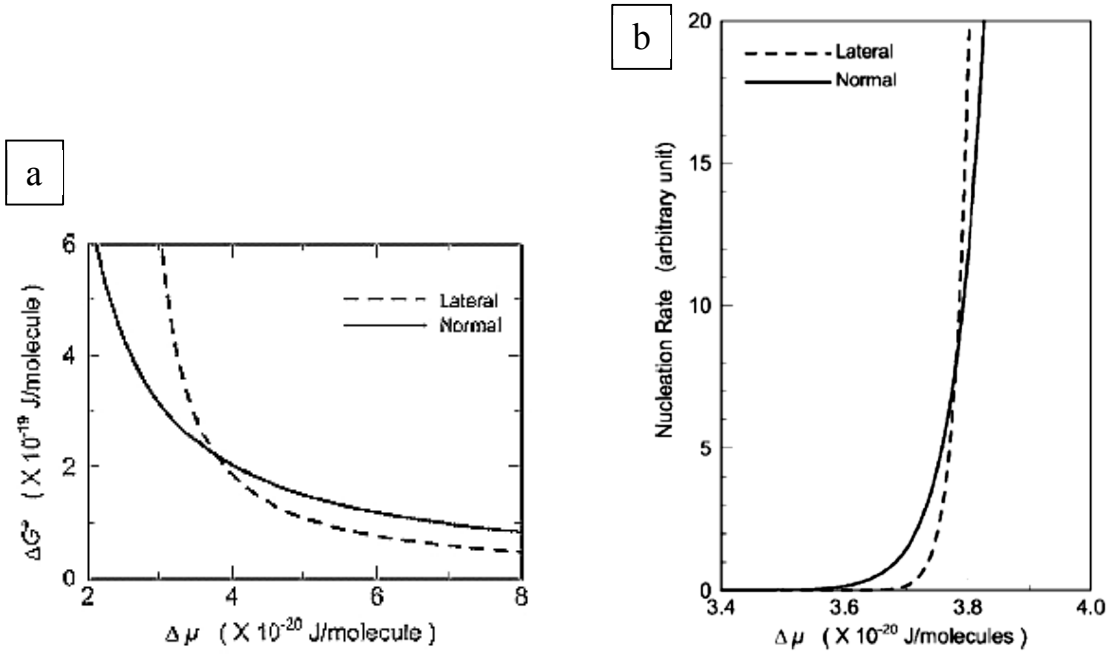

Figure 1.3 a.) Critical free energy of normally and laterally oriented nuclei as a function of chemical potential change; b.) nucleation rate for laterally and normally oriented nuclei as a function of chemical potential change. Figures reprinted from Ref. 5 with permission.

1.3 Organic epitaxy, a growth technique to apply a pattern to organic thin films

Epitaxy is the oriented crystal growth of an overlayer on the crystal structure of a substrate such that the structure of the substrate determines the orientation of the overlayer crystal. Epitaxy is of great importance in industrial applications such as corrosion inhibitors, biocompatible materials, lubrication and optical and electronic devices such as light emitting diodes, field effect transistors, solar cells, sensors, lasers and molecular electronics. In epitaxial growth, interfacial interactions between the crystal faces of the deposit and the substrate provides the possibility of growing particular overlayer morphology in a selective manner. Molecule-molecule interactions as well as molecule-substrate interactions at the deposit-substrate interface act as two competing factors to drive bulk nucleation or epitaxial nucleation[10] of an overlayer on a substrate. The morphologies that are seen in the deposit-substrate interface grown epitaxially cannot be seen in the bulk of deposit alone and form at the expense of deviation from natural form of deposit.

1.3.1 Molecular epitaxy

Generally, the geometric requirement for epitaxy is the availability of proper configuration for registry of an overlayer with substrate lattice points. However, molecular epitaxy can be obtained for different degrees of commensurism, starting from high degrees (point-on-point coincidence) to the lower degrees (point-on-line coincidence) and even to incommensurism. Point-on-point coincidence (Figure 1.4 left) refers to the condition where the overlayer lattice points coincide with the symmetry equivalent points on the substrate, while in point-on-line coincidence (Figure 1.4 right), every lattice point of the overlayer lies on a primitive lattice line of the substrate.[11]

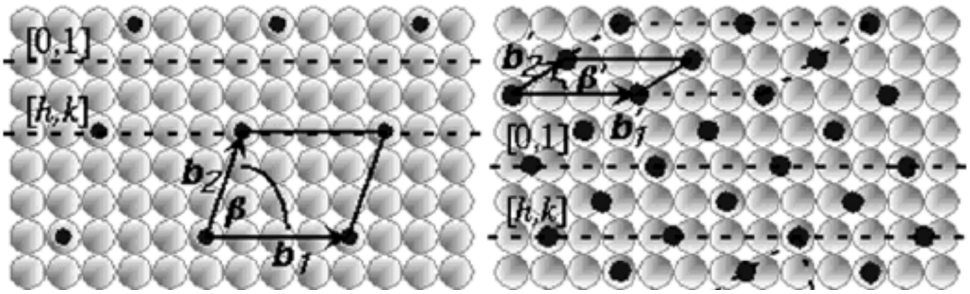

Figure 1.4 Schematic representation of different degrees of epitaxy: (left) point-on-point commensurism; (right) point-on-line commensurism. The small black and larger white circles represent the deposit and substrate lattice points respectively. The solid lines indicate the deposit primitive cells. Figure modified from Figure 2 in Ref. 11 with permission.

Commensurism can be even less than point-on-line coincidence, in which only some lines of the overlayer coincide with the primitive lines of the substrate. In an incommensurate overlayer, there is no distinctive registry between the lattices of the substrate and deposit. But even in this case, preferential directions can exist through a correspondence between the lattice directions of the deposit and substrate.[11] For example, a film of hexabromobenzene forms a uniquely oriented overlayer in registry with the graphite lattice in a small length scale of 80 Å despite a large lattice mismatch (lattice constant of C_6Br_6 is 9.14 Å versus that of graphite 2.46 Å).[11,12] The energetic benefit of coinciding lattice points can distort the overlayer from its natural form and gain some commensurism. However, the resultant strain of lattice point displacement or azimuthal rotation can lead to the formation of smaller ordered domains. The energetic gain of epitaxial growth that distorts the overlayer from its natural form depends on the degree of fit between two lattices, defined as the ratio of coinciding to non-coinciding lattice points.[11]

1.3.2 The driving forces in organic epitaxy

The potential energy involved in epitaxial growth of an organic deposit is the sum of E_{inter} and E_{intra} which describe the energy of interaction between an adsorbed molecule and substrate

(interface energy, E_{inter}), and the lateral molecule-molecule interaction within the organic molecular layer (two-dimensional crystallization or intramolecular energy, E_{intra}). For example the physisorption energies (E_{inter}) in the epitaxy of *n*-alkane/graphite system are from van der Waals and electrostatic interactions. In this system, the van der Waals interactions are larger than electrostatic interactions and the cooperative electrical polarization of two neutral bodies lowers the energy of system.[10,11] In the *n*-alkane/graphite system, E_{intra} is also from van der Waals interactions but is weaker than E_{inter} such that $E_{inter}/E_{intra} \sim 2.5$.[10]

The degree of epitaxy reflects the balance between E_{intra} and E_{inter}. The relative magnitudes of E_{intra} and E_{inter} make for three major categories for epitaxy. In the first case where $E_{intra}<E_{inter}$, the lattice distortion of overlayer leads to a high degree of commensurism. In this case, the energy gained by coinciding lattice points outweighs the penalty associated with the perturbation of E_{intra} from its native structure minimum value. In the second case where $E_{intra}>E_{inter}$, the consequences are either perfect commensurism (if coincidence can be achieved without perturbing the native structure of the overlayer) or a small degree of epitaxy (if a natural epitaxial match is not available). In the third case, $E_{intra} \sim E_{inter}$, epitaxy is possible when overlayer distorts its native structure to gain the benefit of lower interfacial energy by achieving a higher degree of commensurism.[11]

Epitaxial growth includes aggregation of deposit molecules in the energetically favored sites of the substrate that can be formed in quasi-equilibrium condition.[13] Since not all of nucleations take place on the most energetic favorable sites of substrate, it is necessary that growth proceed in quasi-equilibrium condition that ensures the reversible adsorption of molecules on the surface of substrate. The reversible adsorption involves an adsorption/desorption process so that the arriving molecules can diffuse on the surface and join

to the epitaxially growing nuclei. The critical size of epitaxial nuclei is achieved at the expense of desorption of nuclei in the other azimuthal angles (Figure 1.5). This happens when the sum of E_{inter} and E_{intra} at the preferred azimuthal orientation overcomes the sum of surface free energies of deposit and substrate shown as $\gamma_{deposit}$ and $\gamma_{substrate}$ respectively.[11] However, in the case that no commensurism exists between the deposit and substrate lattices, an orientational relationship between deposit and substrate results in an azimuthal order.[13]

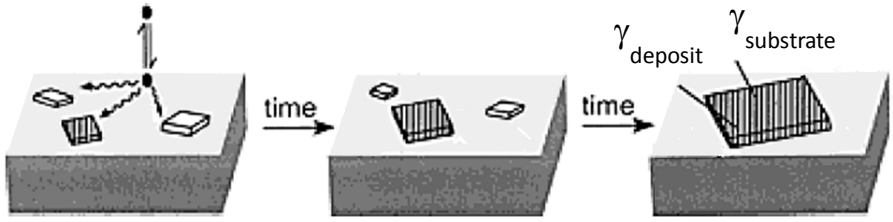

Figure 1.5 Selective growth of a molecular deposit near thermodynamic equilibrium condition that involves re-evaporation of nuclei in non-epitaxial azimuthal orientations to aggregate in the energetically favored epitaxial orientation. Figure reprinted from Ref. 11 with permission.

1.4 Different growth modes for thin films

In the study of film growth, understanding the relationship between the thermodynamics of adsorption and the kinetics of crystal growth are of great importance. There are three modes of crystal growth for a deposit on a crystalline substrate as illustrated in Figure 1.6. Each mode will be discussed as follows. In the Frank-van der Merwe mode (Figure 1.6a), the first deposited atoms/molecules form a complete monolayer on the substrate. The next layer containing the less tightly bound atoms/molecules covers the first layer completely. The decrease in binding energy continues towards the value for a bulk crystal of deposit. This mode happens when the atoms/molecules of deposit are bound to the substrate stronger than to each other. According to minimum Helmholtz free energy thermodynamic argument, crystal A grows in the layer-by-layer

mode (Frank-van der Merwe mode) on crystal B if $\gamma_A + \gamma^* \leq \gamma_B$; where γ_A, γ_B, and γ^* are the surface free energies of the crystal A, crystal B, and interface respectively.[9] By assuming that the surface free energies of the individual crystal A and crystal B are comparable in values, the determining parameter in the above inequity is the surface free energy of interface between A and B crystals, γ^*. A strong interaction between deposit and substrate stabilizes the interface and gives a negative value for γ^* and validates $\gamma_A + \gamma^* \leq \gamma_B$ and the layer-by-layer growth mode.

In contrast, the Volmer-Weber mode (Figure 1.6b) happens when the atoms/molecules of deposit are more strongly bound to one another than to the substrate. In this case, the interface of two weakly bonded crystals is unstable and γ^* has a positive value which makes $\gamma_A + \gamma^* \geq \gamma_B$. In island mode (Volmer-Weber mode), the first incoming atoms/molecules form small clusters directly on the substrate which gradually grow into crystalline islands of deposit. The Stranski-Krastanov mode (Figure 1.6c) is a growth mode in between the layer-by-layer mode and island mode. The $\gamma_A + \gamma^* \leq \gamma_B$ inequity is valid for the initial stages of growth. After forming the first complete monolayer, or a few monolayers, the subsequent layer growth is energetically unfavorable and islands are formed on top of the complete layer(s). Any reason that disturbs the monotonic decrease in binding energy between layers can dominate the island growth over the layer-by-layer growth. The factors that prevent the first monolayer to grow into a bulk crystal can be categorized as the lattice parameters, symmetry, molecular orientation, etc. These changes increase the interface free energy between the layers and lead to the start of island formation.

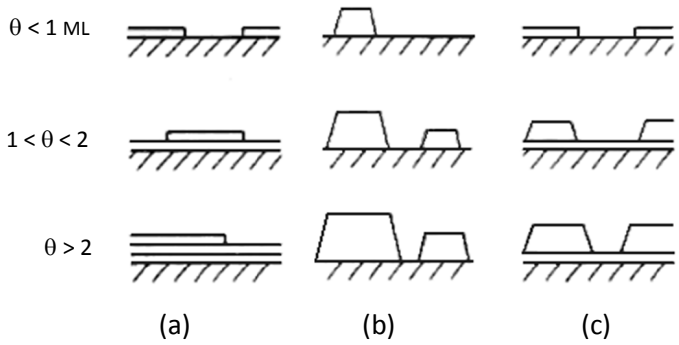

Figure 1.6 Three crystal growth modes: a.) layer-by-layer mode or Frank-van der Merwe; b.) island mode or Volmer-Weber; c.) layer-plus-island mode or Stranski-Krastanov, θ shows the degree of coverage in monolayers. Figure modified from Figure 1 in Ref. 9 with permission.

The thermodynamic equivalent of the three growth modes mentioned above is illustrated in Figure 1.7 in the form of adsorption isotherms. In this figure, the chemical potential change of the growing deposit relative to its bulk crystal ($\Delta\mu$) is represented at different thicknesses (θ in monolayers). The layer-by-layer growth mode can exist at the negative values of $\Delta\mu$, low supersaturation, due to strong binding energy between deposit and substrate (Figure 1.7a). Supersaturation is used in literature as a parameter that is associated with both substrate temperature and deposition rate. On the other hand for island growth mode (Figure 1.7b), the surface concentration of deposit atoms/molecules is very low because of fast re-evaporation due to the weak binding of deposit to the substrate. This mode needs a large positive value for $\Delta\mu$, high supersaturation, to form a crystalline island of deposit on the substrate.[5,7,9] In the layer-plus-island growth mode (Figure 1.7c), the negative $\Delta\mu$ (which is related to the layer-by-layer growth) turns to the positive $\Delta\mu$ (which refers to the island growth) at some finite coverage, or thickness.[9]

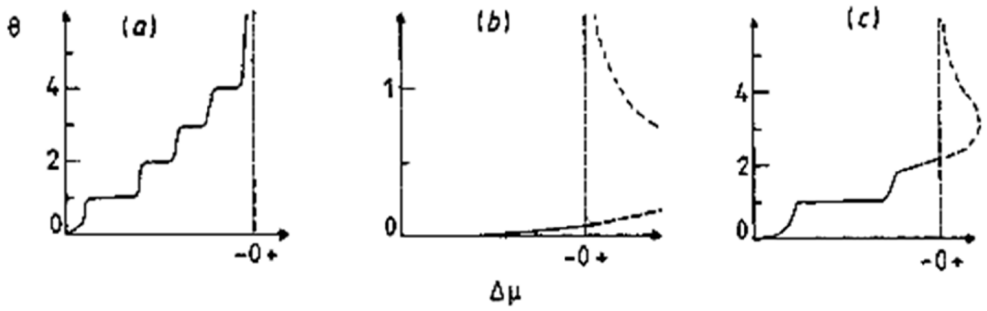

Figure 1.7 Adsorption isotherms corresponding to three modes of film growth. Chemical potential of the growing deposit relative to the bulk (shown in axis X, Δμ) changes as deposit grows (shown in axis Y in monolayers, θ). a.) Frank-van der Merwe mode; b.) Volmer-Weber mode; c.) Stranski-Krastanov mode. Figure modified from Ref. 9 with permission.

1.5 Physical vapour deposition, a growth technique to apply epitaxy

Physical vapour deposition (PVD) is a widely used technique for depositing organic/inorganic/metal thin films. Vapours are prepared by electron beam heating, resistive heating, or sputtering. Before vapour deposition was utilized as a film growth technique, solution deposition was widely used. In 1930, Sloat and Menzies[14] studied the effect of solvent in solution deposition and found out that the orienting ability of a substrate increases as the dielectric constant of the solvent decreases. This led them to the idea that deposition from vapour phase, with the dielectric constant of one, has a better potential for epitaxial growth than solution deposition. Growth parameters such as atomic/molecular flux (deposition rate), flux incidence angle, incident kinetic energy and the substrate temperature can be varied individually in PVD. Controlling morphology and microstructure of the deposit during PVD can be achieved through varying these growth parameters because they influence the processes such as adsorption, desorption and reconstruction of deposit. Therefore, vapour phase deposition became a widespread technique from 1950 onward. To decrease the amount of contamination during

vapour deposition, "vacuum evaporation" is used which facilitated the use of in situ electron based and spectroscopic probes to investigate the interface during the growth process.[15-18]

1.5.1 Growth parameters in PVD

Well-ordered organic thin films can be prepared by physical vapour deposition because the weak binding to the surface allows for the reversible and quasi-equilibrium growth. According to the PVD growth model proposed by Kubono et al.,[7] the initial stages of film growth from the vapour phase include the following steps: 1) adsorption from vapour, 2) surface migration, 3) re-evaporation from the substrate, 4) capture into a laterally or normally oriented cluster, 5) re-evaporation from the cluster and, 6) reorientation (Figure 1.8).[7]

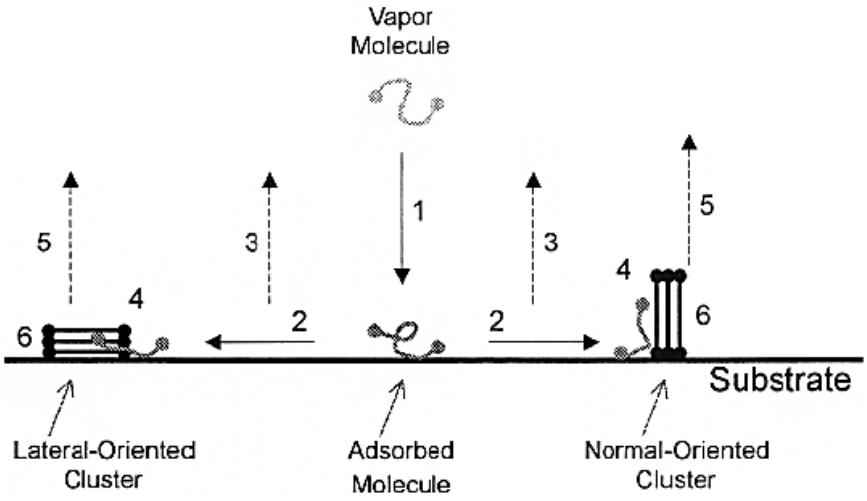

Figure 1.8 Schematic representation of initial stages of film growth from vapour phase, 1) adsorption from vapour, 2) surface migration, 3) re-evaporation from the substrate, 4) capture into a laterally or normally oriented cluster, 5) re-evaporation from cluster, 6) reorientation. Figure reprinted from Ref. 7 with permission.

The diffusion of adsorbed molecules on the substrate plays an important role because the direct capture of molecular vapour to a cluster is negligible.[19] The re-evaporation is noteworthy at high substrate temperatures, as the lateral-oriented clusters exhibit faster re-evaporation due to

larger surface area in contact with the substrate. This can be seen in experiment, as a normally oriented cluster growth is predominant over the laterally oriented cluster growth at high substrate temperatures. However, at low substrate temperatures, the energetic benefit of laterally oriented nuclei makes the nucleation and growth proceed with lateral orientation.[5] Therefore, substrate temperature determines the balance of capture and re-evaporation of normal and lateral orientations, which leads to the nucleation and growth of a specific orientation.[7] As illustrated in Figure 1.9 two categories of parameters are responsible for determination of the sign and value of $\Delta\mu$ (chemical potential change of the growing deposit on the surface with respect to its bulk) and the nucleation and growth behavior of a thin film from vapour phase. The first category includes the experimental variables, such as deposition rate (F) and substrate temperature (T_s); and the second group involves material parameters, such as re-evaporation energy (E_a), diffusion energy (E_d), and binding energy (E_i). Specially, the diffusion and re-evaporation energies are important, because they provide the conditions required for the epitaxial growth in which the clusters of deposit could grow and decay reversibly.[9]

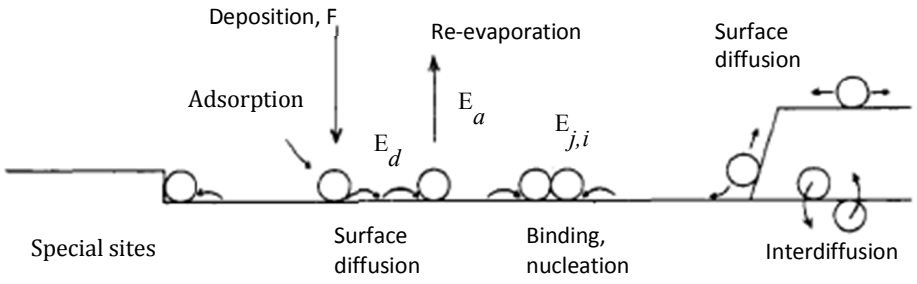

Figure 1.9 Schematic diagram of the processes and energies involved in nucleation and growth of a deposit in physical vapour deposition. Figure modified from Ref. 9 with permission.

1.5.2 Diffusion barrier in PVD

Surface diffusion is an important parameter that affects the structure of the deposit in the PVD technique. Surface diffusion provides the condition in which the adsorbing atoms/molecules can move on the surface to find substrate sites with the least potential energy in order to decrease the surface free energy. A diffusion barrier exists in the process of surface diffusion, as diffusion requires the partial breaking of the deposit-surface bonds to be able to move to the neighboring area and form new bonds. Therefore, an adsorbed atom/molecule has to pass a transition state between two sites of the surface to diffuse.[20] According to Equation (1.4),[21] the surface diffusion rate (D) is a function of substrate temperature (T) that applies kinetic energy to the deposit atoms/molecules and enables them to overcome the diffusion barrier.

$$D = D_0 \exp(-\frac{E_a}{kT}) \quad (1.4)$$

The diffusion pre-factor (D_o) and diffusion energy barrier (E_a) are determined by substrate material.

1.5.3 Molecular orientation in PVD

The molecular orientation in the organic thin films prepared by PVD is controlled by the deposition rate and the degree of *supercooling* (difference between the melting temperature of deposit and the substrate temperature). The degree of supercooling affects molecular motion (translation, rotation and precession modes) and the relative rates of adsorption and re-evaporation processes.[22] In the initial stages of growth, the laterally oriented nuclei can be changed to the normally oriented nuclei by annealing at a higher substrate temperature (lower supercooling), which is considered an irreversible process.[23] It has been reported that the

orientational change of paraffin during annealing occurs for nuclei consisting four or less molecules and that the orientation change cannot occur if the nuclei grow larger.[7,24]

1.6 Indirect epitaxial growth

Indirect epitaxy, first observed by Distler et al.[25] in 1976, is a puzzling variation of well-known epitaxy. In indirect epitaxy, the substrate crystal structure can still be copied onto the deposit even when an amorphous film (an interlayer) separates the deposit and substrate. In multilayer systems of crystalline/amorphous/crystalline type, there are some ideas in favour or against the active role of an interlayer in the oriented growth of deposit. In favor, the electrical polarization of interlayer is believed to be responsible for the oriented crystallization of deposit. Shirokoff and Erb[26] examined the orientation of Au and Ag on NaCl and Si with and without amorphous C and SiO_2 interlayers respectively, and observed two kinds of orientation relationships that depended on the contact planes of the deposit and the substrate. One kind of orientation relationship has a characteristic that occurs even when an interlayer with the thicknesses of up to 20 nm for NaCl and 33 nm for Si separates the substrate and deposit. The other kind of orientation relationship (specific to some contact planes) occurs only if the substrate and deposit are in direct contact.[26,27]

Those opposed to the interpretation of indirect epitaxial growth through an amorphous interlayer believe that structural information is transmitted to the overgrowth through some pinholes in the amorphous interlayer. Yang et al.[27,28] presented evidence showing that in the multilayer system of Si-SiC-diamond, the interlayer of amorphous SiC has pinholes through which Si and diamond interact directly.

1.6.1 Metallic thin films as an intermediate layer

In indirect epitaxy, the metallic thin films make an interesting category of interlayer due to their high polarizability. Long-chain alkanes form highly ordered lamellae structure on metallic substrates due to the strong binding energy. Many studies have shown that *n*-alkanes form a two-dimensional ordered monolayer on the clean surface of most metals such as Ag(111),[1,29] Au(111),[1,30] Cu(100),[31] Pt(111),[1,32] etc. In this ordered monolayer, *n*-alkane molecules with all-*trans* conformation are oriented parallel to the surface with their carbon backbone having flat-on structure. The ordered structure comes from the van der Waals interaction between the fluctuating dipole of *n*-alkane molecule and its image dipole in the metal surface. This van der Waals interaction between an *n*-alkane molecule and metal is greater than alkane-alkane interaction because of higher density of mobile electrons and stronger dipole moment induced on the metal surface.[31] The flat-on orientation is energetically preferred to edge-on, because of imposing a shorter distance between electron cloud of each methylene group of alkane chain and the surface of metal.[31] However, van der Waals interactions can easily be overcome by alkane-alkane intermolecular interactions when *n*-alkane is adsorbed on a contaminated or oxidized metal surface.[33,34] In this case the energetically favored orientation is end-on (normal to the surface). The structure of thicker *n*-alkane films (up to 40 monolayer equivalent) is determined by alkane-alkane intermolecular interactions. Therefore, the films thicker than a monolayer are quasi-crystalline and the plane of carbon backbone is to some extent inclined relative to the surface of metal.[31]

1.6.2 Interfacial dipole formation upon adsorption of *n*-alkane on the metal surface

In the case of indirect epitaxy of *n*-alkane films on ordered substrates through an intervening metal thin film, an *n*-alkane/metal interface forms. Understanding the nature of the

molecule/metal interface is required to predict the electronic properties of molecular electronic devices based on these organic thin films. Upon the formation of the interfacial dipole, the surface properties of deposit and metal are affected and are manifested as (1) the changes in the vibration energies of deposit, and (2) a decrease in the metal work function. IR spectra from *n*-alkanes adsorbed on metals reveal that the C-H stretching shows up at lower frequencies than normal stretching modes of a methylene group. The softening of C-H bond in contact with a metallic surface is explained in three different ways.[30,35,36] Yamamoto et al.[30] proposed that conduction electrons at the metal surface produce the image-dipole that interacts with the transition dipole moment of CH group. Fosser et al.[34] and Ostrom et al.[35] suggested that there is some sort of chemical bonding between metal and *n*-alkane that is responsible for the charge transfer from the metal to the *n*-alkane unoccupied molecular orbitals. In contrast, Pichugina et al.[37] proposed the presence of an electronic transition from the adsorbed hydrocarbon to the metal. They studied the interaction of hydrocarbons with gold clusters of Au_{10} and determined that the alkane-Au cluster interaction increased by 3 times for the charged gold cluster (Au_{10}^{+}). This implies a charge transfer from hydrocarbon to the metal.

In addition, it was also reported that the work function of Au decreases by 0.7 eV upon adsorption of saturated hydrocarbons on the Au due to formation of a dipole interface. Ishii and Seki[38] suggested two reasons for the formation of interfacial dipole: the image effect and the push-back effect. The push-back effect is assigned to perturbations of the electronic structure of metal by Pauli repulsion. This repulsion occurs upon physisorption, when the distortion of metal electrons' wavefunction is required to reduce the overlap between deposit molecule and metal electronic wavefunctions via van der Waals interactions. The distortion of the metal electron

wavefunction increases the kinetic energy of electrons[39] and pushes some of the metallic charge back into the metal.[40,41]

In summary, in a hydrocarbon-metal system the presence of interfacial dipole moment has been experimentally proven in two ways; first, the variation of deposit vibrational energies and second, the variation of metal work function. However, the nature of hydrocarbon-metal interaction is not clear yet and more investigation is needed to assign it to van der Waals/ electrostatic interactions or prove some chemical bonding through charge transfer.

1.7 Application of epitaxy in inorganic strained systems

Epitaxy is a commonly used industrial method for production of semiconductor devices such as transistors, and light emitting diodes. Strained hetero-structure systems can have a modified electronic band structure and improved electron mobility in optoelectronic devices. The ability to measure alloy composition and strain is required for the calibration of growth processes and control of electrical and optical properties of these materials.[42] Figure 1.10 specifically presents the epitaxial growth of a strained SiGe alloy thin film on Si(100) substrate. In the strained SiGe/Si semiconductor system the following changes are observed: lattice distortions (Figure 1.10a), modified spatial distribution of unoccupied molecular orbitals (Figure 1.10b), and the corresponding split band structure (Figure 1.10c).

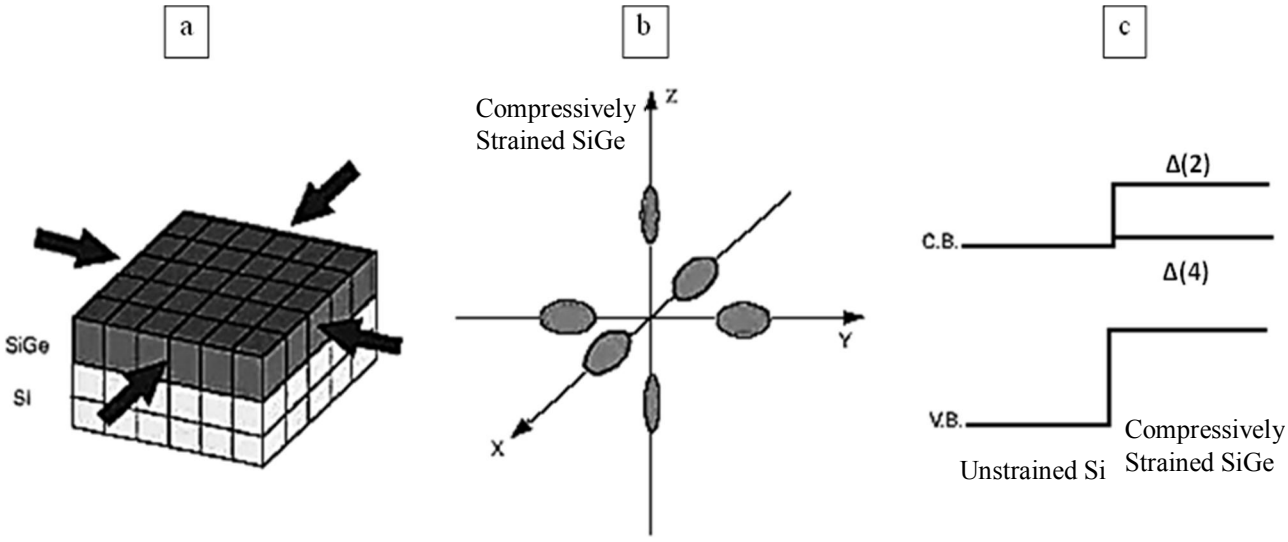

Figure 1.10 a) Compressively strained SiGe alloy on Si(100); b) unoccupied molecular orbitals of strained SiGe; c) band modification of strained SiGe. Figure modified from Figure 2 in Ref. 43 with permission.

1.7.1 $Si_{1-x}Ge_x$ alloys on Si wafer

The epitaxial growth of $Si_{1-x}Ge_x$ hetero-structures on the Si(100) substrate has been used to improve light emitting devices and high speed transistor structures. $Si_{1-x}Ge_x$ alloys are miscible in the whole composition range if they are prepared at the temperatures required for epitaxial growth on Si wafer.[44] The lattice parameter of Ge (5.657 Å) is 4% larger than that of Si (5.431 Å). This causes a biaxial compressive strain, when a commensurate $Si_{1-x}Ge_x$ alloy film is grown on Si(100).[45] Biaxial compression of $Si_{1-x}Ge_x$ layer results in an elastic energy that increases with layer thickness and drives strain relaxation (Figure 1.11a). After a critical thickness, the strain can be relaxed by formation of misfit dislocations (Figure 1.11b).[42] Since the surface free energy of $Si_{1-x}Ge_x$ alloy is lower than Si for very low Ge concentration, the alloy grows in Frank van der Merwe (layer-by-layer) mode on Si wafer. By increasing Ge content, the strain builds up and Stranki-Krastanov growth mode results.[42]

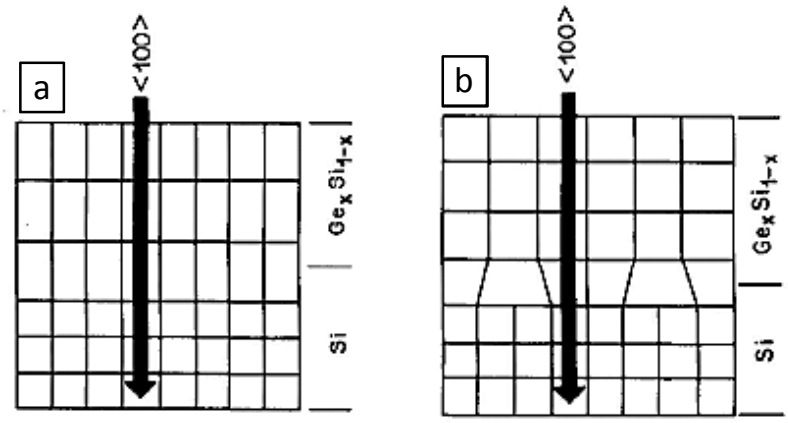

Figure 1.11 Schematic representation of epitaxial growth with different degrees of strain, a.) commensurate and strained; b.) incommensurate and relaxed. Figure modified from Figure 5 in Ref. 46 with permission.

1.7.2 Electronic transitions in the NEXAFS spectra of $Si_{1-x}Ge_x$ /Si systems

Generally, electronic transitions close to the core ionization onset (less than 10 eV above threshold) are assigned to dipole excitations to unoccupied molecular orbitals or conduction bands for solids. In particular, the 1s transitions of solids are related to unoccupied final states of p-character.[47,48] The doublet peak at ~ 1840 eV in the Si 1s NEXAFS spectrum (Figure 1.12) is assigned to the Si 1s → 3p conduction band transition and is commonly seen in the spectra of the crystalline Si and $Si_{1-x}Ge_x$ alloys[47] and also in the calculated plot of partial density of unoccupied p-symmetry states.[49]

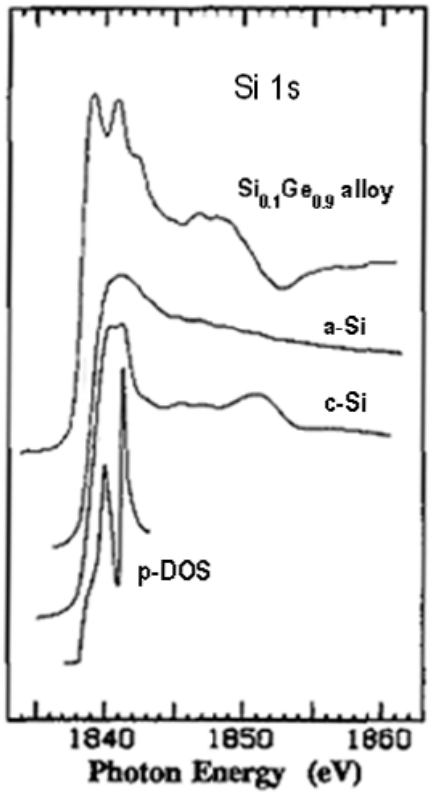

Figure 1.12 Si 1s spectra of $Si_{0.1}Ge_{0.9}$ crystal alloy, amorphous Si (a-Si), crystalline Si (c-Si) and density of p-unoccupied states (p-DOS). Figure reprinted from Ref. 47 with permission.

1.8 Molecular and atomic alignment identification by linear dichroism in near-edge X-ray absorption fine structure (NEXAFS) spectroscopy and microscopy

Structure of *n*-alkane thin films have been studied by various techniques such as low energy electron diffraction (LEED), infrared reflection absorption spectroscopy (IRRAS), helium atom scattering, temperature-programmed desorption and scanning tunneling microscopy (STM).[31] STM provides high spatial resolution imaging and can detect the individual molecules of a monolayer, but is not able to image an *n*-alkane multilayer due to low electric conductivity. The spatial resolution of IR microscopy (5 μm) is much larger than the typical domain size for nanostructured *n*-alkanes. None of these techniques provides characterization of molecular orientation with high spatial resolution for an *n*-alkane multilayer with structures smaller than 500 nm. Synchrotron radiation sources have been used as an independent tool to characterize the

surface properties starting from the 1960s. Near edge X-ray absorption fine structure (NEXAFS) spectroscopy is a synchrotron-based technique that can be used to resolve the electronic structure and orientation of molecules bonded to surfaces.[50] NEXAFS probes the electronic transitions usually from 1s, 2s or 2p of an atomic species into unoccupied molecular orbitals or continuum states. NEXAFS spectra exhibit distinctive features in the energy region below and up to about 50 eV above the absorption edge.[47] A NEXAFS spectrum shows the dependence of the photoabsorption cross section, probability of absorption, on the photon energy in the vicinity of ionization threshold. In organic molecules, the electron transition resonance is observed if the energy of incoming photons matches the energy difference between 1s and the unoccupied molecular orbitals, π^* or σ^* depending on the symmetry, or Rydberg orbitals. Usually π^* and Rydberg orbitals are located below ionization potential and σ^* above the ionization potential (Figure 1.13). The width of a resonance depends on the energy resolution of the instrument and the lifetime of the core-excited state. An increased lifetime broadening of the transitions to σ^* orbitals occurs because they can be found at energies higher than ionization threshold and the large overlap with the continuum increases the probability of electron decay to continuum states.[51]

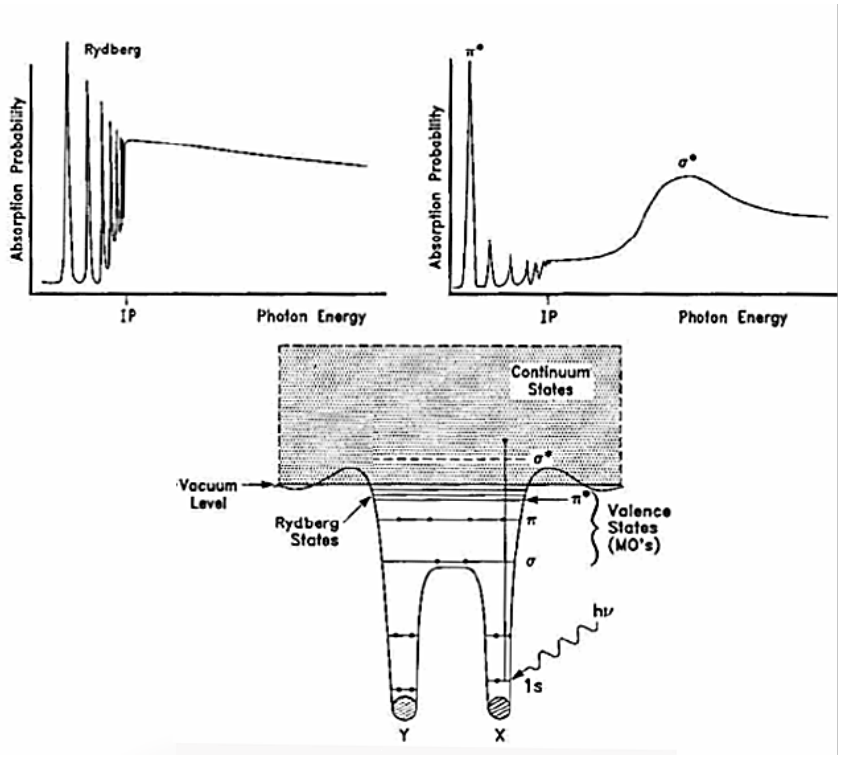

Figure 1.13 (bottom) Schematic potential of a diatomic molecule; (top) NEXAFS spectra corresponding to 1s transitions. Figure modified from Figure 4.2 in Ref. 51 with permission.

1.8.1 Transition dipole moment

The transition dipole moment is the charge separation in the electronic cloud of an absorbing atom induced by electric field of electromagnetic radiation. The magnitude of the transition dipole moment depends on the ability of electron to couple with the electric field and follow the electric force induced by this interaction. The transition dipole moment (μ_{if}) is calculated by Equation (1.5):

$$\mu_{if} = < \psi_i | \mu | \psi_f > \qquad (1.5)$$

where ψ_i and ψ_f are the electron initial and final states and μ is the electric dipole moment operator. For example, when the energy of the radiated light matches the energy difference between s and p orbitals, an electron transition occurs due to interaction of the electric field and electron charge.[52]

1.8.2 Dipole selection rules

In NEXAFS spectroscopy, for the transitions from an atomically localized orbital to an unoccupied molecular orbital, the local symmetry of molecular orbital on the excited atom determines if the transition is allowed. In transitions from the 1s atomic orbital to the unoccupied molecular orbitals, the dipole selection rule dictates that the final state have a p orbital component such that generally, the $\pm\Delta l$ rule should be followed (an exact rule for an atom, a propensity for a molecule). The presence of a node, indicating local p character, in the plot of the molecular orbital is a simple method to check if a transition from 1s to that particular final state is allowed.[51]

In NEXAFS spectroscopy of a molecule, the dipole selection rules require that the transition dipole moment be parallel to the electric field vector of the X-rays for maximum absorption. As shown in Equation (1.6), the intensity of X-ray absorption (I) is proportional to the angle θ between the electric field vector of X-ray (E) and the direction of electronic transition dipole moment (μ_{if}) from the initial state ψ_i to the final state ψ_f.[53]

$$I \propto \left| E \bullet \mu_{if} \right|^2 = \left| E \right|^2 \left| \mu_{if} \right|^2 \cos^2 \theta \qquad (1.6)$$

1.8.3 Orientation analysis of NEXAFS spectroscopy and microscopy

Information regarding the orientation of molecules can be derived from NEXAFS experiments by using the polarization characteristics of synchrotron radiation. X-ray linear dichroism (LD) in NEXAFS spectroscopy, or the polarization dependent absorption of linearly polarized X-ray, can determine the relative orientation of a transition dipole moment. Linear dichroism in NEXAFS spectroscopy and microscopy creates a contrast between differently oriented transition dipole moments within a molecule from which the orientation of the respective molecule can be extracted.

1.9 Linear dichroism in NEXAFS spectroscopy from saturated hydrocarbons

Molecular orientation of the saturated hydrocarbons can be determined by acquiring the angle dependent NEXAFS spectra of the C 1s $\rightarrow \sigma^*_{C\text{-}H}$ and C 1s $\rightarrow \sigma^*_{C\text{-}C}$ transitions, and comparing to those of known reference systems (Figure 1.14). However, some differences must be considered between unoccupied $\sigma^*_{C\text{-}H}$ and $\sigma^*_{C\text{-}C}$ molecular orbitals as discussed below.

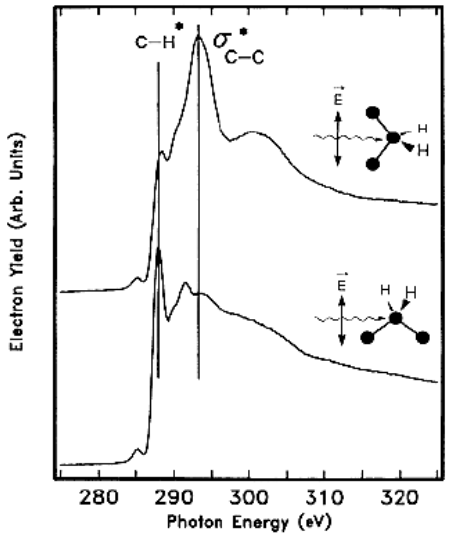

Figure 1.14 NEXAFS spectra from a saturated hydrocarbon focused on a portion of carbon backbone. (Top) X-ray electric field ∥ carbon chain axis, (bottom) X-ray electric field ⊥ carbon chain axis. Figure modified from Figures 1 and 2 in Ref. 54 with permission.

The hydrogen-derived $\sigma^*_{C\text{-}H}$ antibonding orbitals mix with the Rydberg orbitals with similar symmetry and increase the intensity of the corresponding resonance. The mixing of $\sigma^*_{C\text{-}H}$ with Rydberg orbitals draws the $\sigma^*_{C\text{-}H}$ energy level below the ionization potential (Figure 1.15). This makes the comparison of intensities related to C 1s $\rightarrow$ $\sigma^*_{C\text{-}C}$ and $\sigma^*_{C\text{-}H}$ transitions difficult because the former is superimposed on the ionization potential but the latter is not. Decomposing the angle dependent spectra to their components and fitting the ionization step and various transitions makes it possible to compare the net intensity of transitions assigned to $\sigma^*_{C\text{-}C}$ and $\sigma^*_{C\text{-}H}$. However, since the orientation of *n*-alkanes has been studied widely on a variety of substrates by NEXAFS spectroscopy and the energies of different electronic transitions in the hydrocarbon films are known, it is possible to skip the decomposition step and simply compare the relative heights of the peaks assigned to C 1s $\rightarrow$ $\sigma^*_{C\text{-}C}$ and $\sigma^*_{C\text{-}H}$ transitions.[55]

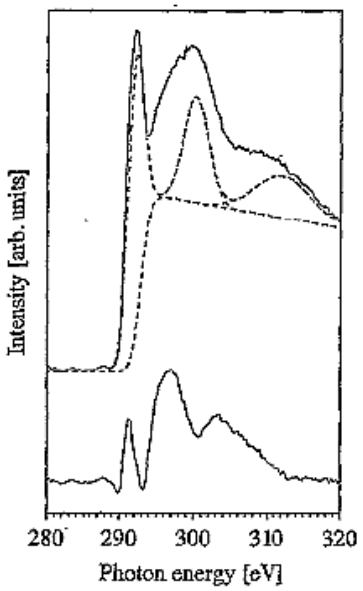

Figure 1.15 (top) Solid line is the summation of NEXAFS spectrum of a saturated hydrocarbon, and C 1s ionization potential; (bottom) C 1s ionization potential is subtracted from the spectrum of hydrocarbon to show C 1s $\rightarrow$ $\sigma^*_{C\text{-}H}$ and C 1s $\rightarrow$ $\sigma^*_{C\text{-}C}$ transitions. Figure reprinted from Ref. 56 with permission.

Fu and Urquhart[57] presented the linear relationship between I and $cos^2\theta$ (Equation 1.6) for *n*-alkane thin films grown on NaCl(001). As shown in Figure 1.16, optical density (proportional to intensity of absorption) exclusively changes with angle θ (top) and $cos^2\theta$ (bottom) dramatically at the X-ray energy corresponding to C 1s → $\sigma^*_{C\text{-}C}$ transition (293.5 eV) which is a direct manifestation of linear dichroism.

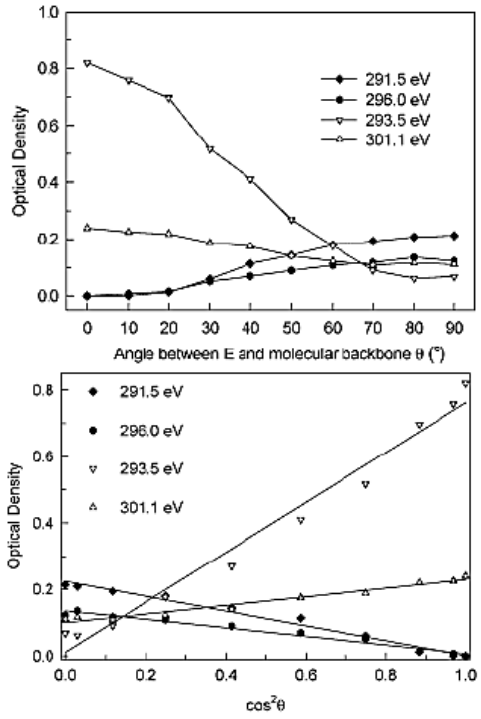

Figure 1.16 Optical density of C 1s → $\sigma^*_{C\text{-}C}$ transition in a saturated hydrocarbon as a function of angle θ (top) and $\cos^2\theta$ (bottom). Figure reprinted from Ref. 57 with permission.

Splitting of the C 1s → $\sigma^*_{C\text{-}H}$ transition

One of the main NEXAFS transitions used in the determination of the orientation of *n*-alkane films that is assigned to C 1s → $\sigma^*_{C\text{-}H}$; this usually appears in the form of a doublet. Stöhr et al.[54] have assigned the doublet peak located at ~288 eV to two electronic transitions such that the first peak at 287.4 eV was assigned to C 1s → $\sigma^*_{C\text{-}H}$ transition and the second peak at 288.1

eV to C 1s → $\pi^*_{C\text{-}H}$ transition. Weiss et al.[58] have assigned the doublet peaks at 288 eV to mixed valence and Rydberg character. They computed that both of peaks are related to the transitions that have π-character while the largest contribution is in the *y* and *z* directions for the first and second peak respectively (Figure 1.17).[58] The Rydberg character of the doublet peaks at 288 eV makes these transitions sensitive to the intermolecular environment and their relative intensity varies with intermolecular distance.[58] Moreover, the azimuthal orientation of an *n*-alkane chain in the *xz* plane can be resolved by comparing the doublet peaks' relative heights. If the electric field vector of the X-ray are oriented along the *x* axis, the *n*-alkane aligned along axis *z* will produce a doublet peak with 1:1 intensities. While, for the *n*-alkane molecule aligned along the *x* axis, the spectrum will show a doublet resonance with a higher intensity in the second peak.

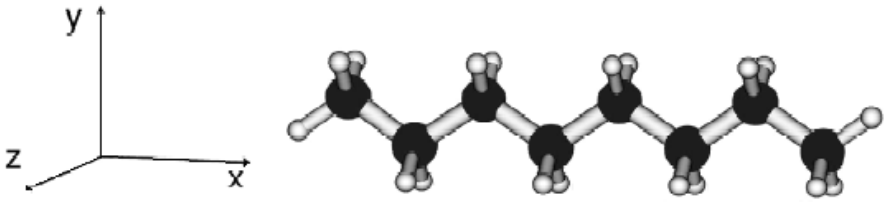

Figure 1.17 The geometry used for calculation of *n*-octane by Weiss et al. Adapted from Figure 1 in Ref. 58.

1.10 Research objective and approaches

Two projects related to epitaxy in organic and inorganic systems are covered in this thesis, and are named as the main and side projects respectively. The main project is built on the conception of thermodynamically stable and kinetically trapped metastable orientations of *n*-alkane thin films. Based on the literature and knowledge learned in Dr. Urquhart's group, this project is intended to assess the balance of the enthalpic interactions and molecular mobility that governs the epitaxial growth of the physical-vapour deposited *n*-alkane thin films. By

understanding the fundamental determining factors in molecular orientation it may be possible to control the growth conditions and the nature of interface between substrate and deposit needed to induce a desired molecular orientation in an organic thin film. Several approaches have been taken to examine different aspects of organic film growth, and to identify these determining factors. To this end in the current thesis, the strength of attractive forces as a thermodynamic factor and several kinetic factors (such as molecular mobility and diffusion rate) will be addressed for epitaxial growth of *n*-alkane thin films on a series of substrates (such as semi-metallic, metallic, ionic, and chemically treated surfaces).

In the side project, the objective is high spatially resolved measurement of the lattice strain in the $Si_{1-x}Ge_x$ alloy thin film grown epitaxially on Si(100). This objective will be investigated by performing two types of measurements. First, the degree of strain in $Si_{1-x}Ge_x$ alloys will be measured by Raman spectroscopy for the samples with variable Ge content. Second, the absolute value of linear dichroism in Si 1s $\rightarrow$ NEXAFS spectra will be measured with respect to the Ge content in these alloys. Finally, the two mentioned measurements will be correlated to obtain a direct relationship between Si 1s polarization dependence NEXAFS spectra and the degree of strain. This technique has the potential for a complementary metrology of strain in semiconductors. For example X-ray photoemission electron microscope (X-PEEM) and scanning transmission X-ray microscope (STXM) with lateral spatial resolutions of <50 nm and <35 nm respectively are capable of mapping the strain on the surface of semiconductors with sub-100 nm length scales. The specific objectives that are sought in the main project (organic epitaxy study) and the corresponding approaches are listed in §1.10.1 to §1.10.3 as follows.

1.10.1 Epitaxial growth of *n*-alkane on the surfaces with tailored functionalities

Well-oriented self-assembled monolayers (SAMs) have a potential of controlling the molecular orientation of deposited organic thin films, by following the alignment of SAMs. It was observed[59] that the *n*-alkane film grown on a SAM with defined orientation duplicates the molecular orientation of the SAM monolayer (Figure 1.18). In the current study, epitaxial growth of *n*-alkane thin films will be examined on the chemically treated SAMs. It is hypothesized that *n*-alkane film orientation can be controlled by tuning the alkane-substrate interactions via changing the nature of alkane-SAM interface.

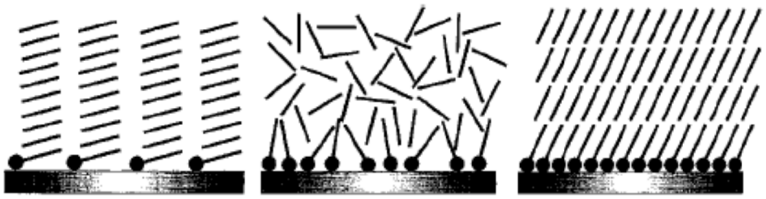

Figure 1.18 Schematic of *n*-alkane multilayer alignment on the laterally oriented SAM, disorder SAM, and normally oriented SAM from left to right. Figure reprinted from Ref. 59 with permission.

Two approaches are proposed based on two thiol SAMs on gold with different functionalities:

a) In the first approach, a normally oriented carboxylic-acid-terminated thiol SAM, such as 11-mercaptoundecanoic acid, will be prepared on gold. This will be chemically treated to produce alkali metal ion end groups (CO_2^- K^+, Figure 1.19). Theoretical calculations by Mauritz et al.[60,61] show that *n*-alkane chains grown on NaCl(001) crystal are aligned along Na^+ ions in <110> direction. Likewise, it is hypothesized that the interaction between CH_2 groups of *n*-alkane and alkali metal ions as end groups of a SAM could align the *n*-alkane molecules in a lateral orientation.

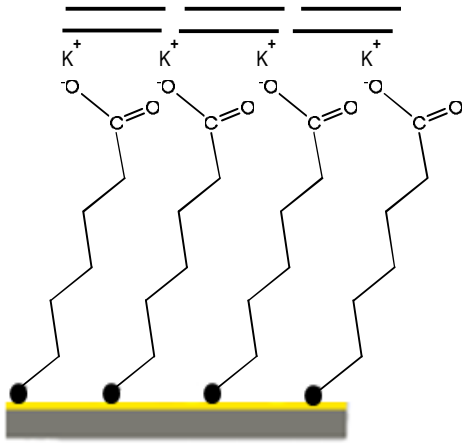

Figure 1.19 Schematic of a normally oriented SAM with end groups of alkali metal ion and hypothesized *n*-alkane orientation. The relative lengths of the SAM and *n*-alkane chain are not proportional.

b) In the second approach, an aromatic thiol SAM will be prepared on gold, where the SAM has tunable alignment. For this purpose, 4-mercaptopyridine is a candidate because of its ability to lie down or stand up on the surface of gold depending on the pH of the depositing solution. The strong π-CH_2 interaction between a laterally oriented aromatic SAM and an *n*-alkane chain is hypothesized to initiate the growth of *n*-alkane film in a lying down orientation.

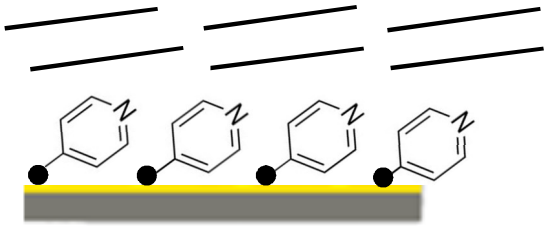

Figure 1.20 Schematic of a laterally oriented aromatic SAM and hypothesized *n*-alkane orientation. The relative lengths of the SAM and *n*-alkane chain are not proportional.

The initial approach to align *n*-alkane films by depositing on the SAMs with predefined orientations proved to be unsuccessful. These results are presented in Appendix. The nature of substrate was changed in the next approach to highly ordered substrates.

1.10.2 Kinetics and thermodynamics of *n*-alkane epitaxial growth on the highly ordered surfaces

After unsuccessful attempts to align *n*-alkane films on SAM coated surfaces, a highly ordered substrate was identified that could potentially align the *n*-alkane thin films more reliably. In this category, the epitaxial growth of *n*-alkane films on NaCl(001) has been studied previously by Fu.[57,62,63] Fu and Urquhart[63] observed that the molecular orientation and morphology of *n*-$C_{36}H_{74}$ (hexatriacontane, C36) thin film on NaCl(001) changes with the substrate temperature during deposition (Figure 1.21, images on the left). Corresponding polarization dependent NEXAFS spectra were acquired to investigate the molecular orientation in each morphology (Figure 1.21, spectra on the right). It was shown that C36 forms combined normal and lateral orientations at room temperature and a normal orientation at 40 °C substrate temperature during deposition. This study was performed on the longer *n*-alkane of *n*-$C_{60}H_{122}$ (hexacontane, C60) that resulted in a more complicated observation.[63]

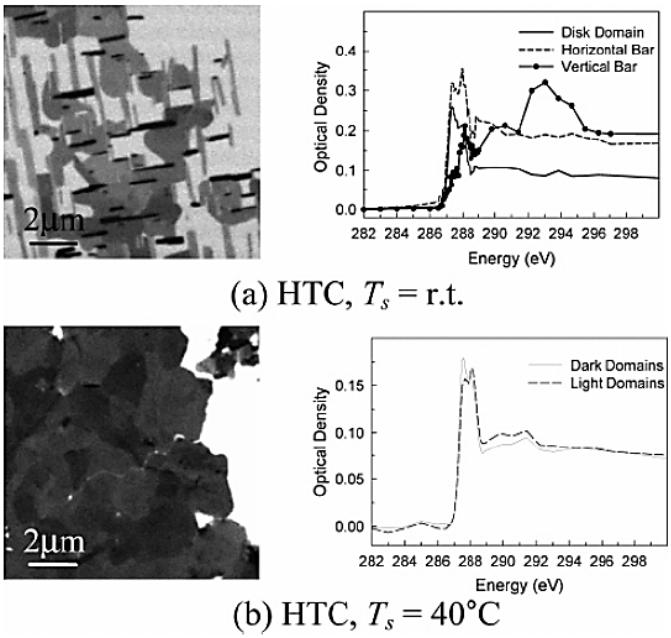

Figure 1.21 X-ray absorption images and the corresponding NEXAFS spectra of C36 film grown on NaCl(001) a.) at room temperature; b.) at substrate temperature of 40 °C. Figure reprinted from Ref. 63 with permission.

In Fu′s study, some questions were left unanswered and a complete morphology study was not performed. For example as shown in Figure 1.22 there is not a clear explanation for (1) the thickness difference of the light and dark domains of C60 thin film on NaCl(001) at the substrate temperatures of 60 °C, (2) the lack of epitaxial growth for C60 on NaCl(001) in the form of orthogonally oriented bar structure (as seen for C36 in Figure 1.21a), (3) the lack of a defined temperature for the formation of normally oriented C60 film on NaCl(001).

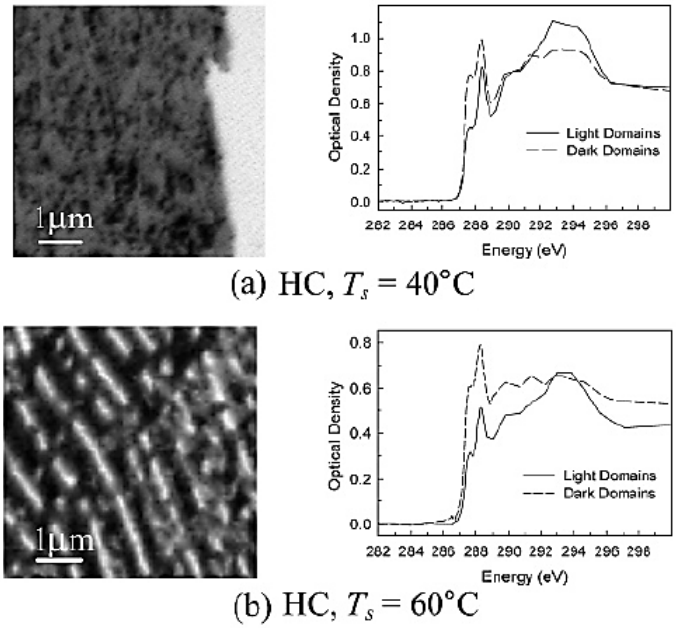

Figure 1.22 X-ray absorption images and the corresponding NEXAFS spectra of C60 film grown on NaCl(001) a.) at substrate temperature of 40 °C; b.) at substrate temperature of 60 °C. Figure modified from Ref. 63 with permission.

Therefore, this study was extended to build a basic understanding of epitaxial growth of *n*-alkane thin films on high symmetry substrates. An appropriate candidate for this approach is highly oriented pyrolytic graphite (HOPG(0001)). Calculations reveal that the primary interactions between *n*-alkane and graphite are van der Waals interaction and the contribution of the electrostatic interactions is very small, different than NaCl(001).[10] The alkane-alkane interactions are of van der Waals type but weaker than the alkane-graphite interactions.[10] For long *n*-alkane chains adsorbed on graphite, the ratio of two-dimensional crystallization energy to the adsorption energy is 2:5 to 3:5.[10] Therefore, the relatively strong π-CH_2 enthalpic interactions lead the *n*-alkane molecules adsorbed in the closed-packing assembly on HOPG(0001).[10] According to Groszek model,[64] the close match of graphite hexagon spacing with *n*-alkane CH_2-CH_2 bond length meets the requirement for the epitaxial growth and the transfer of 6-fold

symmetry pattern of HOPG(0001) to the *n*-alkane thin film. Epitaxially grown films of *n*-alkane on HOPG(0001) exhibit a 2D order in which the *n*-alkane carbon backbones orient along the direction that achieve the best 1D lattice matching with HOPG(0001) (along direction *a* in Figure 1.23). Order in the second dimension (along direction *b* in Figure 1.23) establishes more commensurism at the expense of disturbing intermolecular spacings.[11]

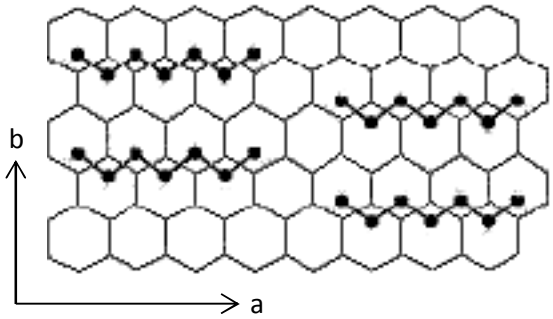

Figure 1.23 Schematic of geometrical match between the *n*-alkane chain and HOPG(0001) hexagons. Figure adapted from Figure 5 in Ref. 65.

Molecular mobility as a kinetic controlling factor plays different roles in epitaxial growth. Mobility enables the deposit molecules to transfer to the epitaxial sites of substrate that have minimum potential energy. However, high molecular mobility can overcome the deposit-substrate interactions and prevent epitaxial growth.

In summary, epitaxial growth of *n*-alkane thin films on HOPG(0001) will be investigated through three approaches, by monitoring the morphology and molecular orientation changes in different experimental condition. First, applying different substrate temperatures during growth will make it possible to tune the mobility of *n*-alkane molecules and the molecular diffusion barrier. Second, growing *n*-alkanes with different chain lengths at similar supercooling temperatures (*n*-alkane melting point – substrate temperature) will tune the *n*-alkane/graphite attractive forces. Longer *n*-alkane chains interact stronger with graphite due to larger number of interacting CH_2 groups. Third, varying the deposition rate at a constant substrate temperature

will provide a means to assess the effective molecular mobility. The results of first two approaches will be presented as a published manuscript in Chapter 3 and the results of third approach will be discussed in Chapter 4.

1.10.3 Indirect epitaxial growth of *n*-alkane on the modified highly ordered surfaces

The results obtained towards the objectives of §1.10.2 showed that the form of epitaxy varies with different growth conditions. It was found that an *n*-alkane film grows epitaxially in the form of uniform thickness film on HOPG(0001) at low substrate temperatures while the same *n*-alkane forms ordered separate bars at higher substrate temperatures. It was also shown that epitaxial growth of *n*-alkane on the highly ordered substrate is achievable under some specific growth condition. For example, it was seen that epitaxial growth cannot be obtained at high substrate temperatures and the substrate surface treatment is required to maintain epitaxy. The goals of (1) controlling the form of epitaxy, and (2) maintaining the epitaxial growth at the extended substrate temperature range were sought by developing the concept of indirect epitaxy. It was hypothesized that attractive forces of the highly ordered substrate can act through the thin interlayer film in indirect epitaxy. Therefore, *n*-alkane films were grown on the treated highly ordered substrates as follows.

a) Surface treatment is intended in cases when low substrate temperature does not provide adequate molecular mobility. The surface of a highly ordered substrate can be modified to provide a higher diffusion rate for deposit molecules, by treating the surface with an organic compound that is hypothesized to play the role of lubricant. Liquid crystals will be explored as "molecular lubricants" to change the form of epitaxy to the ordered bars in conditions where molecular mobility might otherwise be inadequate. The results of modifying the surface of a highly ordered substrate with a liquid crystal thin film led us to modify the same substrate with a

thin film of a short *n*-alkane alternatively. Results of Chapter 3 show how short and long *n*-alkanes can form different morphologies as a function of substrate temperature and suggest how a short *n*-alkane can act as a template for the longer *n*-alkane. The results of this section are presented in Chapter 4.

b) Another type of indirect epitaxy will be applied for the cases where high substrate temperature disturbs the transfer of the substrate ordered pattern to deposit. Increasing the deposit-substrate interaction or quenching the deposition enthalpy of the arriving molecules are potential solutions. Since the major attractive forces participating in the epitaxial growth of *n*-alkane films are van der Waals interactions, increasing the polarizability of the substrate is hypothesized to result in stronger deposit-substrate interactions. Metals have higher density of valence electrons and are more polarizable than other materials. A thin film of a metal can potentially improve the attractive forces of a high symmetry substrate provided that the metal coating transfers the primitive forces of substrate. Additionally, metals have high thermal conductivities that can affect the relative mobility of condensing molecules by diffusing the deposition enthalpy. For this approach, indirect epitaxy of *n*-alkanes across different intervening metals film will be investigated. The results and discussion are presented in Chapters 5 and 6.

1.11 Summary

In this section, the materials that will be covered in the thesis are summarized as described in below:

In Chapter 2, the samples of *n*-alkane and the substrates that are studied for the main project (organic epitaxy) are described along with the characterization techniques used. Chapter 3 is presented as the published manuscript and is related to the objectives introduced in §1.10.2. In this chapter, *n*-alkane chain length and the substrate temperature are studied as thermodynamic

and kinetic determining factors in the process of epitaxial growth. The effect of deposition rate on the *n*-alkane epitaxial growth is studied in Chapter 4. Chapter 5 describes the results and discussion of indirect epitaxy of *n*-alkane films through organic and metallic thin films. In this chapter the indirect epitaxy of *n*-alkane films is shown as a complementary approach to change the substrate surface properties and induce an altered morphology on the treated surfaces of highly ordered substrates. A specific study on the indirect epitaxy of *n*-alkanes through a gold thin film is presented in Chapter 6 in the form of a submitted manuscript. The results of the study related to the side project (strain in inorganic system) are presented in Chapter 7, in which the strain of SiGe thin films is measured by linear dichroism in NEXAFS spectroscopy. Chapter 8 presents a summary of results and discussions obtained for the entire thesis. Chapter 9 provides a view to the future work that can be pursued to complete the studies presented in this thesis. Chapter 10 summarises the unsuccessful results for the objectives and approaches described in §1.10.1 in which SAMs were used as substrates for epitaxial growth of *n*-alkane films.

CHAPTER 2: EXPERIMENTAL

2.1 *n*-Alkane candidates

The *n*-alkanes used in this project are octacosane (*n*-$C_{28}H_{58}$, 99%), hexatriacontane (*n*-$C_{36}H_{74}$, 98%), tetratetracontane (*n*-$C_{44}H_{90}$, 99%), pentacontane (*n*-$C_{50}H_{102}$, 97%) and hexacontane (*n*-$C_{60}H_{122}$, 98%), purchased from Sigma-Aldrich and used without purification. The shorthand C28, C36, C44, C50, and C60 will be used in this thesis to refer to these *n*-alkanes respectively. These are chosen based on their melting point and suitability to be deposited by the PVD.

2.2 Preparation of substrates and *n*-alkane samples

As mentioned in Chapter 1, chemically modified SAMs and naturally ordered materials with and without surface treatment will be considered as substrates to grow *n*-alkane thin films epitaxially. SAMs of 11-mercaptoundecanoic acid (MUA, 99% Aldrich) and 4-mercaptopyridine (4MP) on Au(111) will be treated chemically as follows in §2.2.1.

The naturally ordered substrates are HOPG and NaCl. HOPG will be modified by organic and metallic coatings, while NaCl will be modified with a gold thin film. These substrates will be transferred into the vacuum chamber and used to grow epitaxial *n*-alkane thin films at defined growth conditions such as controlled evaporation rate and substrate temperature.

2.2.1 Preparation of SAM substrates on gold

a) Preparation and treatment of 11-Mercaptoundecanoic acid SAM on Au(111)

Based on the literature it was assumed that incubating the Au(111) substrate in a thiol solution for 24 hour forms a normally oriented thiol monolayer in which the main backbone is

approximately perpendicular to the surface.[66] The SAM of 11-mercaptoundecanoic acid is prepared by incubating a gold coated Si wafer in 1 mM 11-mercaptoundecanoic acid solution in ethanol. Figure 2.1 presents the schematic diagram of the SAM sample preparation.

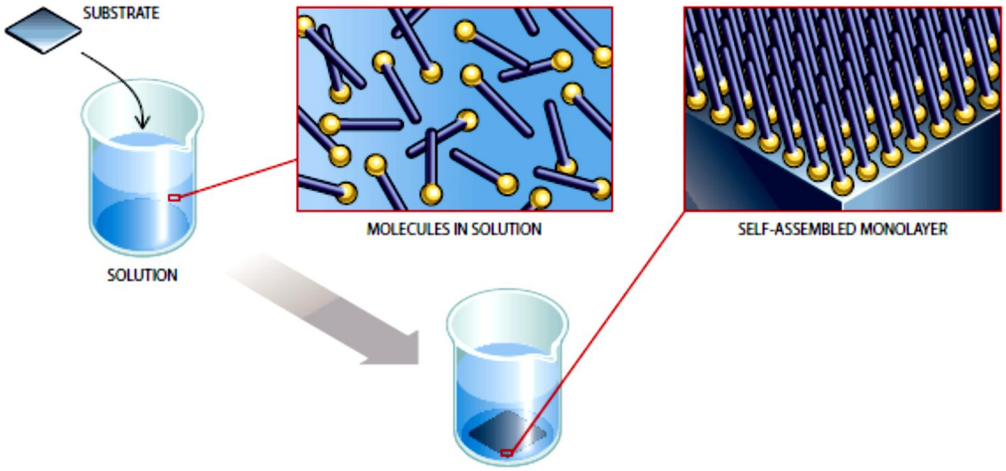

Figure 2.1 Schematic of SAM preparation. Figure reprinted from Ref. 67 with permission.

Two samples of 11-mercaptoundecanoic acid on gold were prepared with different solvents to prepare the end groups with COOH and COO^-K^+ functional groups. This was to study the effect of end group interaction with *n*-alkane CH_2 units. Rosendahl and Burgess[66] reported that by immersing a gold substrate in SAM solution a mixture of hydrogen bonded COOH end group, non-hydrogen bonded COOH end group, and deprotonated carboxyl end group is formed. In order to have non-hydrogen bonded COOH end groups, 5% acetic acid 95% ethanol was used as a solvent. If the SAM with all COOH end group is rinsed with KOH solution (pH = 12), a SAM with COO^-K^+ end group is formed as shown in Figure 2.2.[68] Samples were rinsed with Millipore water at the end.

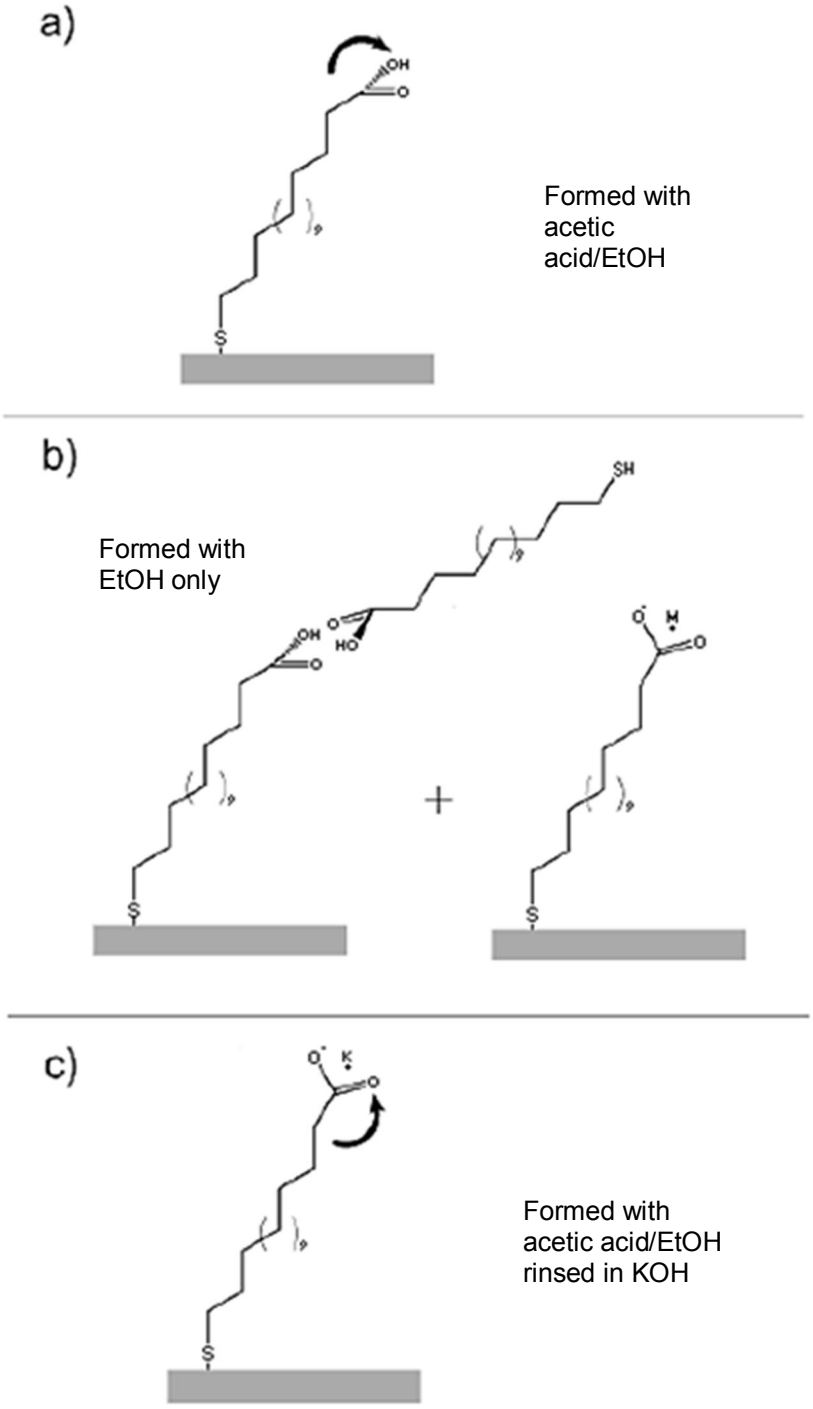

Figure 2.2 Schematic of orientation of a mercapto alkanoic acid on gold. a.) EtOH/AcOH mixture solvent; b.) EtOH solvent; c.) EtOH/AcOH mixture solvent; rinsed next with KOH solution. Figure reprinted from Ref. 68 with permission.

b) Preparation of 4-mercaptopyridine on Au(111)

Another SAM to be studied in this project is 4-mercaptopyridine which has a potential of being oriented parallel or normal to the surface, when grown from solutions with different pHs. The strong interaction between the π electrons of aromatic ring of 4-mercaptopyridine and an *n*-alkane chain makes it possible to align the *n*-alkane film laterally on a lying down aromatic SAM. The SAMs of 4-mercaptopyridine on gold were made by immersing a gold coated Si wafer in 0.1 mM aqueous solution of 4-mercaptopyridine in 0.1 M $NaClO_4$ with the pHs of 1, 5 and 10 for 5 minutes. The pH of 4-mercaptopyridine solution was adjusted to 10 and 1 by using 0.1 M aqueous solutions of KOH and $HClO_4$. All samples were rinsed with Millipore water at the end.

2.2.2 Preparation of naturally ordered substrates

The substrate HOPG (10 x 10 x 2 mm, ZYH grade, mosaic angle is 3.5° +/- 1.5°, NT-MDT) was prepared by cleaving the topmost layer with scotch tape. The substrate NaCl (International Crystal Labs) was air-cleaved by a razor blade to expose a fresh surface. For X-ray spectroscopy and microscopy experiments, it is necessary to grow *n*-alkane thin films onto self-supported X-ray transparent graphene or thin graphite substrates. Graphene, prepared by chemical vapour deposition on Ni (Graphene Supermarket) was transferred onto a TEM grid or a Si_3N_4 window after etching the Ni layer with 12 M HCl(aq) and picking up floating graphene layer. Self-supported thin graphite films were prepared from ZYH grade graphite flakes. Thin graphite flakes attached to scotch tape were separated onto a SiO_2 wafer surface (300 nm SiO_2 on silicon) and then were transferred onto a holey-carbon coated TEM grid with a drop of isopropyl alcohol. These TEM grids were separated from wafer by a drop of 30% KOH solution and rinsed with Millipore water.[69]

2.2.3 Preparation of metal coated ordered substrates

Thin metal films of Au (wire), Cr (Chrome plated tungsten rod), Bi (powder), Pb (granule) and Se (powder) were vapour deposited on the substrates of HOPG(0001) and NaCl(001). A few milligram of each metal was placed in a tungsten boat and was evaporated in the vacuum chamber at the pressure of 10^{-7} torr with a deposition rate of 0.2 Å/s. The vacuum evaporator is described in §2.3.

2.2.4 Preparation of *n*-alkane thin films

The thin films of *n*-alkanes were prepared on different substrates by physical vapour deposition method in the vacuum chamber at a pressure of 10^{-7} torr. In the vacuum chamber *n*-alkane is evaporated and deposited on the substrate by tuning the power of a resistive heater so that the evaporation rate is kept constant in the range of 0.3 - 1 Å/s. As the rate of evaporation is decreased it should get closer to the equilibrium growth condition, so *n*-alkanes were evaporated at the minimum rate that was achievable with the present setup.

2.3 Vacuum chamber

The vacuum chamber (DataComp Scientific) (Figure 2.3) is equipped with a diffusion pump (base vacuum of 10^{-7} torr), tunable resistive heater (to evaporate solid samples from a tungsten boat), a quartz crystal microbalance (to measure the rate of evaporation and thickness of samples), and a substrate holder. The substrate holder includes a Peltier thermoelectric module (TE Technology) mounted on a water cooler. The temperature of the substrate is measured by a thermistor which is connected to the Peltier heater surface.

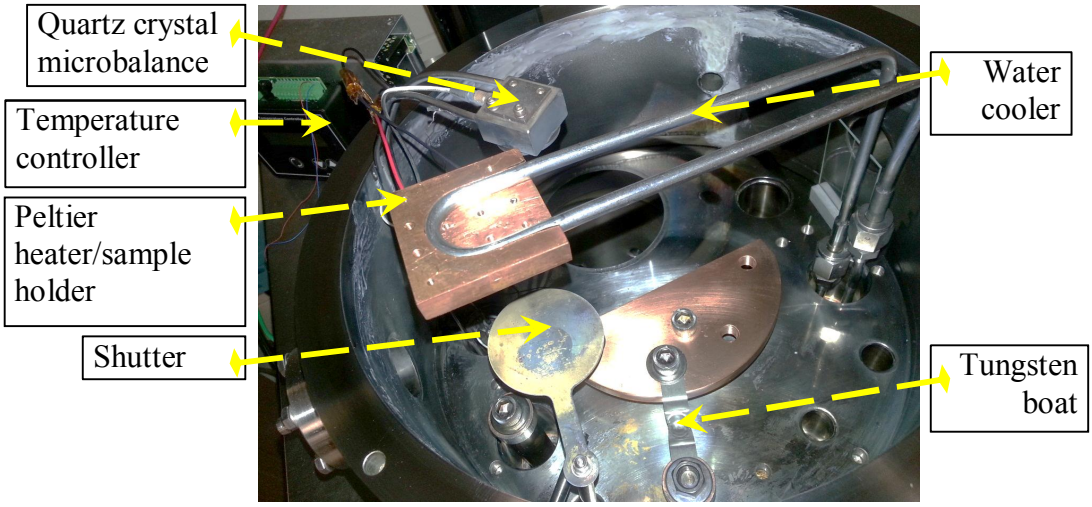

Figure 2.3 Top view from inside of vacuum evaporator.

2.4 Development and repair of vacuum evaporator

2.4.1 Development of a variable temperature sample holder

In previous studies, the substrate temperature was controlled by using a 12V quartz-halogen light bulb mounted to the back side of sample holder. As mentioned in §1.10, the objective of this project requires keeping the substrate at the predefined and controlled temperature. To heat up the substrate in small intervals with high accuracy, a Peltier heater controlled by a temperature controller was used (Figure 2.4). The Peltier heater operates by the thermoelectric effect. When current flows through the heater, heat is transferred from one side to the other so that one side gets hotter and the other side gets cooler. If the cold side is not attached to a heat sink it will get hot due to the very small distance between the plates and consequently the temperature of the whole device will rise in an uncontrolled way. To use a Peltier element as a heater, the temperature of the cold side should be kept low. Therefore, a water cooler is

connected by a stainless steel tube to surround the copper sample holder to cool down the cold side of the Peltier module inside the vacuum chamber as shown in Figure 2.3.

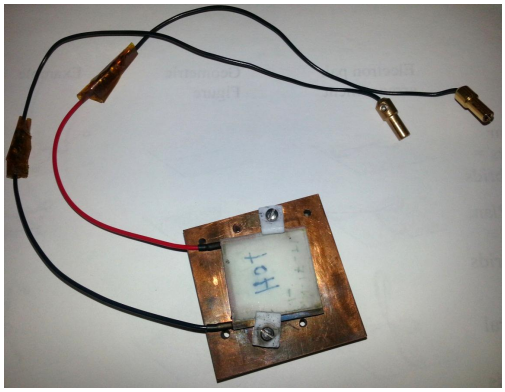

Figure 2.4 Image of Peltier heater attached to the copper holder. The holder is cooled by the stainless steel tube water cooler as shown in Figure 2.3.

2.4.2 Identification of reproducibility and contamination artefacts in the evaporator

One of the big challenges of the sample preparation in the vacuum chamber was the lack of reproducibility of the prepared sample morphology. It was likely assumed that the lack of reproducibility came from vacuum contamination, which was usually solved by cleaning the bell jar walls with ethanol, and sonicating all removable parts with soap and ethanol. In one special case, contamination was not removed by this normal cleaning procedure. This was detected by monitoring the morphology of C40 samples grown on HOPG at room temperature, as shown in Figure 2.5. The image on the left (Figure 2.5a) is the sample before contamination in which very narrow bars can be distinguished by the optical microscope image, but the one on the right (Figure 2.5b) is the sample after contamination that shows a disordered film with no visible bar structure.

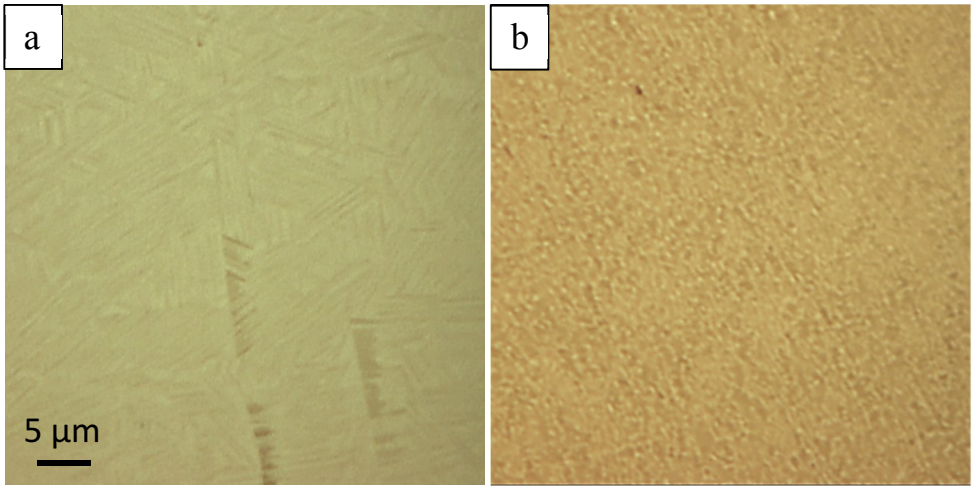

Figure 2.5 Optical microscopy images of a.) 10 nm C40 deposited on HOPG(0001) before contamination; b.) 50 nm C40 deposited on HOPG(0001) after contamination. Both of depositions were performed at room temperature.

Therefore, a more effective cleaning process such as plasma cleaning was required to remove the hydrocarbons inside the chamber. To this end a mixture of N_2/O_2 gas (air, pressure = 1.7×10^{-1} torr) was let to the chamber and a DC voltage (I = 10 mA, V= 2.5 kV) was applied to a SHV feed-through for about a minute. This produced plasma in the vacuum chamber. In the second step, the chamber was baked at 100 °C for 24 hours and then was wiped with EtOH at the end. The C40 samples that were prepared afterwards remained distorted and no significant improvement was achieved with this harsher cleaning method.

After failing to reproduce the morphology of C40 with the fine bar structure despite all cleaning processes it was hypothesized that the source of contamination could be within the diffusion pump oil. Therefore, the old Santovac pump oil was removed and the diffusion pump was dismantled completely and all the interior parts of the diffusion pump were washed with soap and ethanol. New Santovac pump oil was charged, and a new C40 sample was prepared to assess the results. Interestingly the bar structure could be seen again and the chamber was

considered free from contamination. Since this contamination occurred after evaporating a few C28 samples in the vacuum chamber it was concluded that, the short *n*-alkane can get trapped inside the Santovac pump oil and can get released gradually into the vacuum chamber and change the morphology of longer *n*-alkanes. It is hypothesized that a short *n*-alkane with higher molecular mobility acts like a plasticizer and causes an interruption in the crystallization process of longer *n*-alkanes.

This problem repeated again when liquid crystal coated substrates were examined in the vacuum chamber. In the related study, it was assumed that the liquid crystal coating would be replaced by *n*-alkane molecules that were deposited in the vacuum chamber. It was concluded that liquid crystal acted similar to the short *n*-alkane because it caused a similar morphology variation. This problem was solved in a similar way by another replacement of the Santovac pump oil. Therefore, no more samples were prepared with the *n*-alkanes shorter than C36, and liquid crystal coated substrates were not used in the vacuum chamber after this point.

2.5 Characterization of *n*-alkane thin films

2.5.1 Optical microscopy

Optical microscope visualizes surface structures down to ~ 0.2 μm scale and can examine the surface morphology. In this project, a standard optical reflection microscope (Nikon Eclipse ME600, with a Q-Imaging CCD camera) is used as shown in a schematic view in Figure 2.6. The sample is illuminated through the objective lens by a filament lamp. The objective lens forms a real inverted image that is magnified more by the eyepiece. The eyepiece forms a virtual image of the object. The total magnification is the product of the eyepiece and objective magnifications. The bright field imaging that is used in this project is a commonly used technique in which the

entire sample is illuminated and the structures appear as a dark image against a brightly lit background.[70]

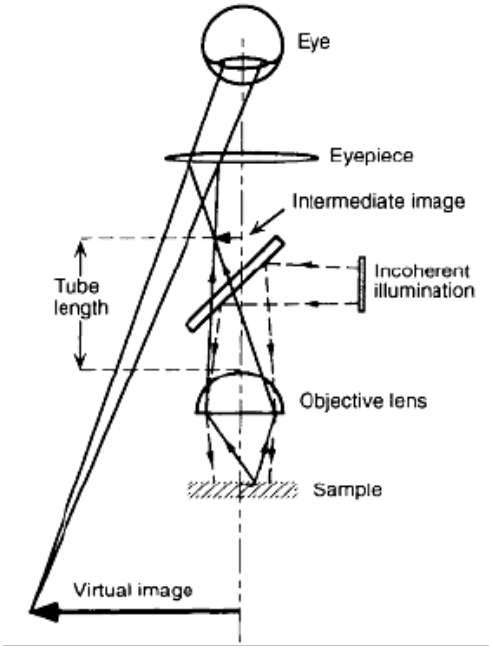

Figure 2.6 Schematic of a standard optical reflection microscope. Figure reprinted from Ref. 70 with permission.

Polarized optical microscopy (POM)

In a polarized optical microscope, as shown in Figure 2.7, light is polarized by a polarizer before hitting the sample. Linearly polarized light has the electric field vector of the electromagnetic radiation oriented in one direction. Polarized light in an optical microscope enhances the contrast of anisotropic materials and facilitates the study of optical crystallographic properties of a birefringent material. Birefringence relies upon the refractive indexes of an optically anisotropic material. Polarized light is split into two orthogonally polarized rays by the birefringent sample. The split rays travel with different velocities because of different refractive index of sample in different directions and experience a phase difference after exiting the

sample. The rays with a phase difference reunite after passing through the analyzer that is aligned at a right angle to the polarizer.

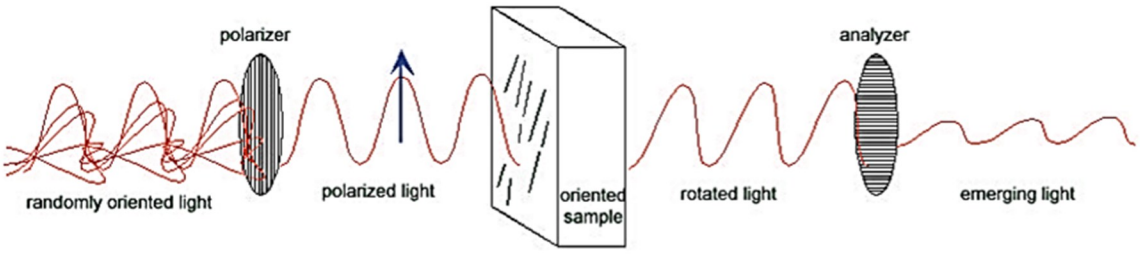

Figure 2.7 Randomly oriented light is polarized as it passes through the polarizer. The oriented sample rotates the polarized light by some angle, and finally this rotated light enters the analyzer, oriented 90° to first polarizer. Only the portion of rotated light that is parallel to the analyzer is transmitted, providing an image contrast driven by sample birefringence. Figure reprinted from Ref. 71 with permission.

The splitting of the polarized light inside the birefringent sample and the consequent phase difference between the split rays can be simplified such that the polarized light is rotated by the birefringent sample. The intensity of light passing through different parts of a polycrystalline material depends on the degree of rotation of the polarized light in each crystal as shown in Figure 2.8 and is calculated by Equation (2.1):

$$I = I_o \, sin^2 (2\theta) sin^2 (\frac{\delta}{2}) \tag{2.1}$$

In Equation (2.1), I_o is the intensity of light passing through the polarizer, θ is the angle between the light and the direction of sample having a larger refractive index (n_1), and δ is retardation that is calculated by Equation (2.2):

$$\delta = \frac{2\pi \, \Delta n}{\lambda} \tag{2.2}$$

δ is a function of birefringence ($\Delta n = n_1$-n_2, refractive index differences in a crystal) and the wavelength of the light (λ).[71]

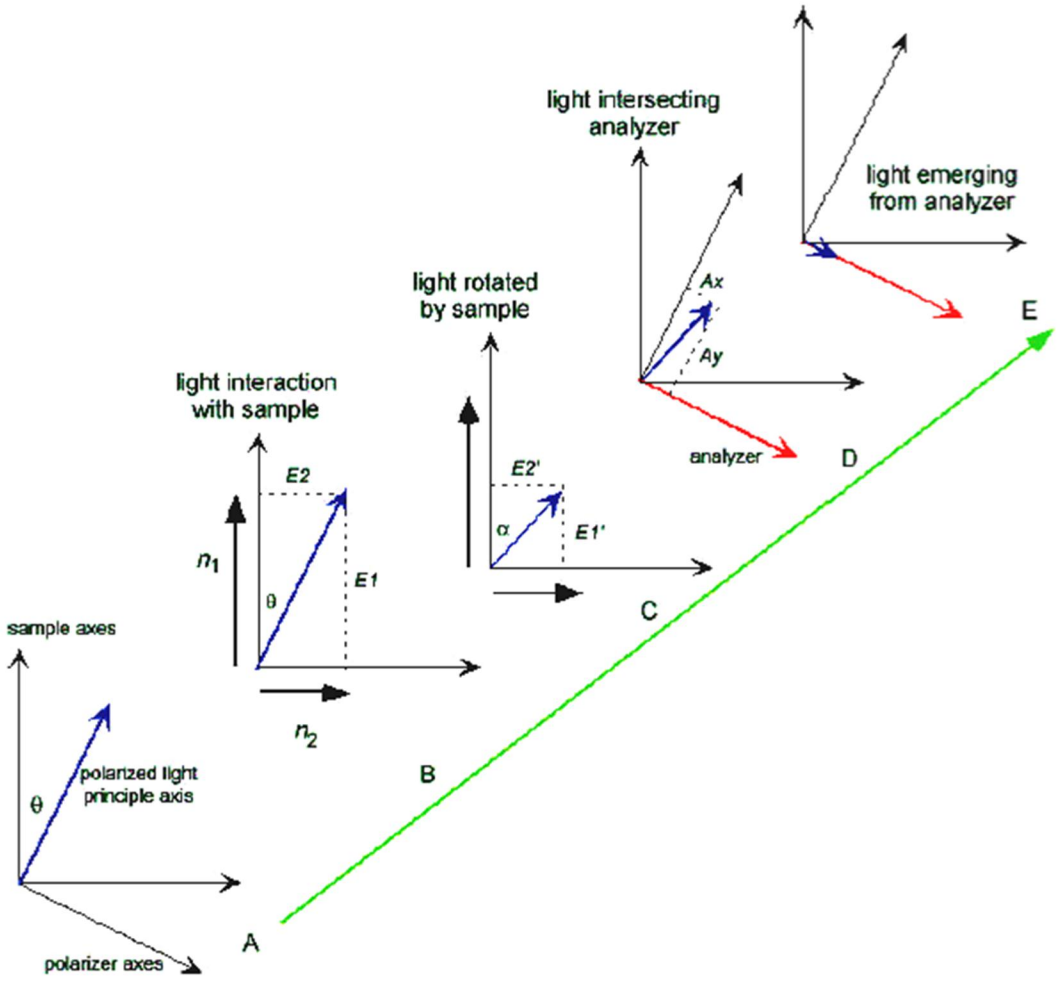

Figure 2.8 The polarizer is oriented at angle θ relative to the principle axes of sample with the refractive indices of n_1 and n_2. The light that has passed the polarizer is decoupled into two orthogonal vectors E_1 and E_2 and enters the sample which retards the E_1 and E_2 vectors differently based on the corresponding refractive indices and makes new vectors of E_1' and E_2'. Coupling E_1' and E_2' forms the rotated light with the new angle of α which can be decoupled to A_x and A_y vectors from which just the one parallel to the analyzer passes through. Figure reprinted from Ref. 71 with permission.

2.5.2 NEXAFS spectroscopy and microscopy

To identify the orientation of the alkane chains deposited on top of different substrates, the carbon 1s NEXAFS spectra were acquired using a Scanning transmission X-ray microscope (STXM) at soft X-ray spectromicroscopy (SM) beamline at the Canadian Light Source and also at beamline 532 at the Advanced Light Source.

Scanning transmission X-ray microscopy (STXM)

STXM images are produced based on the NEXAFS contrast and can be used to prepare a surface orientational map of an organic film with spatial resolution better than 35 nm. The advantage of STXM over other microscopy techniques is its ability to provide combined spectroscopy and microscopy by imaging at a specific energy and acquiring NEXAFS spectra at the desired region. STXM transmission images are recorded by raster scanning samples through an X-ray beam focused by a Fresnel zone plate. The zone plate is a diffractive lens that moves forward and backward to maintain focus at different photon energies because the focal length changes with photon energy. As shown in Figure 2.9, the sample is illuminated with the first order focused X-ray spot of a Fresnel zone plate. Varying the energy of incident beam energy allows visualization of micro-scale structures by adjusting the absorption contrast.

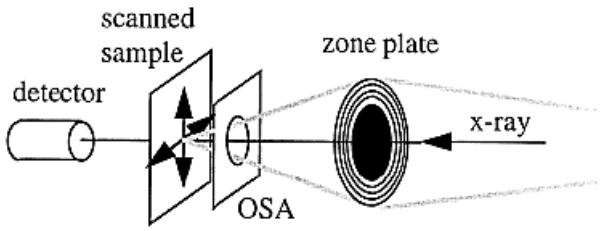

Figure 2.9 Schematic diagram of STXM microscope. Figure reprinted from Ref. 72 with permission.

The unfocused zero order radiation is blocked by the zone plate central stop, and the order sort aperture, OSA, blocks higher order diffraction (Figure 2.10). The sample moves on a scanning x/y stage and the transmitted intensity is recorded to form an absorption image.[72]

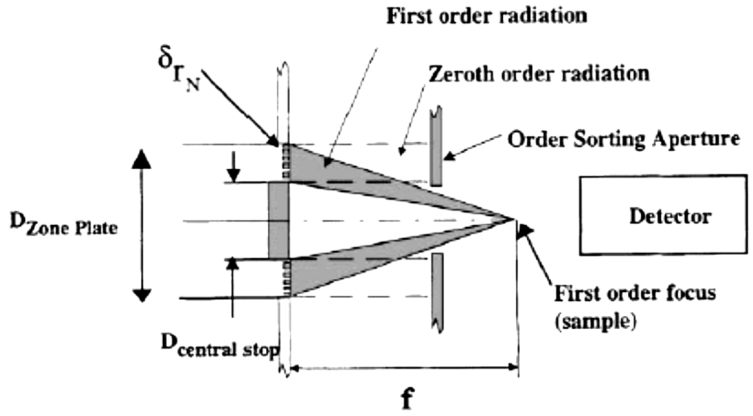

Figure 2.10 Role of the OSA and the central stop of the zone plate in blocking higher order foci of the zone plate (OSA) and undiffracted (zero order) light (central stop). Figure reprinted from Ref. 73 with permission.

X-ray polarization

An electromagnetic wave includes orthogonal electric and magnetic fields perpendicular to the wave motion. The direction of electric field changes with time and can make circularly or elliptically polarized wave, but in some cases the electric field direction is fixed to make a linearly polarized wave. As shown in Figure 2.11 the electromagnetic wave polarization angle (φ) can vary between 0° (green line) and 90° (blue line).

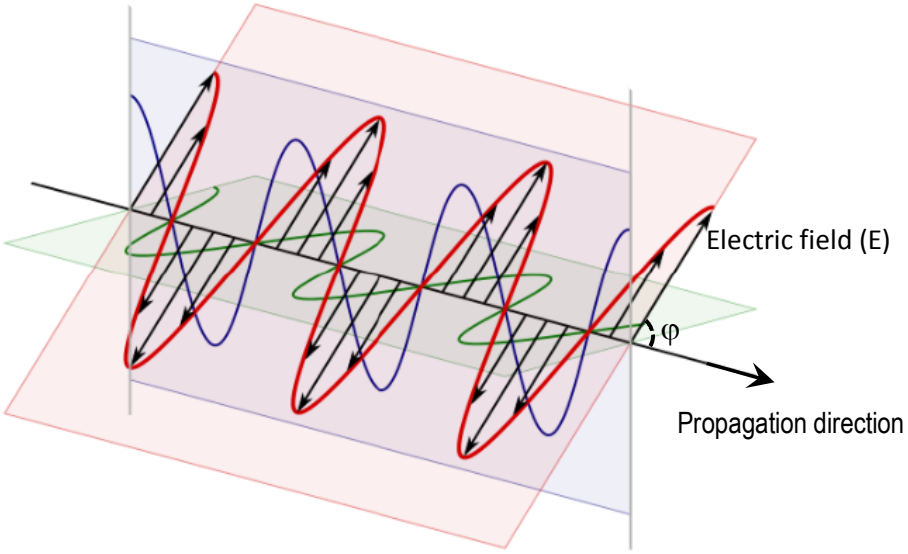

Figure 2.11 Schematic of electromagnetic wave polarized linearly in different angles. Reprinted from Wikipedia Commons under a creative commons licence.

The X-rays polarization is controlled by an elliptically polarized undulator (EPU) to the degree of 100% (+0 / -0.1%) at the Canadian Light Source.[57] EPU is a X-ray source that is made up of four rows of parallel periodic permanent magnets and the electron beam passes through these magnets as shown in Figure 2.12. Two rows of magnets are fixed and the other two are movable along the electron beam path. Changing the relative position of the magnet rows can provide a radiation with continuous variation of polarizations such as arbitrary inclined linear polarization, circular polarization and elliptical polarization.

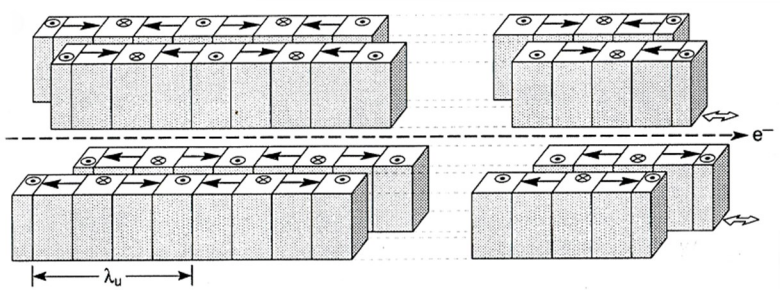

Figure 2.12 Schematic structure of four magnets in EPU for generating variably polarized radiation. Figure reprinted from Ref. 74 with permission.

X-ray linear dichroism in C 1s NEXAFS spectroscopy

NEXAFS spectroscopy includes the excitation and ionization of core electrons by X-ray absorption. X-ray linear dichroism in NEXAFS spectra works based on the sensitivity of this technique to the symmetry of final state unoccupied orbitals. The intensity of absorbed X-ray is related to the degree of alignment of electric field vector of X-ray and transition dipole moment from an atomic core level to the unoccupied orbitals (see Equation 1.6).

For *n*-alkane oriented films, the polarized unoccupied molecular orbitals associated with the C-C and C-H transition dipole moments (TDM) can be used for angular dependent carbon 1s NEXAFS measurements. As shown in Figure 2.13, the TDM for transition of C 1s $\rightarrow \sigma^*_{C\text{-}C}$ in an *n*-alkane chain is oriented along the carbon backbone and it has the greatest intensity when *E* is parallel to the *n*-alkane chain. But the transition of C 1s $\rightarrow \sigma^*_{C\text{-}H}$ has the highest intensity when *E* is perpendicular to the *n*-alkane chain oriented normally or laterally.[57]

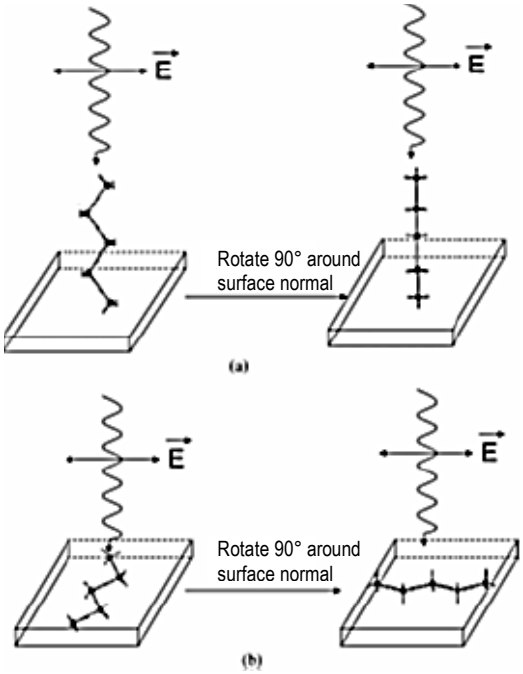

Figure 2.13 Schematic of relative alignment of *n*-alkane to the electric field vector of X-ray, a.) *n*-alkane oriented normal to the surface; b.) *n*-alkane oriented laterally. Figure reprinted from Ref. 57 with permission.

STXM image contrast follows from Equation (2.3),[53]

$$I = I_o \exp(-\mu.\rho.t) \qquad (2.3)$$

where I is the intensity of transmitted X-ray, I_o is the intensity of incident X-ray flux, μ is the mass absorption coefficient and is a measure of atomic photoionization cross-section, t and ρ are the thickness and density of sample. NEXAFS spectra are reported on optical density (OD) scale as shown in Equation (2.4),[53]

$$OD = -\ln(I/I_o) = \mu.\rho.t \qquad (2.4)$$

Radiation damage

In NEXAFS spectroscopy and microscopy radiation damage is shown as changes to chemical bonds or mass loss. In X-ray linear dichroism microscopy (XLDM) of oriented samples, the changes in molecular orientation is seen at a much lower radiation dose than is needed for chemical damages.[53] To avoid faulty results in X-ray studies two different approaches were used. First, the X-ray images and spectra were repeated in a few different spots on the sample to get reproducible results with minimal radiation dose. Specifically, the relative intensities of C 1s $\rightarrow \sigma^*_{C\text{-}C}$ and C 1s $\rightarrow \sigma^*_{C\text{-}H}$ transitions were monitored to be reproducible in the repetition acquisitions as an indicator of linear dichroism. Second, the X-ray spot was defocused to reduce the radiation dose and fresh areas were scanned each time.

CHAPTER 3: EFFECT OF SUBSTRATE TEMPERATURE ON THE EPITAXIAL GROWTH OF *N*-ALKANE ON GRAPHITE

This section analyzes the effect of substrate temperature on the epitaxial growth of oriented *n*-alkane thin films on graphite. The results of this section are related to the objectives explained in §1.10.2 in which the highly ordered substrate of graphite was chosen to study the determining parameters for the orientation and epitaxial growth of *n*-alkane thin films. The results show the common trend of morphology variation with supercooling temperature for four *n*-alkanes with different chain lengths. The corresponding polarization dependent NEXAFS spectra determine the *n*-alkane molecular orientation for each film morphology. NEXAFS spectra support the hypothesis of layer-by-layer growth mode at low substrate temperatures and layer-plus-island mode at high substrate temperatures. The layer-by-layer growth mode has not been reported for the epitaxially grown *n*-alkane film on graphite by other researchers. This work has been published in *Langmuir*, 2012, 28, 12493-12501 and is presented here in the published form.

The author of this thesis investigated the conception of *n*-alkane epitaxial growth on graphite by physical vapour deposition with varied substrate temperature, developed the sample preparation methods, prepared the samples, and acquired the optical microscope images and NEXAFS spectra. Dr. S. G. Urquhart provided guidance throughout the experiments and collaborated closely in editing this manuscript. The author of this thesis obtained Dr. Urquhart's agreement to present the work in this thesis.

The references of this chapter are presented in the form of *(Chapter No.).(Ref. No.)*.

The Effect of Substrate Temperature on the Epitaxial Growth of Oriented *n*-Alkane Thin Films on Graphite

Mitra Masnadi and Stephen G. Urquhart[1]

Department of Chemistry, University of Saskatchewan, Saskatoon, SK, Canada S7N 5C9

Abstract

A complex orientational morphology is observed when *n*-alkane thin films are vapour deposited on highly oriented pyrolytic graphite surfaces. Substrate temperature can be used to tune the orientation and morphology of *n*-alkane thin films. The molecular orientation changes from lateral to normal to the surface when the substrate temperature is raised sufficiently. Under specific substrate temperature conditions, the *n*-alkane molecules are aligned in the plane of the sample surface, in directions reflecting the six-fold symmetry of the graphite substrate. A series of different morphologies, from uniform thin films to oriented bars, are observed as a function of chain length and substrate temperature. The systematic evolution of these oriented morphologies is mapped as a function of deposition conditions, and the kinetic and thermodynamic factors that govern the formation of different in-plane and normal domains are considered.

1. Introduction

Organic thin films, prepared by vacuum or solution deposition, can display a complex orientational nanostructure. The thermodynamic and kinetic variables that drive the formation of these orientated nanostructures can potentially be used to define and pattern the formation of oriented nanostructures. This could lead to the development of functional nano-

1 Corresponding Author, email: stephen.urquhart@usask.ca

materials that rely on molecular order and orientation at the nanoscale, such as organic electronic devices, meta-materials, waveguides and liquid crystal-based devices.

In this paper, we study the morphology of vacuum deposited *n*-alkane thin films on the surface of highly oriented pyrolytic graphite (HOPG(0001)) as a function of the *n*-alkane chain length and the substrate temperature during deposition. Fundamental knowledge developed in the study of model materials, such as *n*-alkane thin films, can be extended to complex organic molecules such as polymers, lipids, oils and fats and a variety of organic coatings that contain hydrocarbon chains as a part of their main chain. Graphite is selected as its high symmetry can lead to the formation of oriented overlayers through epitaxial growth.[3.1] The morphology and orientation of thin films of *n*-alkane molecules, deposited on HOPG(0001) by physical vapour deposition, are characterized by optical and X-ray microscopy.[3.2]

When *n*-alkanes are deposited on surfaces, in-plane and normal-oriented structures are observed.[3.3-3.5] In-plane oriented structures (also known as lateral structures) have the long-axis of the *n*-alkane molecule aligned in the surface plane, while normal-oriented structures have the long-axis of the *n*-alkane molecule aligned, in an all-*trans* configuration, normal to the sample surface. The molecular orientation depends on the deposition conditions (substrate temperature and evaporation rate) as well as the substrate identity. For example, an X-ray diffraction study (*n*-$C_{23}H_{48}$ to *n*-$C_{27}H_{56}$, deposited on glass and polyimide substrates) showed that a mix of lateral and normal orientations dominated at lower substrate temperatures and faster evaporation rates, while films with only normal orientation were present at higher substrate temperatures and slower evaporation rates.[3.3] When an *n*-alkane film consisting of coexisting normal and laterally oriented *n*-alkane domains (*n*-$C_{27}H_{56}$ and *n*-$C_{33}H_{68}$, deposited on glass) was annealed to a temperature just below the melting point, a normally oriented thin film was formed through an

irreversible process.[3.6] This observation suggests that normal orientation of the *n*-alkane chains is the thermodynamically most stable form. The observation of an in-plane *n*-alkane orientation at faster evaporation rates suggests a kinetic barrier to the formation of the normal oriented equilibrium state.[3.3]

Some hints about the thermodynamics of film growth can be elucidated by considering the magnitude of intermolecular and molecule-substrate interactions in a multilayer film. A sufficiently thick film can be considered as a bulk crystal with a single face in contact with the substrate. The intermolecular interactions in the bulk of the crystal will not depend on the crystal orientation, but the interaction of the first monolayer with the substrate will depend on this molecular orientation. Normal-oriented *n*-alkanes will experience a solid-surface interaction via the methyl ($-CH_3$) group, while laterally oriented *n*-alkanes experience a solid-surface interaction via the entire length of the *n*-alkane molecule. When the molecule-substrate interaction is strong it will govern the lateral orientation of the first monolayer and the subsequent layers; otherwise entropic effects will be responsible for the thermodynamic stability of the normal oriented film. The relative significance of the molecule-substrate interactions can be tuned by varying the substrate temperature, which can allow one to control the orientation of the film during the vapour deposition.

The presence of laterally oriented *n*-alkane chains is understood to represent a kinetically trapped structure.[3.5] Kubono et al.[3.7] developed a kinetic model for thin film growth, where the rates of deposition, re-evaporation, surface migration, reorientation, and capture into laterally and normally oriented clusters were considered numerically. The observed molecular orientation is found to depend on the variation in re-evaporation rate and surface adsorption with molecular orientation. At lower temperature, the density of crystal nuclei determines the growth rate,

leading to a preponderance of laterally oriented crystals. At higher temperature, laterally oriented domains will evaporate faster, leading to a preponderance of normally oriented clusters.[3.4] This model does not account for the effect of molecular flux, which Matsuzaki et al.[3.8] consider within a "supersaturation" measure that combines evaporation rate and substrate temperature. In a subsequent model, Kubono et al. used classical nucleation theory[3.4] to consider the nucleation of oriented domains, followed by their growth. This growth depends on $\Delta\mu$, the critical chemical potential change for nucleation. Below this calculated $\Delta\mu$ value, normal oriented nucleation occurs; above this value, lateral oriented nucleation occurs. Within the vicinity of the critical $\Delta\mu$, both orientations coexist. The model also shows that lateral orientation becomes preferable as the molecule-substrate interaction increases,[3.4] providing a rationalization for the observed in-plane molecular orientation, particularly at lower substrate temperatures.

The symmetry of the surface will also affect the orientation of laterally oriented domains. When *n*-alkanes are deposited onto NaCl(001) (four-fold symmetry) or HOPG(0001) (six-fold symmetry), oriented structures are formed that reflect this symmetry.[3.1,3.5,3.9] This orientation arises from organic epitaxy, where the *n*-alkane chains align along energetically favorable directions on the substrate. Epitaxial growth can vary between the extremes of commensurate and incommensurate growth, but some degree of epitaxy is enough to induce a molecule to align in a particular orientation.[3.10,3.11] For example, *n*-alkane molecules align along the rows of sodium cations (the (110) axis) on the NaCl(001) surface due to favorable Coulombic and van der Waals interactions in this geometry.[3.9] Likewise, *n*-alkanes deposited on HOPG(0001) surfaces reflect the six-fold symmetry of the surface through partial epitaxy.[3.11-3.13] In the Groszek model,[3.14] these *n*-alkane chains align so that each methylene is located in the centre of a graphite hexagon, and the chain is oriented along the (100) direction on the graphite surface.[3.1]

This alignment will be referred as flat-on orientation versus edge-on orientation, in which every other methylene group is located on the surface and the rest of methylene groups are above the surface. The early flat-on model has been substantiated by STM investigations[3.1,3.15] and theoretical modeling.[3.16] Subsequent studies have shown that, at surface coverage greater than a monolayer, the vapour deposited alkane film does not follow Groszek's model completely, and the alkane molecules alternate between a flat-on and an edge-on orientation.[3.12,3.17] Even though the substrates are very different, the interaction of alkanes with NaCl(001) and HOPG(0001) have a similar strength. Alkanes, aligned along the <110> direction on NaCl(001) have an interaction energy of 11.2 kJ mol^{-1} CH_2^{-1},[3.9] while on HOPG(0001), the interaction energy is 10.4 kJ mol^{-1} CH_2^{-1} for edge-on and 12.1 kJ mol^{-1} CH_2^{-1} for flat-on orientation.[3.16]

When *n*-alkanes are grown on NaCl(001) or HOPG(0001), a variety of different morphologies have been observed. In our previous work (*n*-$C_{60}H_{122}$ and *n*-$C_{36}H_{74}$ on NaCl(001)), *n*-alkane thin films had an in-plane molecular alignment with four-fold symmetry. C60 thin films grown on NaCl(001) at substrate temperature from room temperature to 60 °C consisted of orthogonally oriented domains of uniform thickness.[3.5] The lateral size of the oriented domains increased with the substrate temperature, presumably as the nucleation density decreases. Shorter chains, of C36 thin films grown on NaCl(001) show a mix of orthogonally oriented bars formed from laterally oriented *n*-alkanes, and islands of normal oriented *n*-alkane chains.[3.5] These "bars" are high aspect ratio structures that have a greater thickness than the regions around the bars. The *n*-alkane chains in the bars are oriented along preferential directions on the NaCl(001) surface. Thin films of *n*-alkanes deposited on HOPG(0001) also show the formation of high aspect ratio bars, formed from laterally oriented *n*-alkane chains.[3.1]

In the deposition of *n*-alkanes on NaCl(001), several different growth modes have been implied, depending on growth conditions and chain length. The growth of C60 on NaCl(001) appears to occur by a van der Merwe (layer by layer) mechanism,[3.18] as an oriented film of uniform thickness is observed.[3.5] On the other hand, C36 thin films grown on NaCl(001) at 22 °C consist of normally oriented islands and laterally oriented bars,[3.5] suggesting a Strainski-Krastanov (layers plus island) growth mechanism.[3.18] Leunissen et al.[3.1] have indicated that the growth of laterally oriented bars from the deposition of *n*-alkanes on HOPG(0001) occurs via the Strainski-Krastanov growth mechanism, where the entire surface is first covered by a *n*-alkane monolayer, upon which 3D nucleation occurs.[3.13] When mobility permits the growth of 3D islands, the stronger side-to-side *n*-alkane intermolecular interactions will drive growth at the narrow end of the bars, as the *n*-alkane chains are known to be aligned perpendicular to the long axis of these bars.[3.5] This growth mechanism leads to the formation of these high aspect ratio structures. The magnitude of kinetic trapping and surface mobility during deposition are clearly important variables in the formation of different oriented morphologies.

Some caution must be taken in reviewing the literature and the discussion of growth mechanisms. Wide ranges of different growth conditions (chain length, substrate temperature, substrate identity, evaporation rate, etc.) have been used, leading to a wide range of observations (varied morphologies, and lateral and normal orientation). Likewise, the language for the epitaxial growth of atomic thin films must be extended to molecular thin films with caution: crystal strain is unlikely to have the same importance in organic thin films as in semiconductors, while molecular shape, orientation and flexibility are unique issues for molecular thin films. Surface mobility and the trapping of metastable states are universally important variables.

In order to control the growth of oriented nanostructures on high symmetry surfaces, and in the future, surfaces tailored to create an engineered orientation, an understanding of these thermodynamic and kinetic factors is required. To improve these models, and build a clearer picture of the thermodynamic and kinetic factors that govern orientation and directional control, further experimental studies are required. To this end, we have systematically explored the chain length and temperature dependence in the deposition of *n*-alkane thin films on HOPG(0001), at a fixed deposition rate. We observe a wide range of orientational morphologies, beyond that previously observed. The variation of orientation and morphology with these conditions, and the mechanistic origin of these morphologies are explored. We have developed a general interpretive framework into which the previous observations are subsumed.

Previous studies of *n*-alkane thin films, on a variety of substrates, have examined how the *n*-alkane molecular orientation varies with substrate temperature, in annealing performed after growth,[3.17,319,3.20] deposition rate,[3.3,3.20] and substrate identity.[3.1,3.9] "Bulk" probes such as X-ray and neutron diffraction[3.3,3.17,3.20] do not provide spatially resolved information to relate molecular orientation with sample morphology. On the other hand, most microscopy techniques[3.1,3.19] only provide an indirect molecular orientation information. Here, X-ray spectroscopy and microscopy can provide a direct and spatially resolved morphology and orientation characterization of *n*-alkane thin films on the surface of HOPG(0001). This is correlated with polarized optical microscopy.

2. Experimental

2.1 Samples and Sample Preparation

Samples: Hexatriacontane (*n*-$C_{36}H_{74}$, 98%), Tetratetracontane (*n*-$C_{44}H_{90}$, 99%), Pentacontane (*n*-$C_{50}H_{102}$, 97%) and Hexacontane (*n*-$C_{60}H_{122}$, 98%) were purchased from Sigma-Aldrich and used without purification. The shorthand C36, C44, C50, and C60 will be used in this paper to refer to these *n*-alkanes.

For optical microscopy experiments the substrate was Highly Oriented Pyrolytic Graphite (HOPG(0001)) (10 x 10 x 2 mm, ZYH grade, mosaic angle is 3.5° +/- 1.5°), from NT-MDT. The surface of HOPG(0001) was prepared by cleaving with scotch tape to expose a fresh graphite surface.

For X-ray spectroscopy experiments, samples were prepared on self-supported graphene or graphite thin films. Graphene, prepared by chemical vapour deposition on Ni (Graphene Supermarket) was transferred onto a TEM grid or Si_3N_4 window after etching the Ni layer with 12 M HCl(aq). Self-supported thin graphite films were prepared from ZYH grade graphite flakes. Thin graphite flakes, separated onto a SiO_2 wafer surface (300 nm SiO_2 on silicon) were transferred onto a holey-carbon coated TEM grid with a drop of isopropyl alcohol. These TEM grids were separated from wafer by a drop of 30% KOH solution. The *n*-alkane thin films were then evaporated onto these grapheme or graphite layers.

Sample preparation: The evaporation of *n*-alkane thin films onto HOPG(0001) was performed by physical vapour deposition from a resistively heated tungsten boat, at pressures below $10^{-3.7}$ torr. The film thickness and rate of the deposition were tracked with a quartz crystal microbalance; a rate of 0.3 ± 0.2 Å/s was used for all depositions and the total sample deposited thickness was 50 nm unless otherwise noted. During the deposition, the

temperature of the substrate was controlled in the range of 6 to 88 ± 0.1 °C with a Peltier thermoelectric module. The temperature was measured with a thermistor.

The substrate temperature was selected to explore different "super-cooling" temperatures (T_{SC}). Super-cooling is defined as the difference between the substrate temperature (T_S) and the melting point of the *n*-alkane (T_{fus}),[3.20,3.21] as shown in Equation 1:

$$T_{SC} = T_{fus} - T_S \quad (1)$$

This super-cooling measure is used to compare the morphology and growth of *n*-alkanes that have very different melting points. All four *n*-alkanes were deposited at similar super-cooling temperatures, to normalize for the difference between different *n*-alkane chain lengths. The *n*-alkane melting points used were taken from Dirand et al.[3.22]

2.2. X-ray Spectroscopy and Microscopy and Optical Microscopy Characterization

Samples were characterized by polarized optical microscopy (Nikon Eclipse ME600, with a Q-Imaging CCD camera). Images were acquired in bright field, with the use of polarizers to provide contrast based on the birefringence of the oriented thin film samples.

Scanning Transmission X-ray Microscopy (STXM) was used to acquire NEXAFS images and spectra in order to characterize orientation in selected samples. STXM experiments were performed at the Spectroscopy and microscopy beamline (10ID-1) at the Canadian Light Source.[3.23] With the linear polarization control of the elliptically polarized undulator source, X-ray Linear Dichroism Microscopy (XLDM) imaging can be performed easily.[3.2] This XLDM study was done by recording images at the energy of the Carbon 1s $\rightarrow \sigma^*_{C\text{-}H}$ band (287-288 eV). In these STXM experiments, the X-ray beam is oriented normal to the sample plane. The orientation of the X-ray linear polarization can be varied arbitrarily through the elliptically

polarized undulator settings, from horizontal polarization ($\theta = 0°$), where the electric field vector is oriented along the x-axis of the STXM images, to vertical polarization ($\theta = \pm 90°$), where the electric field vector is oriented along the y-axis. The inclination of the X-ray linear polarization can be varied from -90° to +90° for XLDM spectroscopy and microscopy. NEXAFS spectra extracted from different sample regions in the STXM microscope are reported as optical density ($OD = -\ln (I/I_o)$) versus energy.

3. Experimental Results

3.1. Polarized Optical Microscopy Results

The morphology and orientation of *n*-alkane films deposited on HOPG(0001) surfaces have been examined as a function of chain length (C36, C44, C50 and C60) and the substrate temperature during deposition. We observe that the morphology of the *n*-alkane thin films evolves systematically, and that similar morphologies are observed when *n*-alkanes of different length are deposited at a similar super-cooling temperature (T_{SC}).

Figure 1 presents polarized optical microscope images of C36 thin films deposited on HOPG(0001) at a series of different substrate temperatures. This trend starts at low temperature (Figure 1a; $T_{SC} = 69.8$ °C) with a film of uniform thickness; the thickness uniformity is later confirmed by X-ray microscopy. Within this film are domains with three different brightness levels. The contrast for these domains changes systematically as the polarizer is rotated. The domains likely correspond to three different regions of *n*-alkane alignment, reflecting alignment with the six-fold symmetry of the HOPG(0001) surface. This observation is similar to our previous observations for C60 deposited at room temperature onto NaCl(001),[3.5] where

orthogonally oriented domains of uniform thickness were observed, reflecting the four-fold symmetry of the surface.

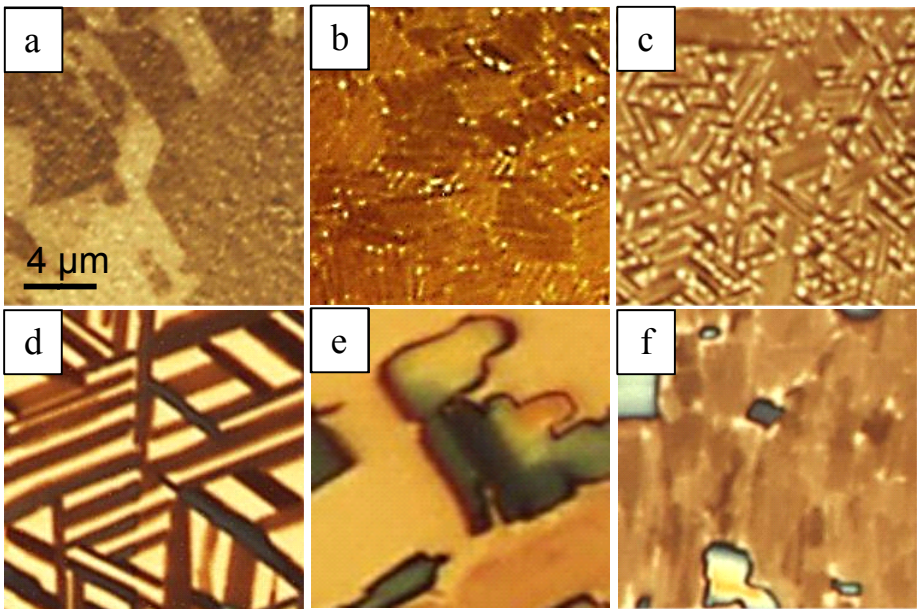

Figure 1: Polarized optical microscope images of C36 evaporated on HOPG (0001) at a range of substrate temperatures: a.) 6 °C (T_{SC} = 69.8 °C); b.) 25 °C (T_{SC} = 50.8 °C); c.) 30 °C (T_{SC} = 45.8 °C); d.) 50°C (T_{SC} = 25.8 °C); e.) 56 °C (T_{SC} = 19.8 °C); f.) 65 °C (T_{SC} = 10.8 °C).

When the substrate temperature is increased (Figure 1b, T_{SC} = 50.8 °C), distinct narrow bars appear within the wider domains; these maintain their pattern of three levels of birefringence contrast. The bars separate more and clearly show six-fold symmetry in Figure 1c (T_{SC} = 45.8 °C). The six-fold symmetry becomes distinct at higher temperature in Figure 1d (T_{SC} = 25.8 °C), as separate, wider and better-ordered bars are observed. After this point, a pseudo-rectangular morphology is observed (Figure 1e, T_{SC} = 19.8 °C); these features lack visible birefringence. Finally in Figure 1f, (T_{SC} = 10.8 °C), a flat film is observed along with domains with a pseudo-rectangular morphology.

Figure 2 presents polarized optical microscope images of C44 thin films deposited on HOPG(0001) at different substrate temperatures. At the lowest substrate temperature, domains of uniform thickness are observed (Figure 2a, $T_{SC} = 79.6$ °C), with three levels of contrast. These domains are smaller than those for C36 at a similar deposition temperature, which corresponds to a larger degree of super-cooling. The lateral size of domains increases with deposition temperature; Figure 2b ($T_{SC} = 60.6$ °C) corresponds closely to a similar C36 morphology (Figure 1a). In Figure 2c ($T_{SC} = 39.6$ °C), where narrow ordered bars are seen in oriented clusters. In Figure 2d ($T_{SC} = 34.6$ °C), bars are wider but still maintain the six-fold symmetry. At higher temperature the bars merge (Figure 2e, $T_{SC} = 24.6$ °C), and a pseudo-rectangular shape dominates. In Figure 2f, ($T_{SC} = 9.6$ °C), a flat film with some pseudo-rectangular domains is observed.

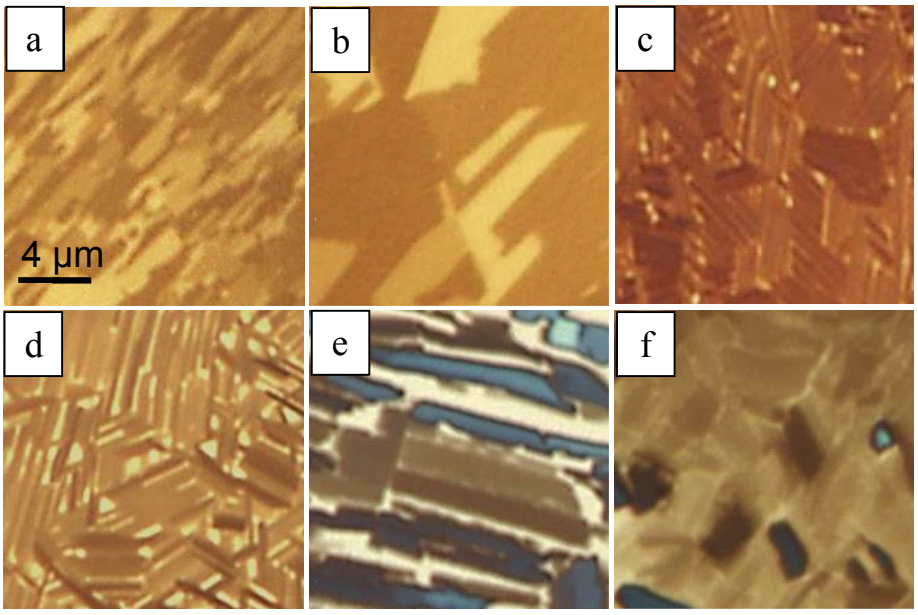

Figure 2: Polarized optical microscope images of C44 evaporated on HOPG (0001) at a range of substrate temperatures: a.) 6 °C ($T_{SC} = 79.6$ °C); b.) 25 °C ($T_{SC} = 60.6$ °C); c.) 46 °C ($T_{SC} = 39.6$ °C); d.) 51 °C ($T_{SC} = 34.6$ °C); e.) 61 °C ($T_{SC} = 24.6$ °C); f.)76 °C ($T_{SC} = 9.6$ °C).

Figure 3 presents polarized optical microscope images of C50 thin films deposited on HOPG(0001) at different substrate temperatures. A similar trend can be observed as following: (a) small domains of a uniform thickness in Figure 3a (T_{SC} = 67.1 °C); (b) larger domains showing initial signs of parallel narrow bars in Figure 3b (T_{SC} = 46.1 °C); (c) clusters of narrow bars with six-fold-symmetry in Figure 3c (T_{SC} = 43.1 °C), similar to the morphology of C44 at the super-cooling of 39.6 °C; (d) ordered but wider bars in Figure 3d (T_{SC} = 35.1 °C); (e) pseudo-rectangular domains in Figure 3e (T_{SC} = 23.1 °C), similar to the morphology of C44 at a super-cooling of 24.6 °C; (f) flat film plus pseudo-rectangular shapes in Figure 3f (T_{SC} = 11.1 °C).

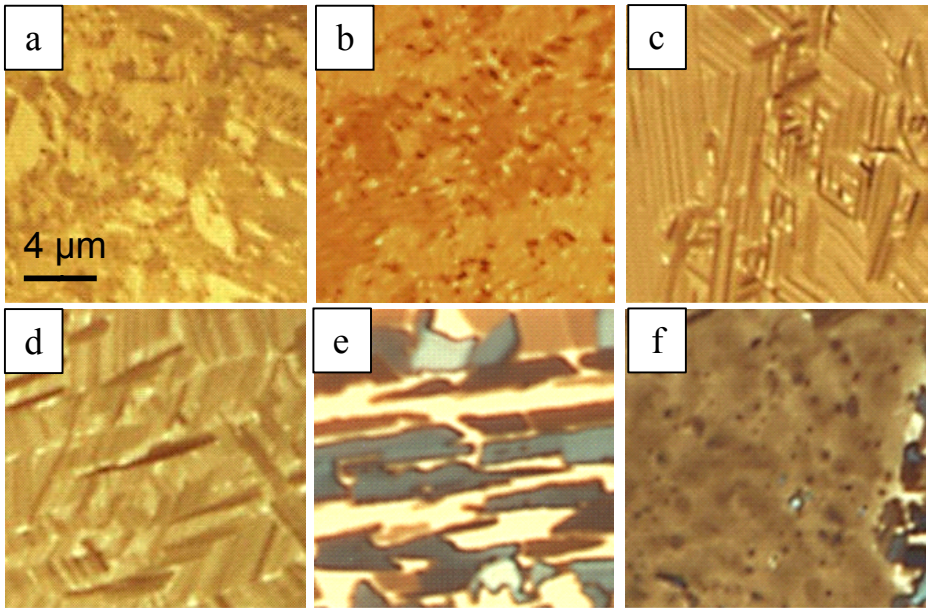

Figure 3. Polarized optical microscope images of C50 evaporated on HOPG (0001) at a range of substrate temperatures: a.) 25 °C (T_{SC} = 67.1 °C); b.) 46 °C (T_{SC} = 46.1 °C); c.) 49 °C (T_{SC} = 43.1 °C); d.) 57 °C (T_{SC} = 35.1 °C); e.) 69 °C (T_{SC} = 23.1 °C); f.) 81 °C (T_{SC} = 11.1 °C).

Figure 4 presents polarized optical microscope images of C60 thin films deposited on HOPG(0001) at different substrate temperatures. A similar trend is observed as for the shorter *n*-

alkanes (C36, C40 and C50), at super-coolings from 74.3 to 16.3 °C respectively. The systematic trends for the observation of uniform oriented thin films, oriented bars, pseudo rectangular morphologies and normal oriented thin films will be identified and discussed in detail in the discussion section below.

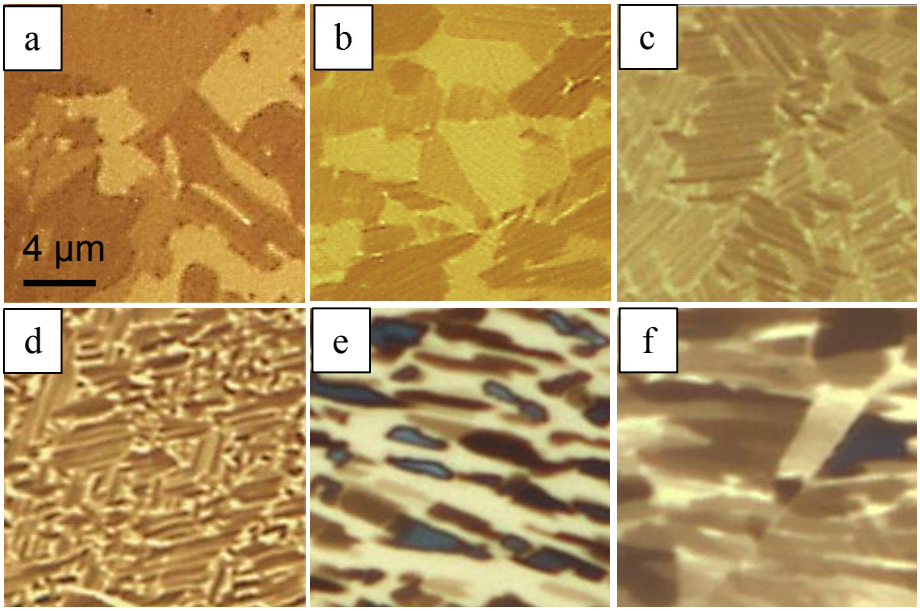

Figure 4. Polarized optical microscope images of C60 evaporated on HOPG (0001) at a range of substrate temperatures: a.) 25 °C (T_{SC} = 74.3 °C); b.) 58 °C (T_{SC} = 41.3 °C); c.) 63 °C (T_{SC} = 36.3 °C); d.) 70 °C (T_{SC} = 29.3 °C); e.) 79 °C (T_{SC} = 20.3 °C); f.) 83 °C (T_{SC} = 16.3 °C).

3.2. X-ray Spectroscopy and Microscopy Results

While polarized optical microscopy shows the evolution of micron-scale morphologies in two dimensions, NEXAFS spectroscopy can provide a three-dimensional view of the molecular orientation based on linear dichroism (the anisotropic absorption of linearly polarized radiation).[3.24,3.25] Linear dichroism in the NEXAFS spectroscopy, recorded in a STXM microscope, is a direct probe of molecular orientation, as the intensity of features assigned as Carbon 1s → $\sigma^*_{C\text{-}H}$ (at ~288 eV)[3.12] and Carbon 1s → $\sigma^*_{C\text{-}C}$ (at ~293 eV) depend on the relative orientation of the X-ray electric field vector and the transition dipole moment (TDM) for the

electronic transition. The TDM for the Carbon 1s → $\sigma^*_{C\text{-}H}$ transition is oriented in the plane perpendicular to the alkane chain, while the TDM for the Carbon 1s → $\sigma^*_{C\text{-}C}$ transition is directed along the alkane backbone. Fu et al.[3.25] (and references within) present a comprehensive discussion on the transition dipole moments of the Carbon 1s → $\sigma^*_{C\text{-}H}$ and $\sigma^*_{C\text{-}C}$ transitions and the assignments for the NEXAFS spectra of oriented linear alkanes.

Figure 5 presents STXM data for an *n*-alkane film representing an oriented uniform film morphology, from the evaporation of C50 at 35 °C (T_{SC} = 57.1 °C) onto a graphene thin film. The STXM image (Figure 5a), recorded at the energy of the Carbon 1s → $\sigma^*_{C\text{-}H}$ band (287.4 eV), shows domains with different transmission intensity. The domain structure for *n*-alkanes grown on graphene is not as well ordered as for similar growth on HOPG(0001). This could arise from a different surface quality, the presence of contaminants from the graphene substrate etching process, or differences in substrate heat conductivity that will affect the actual surface temperature during growth. Regardless, the lower quality morphologies are adequate for our NEXAFS studies.

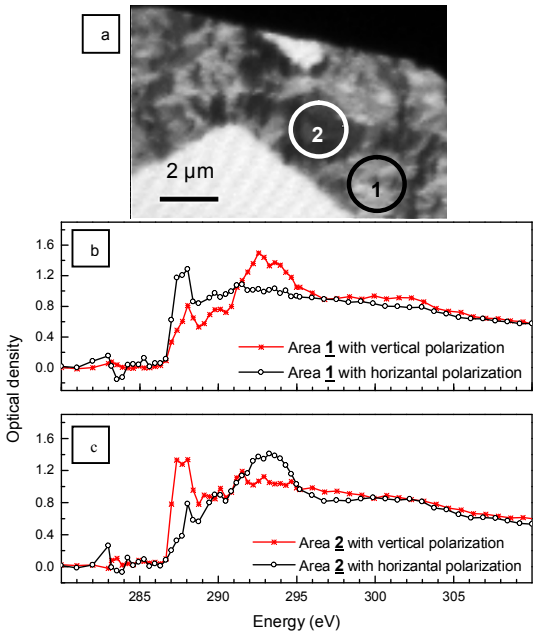

Figure 5. a.) Transmission X-ray image recorded at 287.4 eV with vertical polarization from C50 grown on graphene/TEM-grid at 35 °C (T_{SC} = 57.1 °C); b.) and c.) corresponding NEXAFS spectra of region 1 (light region in Figure 5a) and region 2 (dark region in Figure 5a), recorded with horizontal and vertical polarization.

The Carbon 1s NEXAFS spectra presented in Figures 5b and 5c are extracted from area 1 (light area in Figure 5a) and area 2 (dark area in Figure 5a), acquired with vertically and horizontaly polarized X-rays. The change in the intensity of the C-H (287-288 eV) and C-C band (293 eV) with the polarization change provides direct evidence that the *n*-alkane chains are aligned in-plane (after Fu et al.[3.25]). On the HOPG(0001) surface, different *n*-alkane domains are expected to be oriented 60° apart. When the X-ray polarization is oriented along orthogonal directions (horizontal, along the x-axis, and vertical, along the y-axis), different relative intensities of the Carbon 1s $\rightarrow \sigma^*_{C\text{-}H}$ and the Carbon 1s $\rightarrow \sigma^*_{C\text{-}C}$ bands will be observed for the different oriented domains. This is reflected in the relative intensity of these bands in Figures 5b and 5c. The intensity in the atomic-like NEXAFS continuum (>305 eV) is the same for all locations, indicating that the film has a uniform thickness. Additional data (see accompanying

data), recorded at a wider range of X-ray polarization, provides unambiguous evidence of six-fold symmetry; only two angles are shown in Figure 5.

Figure 6 presents STXM data for an *n*-alkane film representing a pseudo-rectangular morphology, from the evaporation of C36 at 56 °C (T_{SC} = 19.8 °C) onto graphene transferred to a TEM grid. Figure 6a presents a STXM image recorded at the energy of the Carbon 1s → $\sigma^*_{C\text{-}H}$ transition (288 eV) and the corresponding NEXAFS spectra are presented in Figure 6b. The morphology of C36 on graphene is similar to that was seen on HOPG(0001) in Figure 1e. An inversion of C-H and C-C absorption peaks (at ~288 eV and ~293 eV respectively) can be seen when vertical and horizontally polarized X-rays are used; this is similar to the observations for Figure 5, which was discussed in detail above. These results show that the domains consist of chains oriented laterally, in the plane of the substrate.

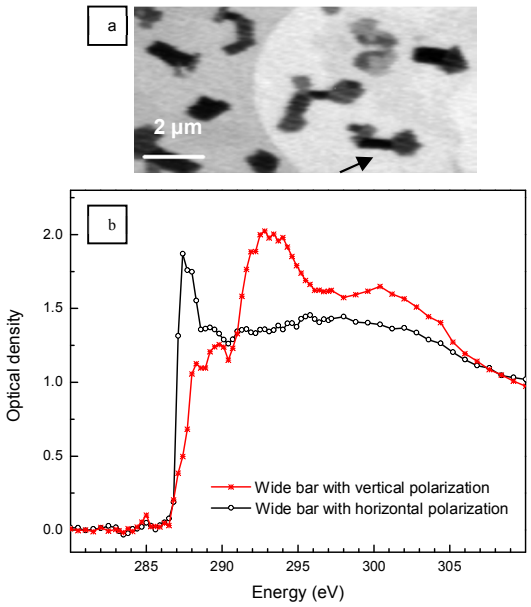

Figure 6. a.) Transmission X-ray image recorded at 288 eV with horizontal polarization from C36 grown on graphene/TEM-grid at 56 °C (T_{SC} = 19.8 °C); b.) corresponding NEXAFS spectra with the horizontal and vertical polarization.

Figure 7 presents STXM data for an *n*-alkane film representing a thin flat film and bar morphologies, from the evaporation of C36 at at 65 °C (T_{SC} = 10.8 °C) onto graphene transferred to Si_3N_4 window. Figure 7a presents a STXM image recorded at the energy of the Carbon 1s → $\sigma^*_{C\text{-}H}$ transition (288.2 eV) and the corresponding NEXAFS spectra are presented in Figures 7b and 7c from two regions. A thin flat film is expected coexist with pseudo-rectangular shapes in these deposition conditions. However, narrow bars are observed instead. The presence of narrow bars can be attributed to the different thermal conductivity and/or surface state of graphene, as discussed above. NEXAFS spectra were acquired from the thin flat film (indicated by region 1) and from a bar domain, with vertical and horizontally polarized X-ray beams. Spectra from area 1 show a maximum absorption in the C-H band (288 eV) for the both polarizations. This indicates that the C36 chains are standing up (normal to the surface), as the polarization is aligned along the C-H transition dipole moment in all cases. In contrast, spectra from the bar domain show a variation in the intensity of the C-H and C-C bands with change in the linear polarization, indicating that the *n*-alkane chains are laterally oriented. As well, the oriented bar domain is thicker than region 1 (optical density of ~0.4 vs 0.2 at the post edge). On the basis of these spectra, the thin flat film regions are chains standing normal to the substrate.

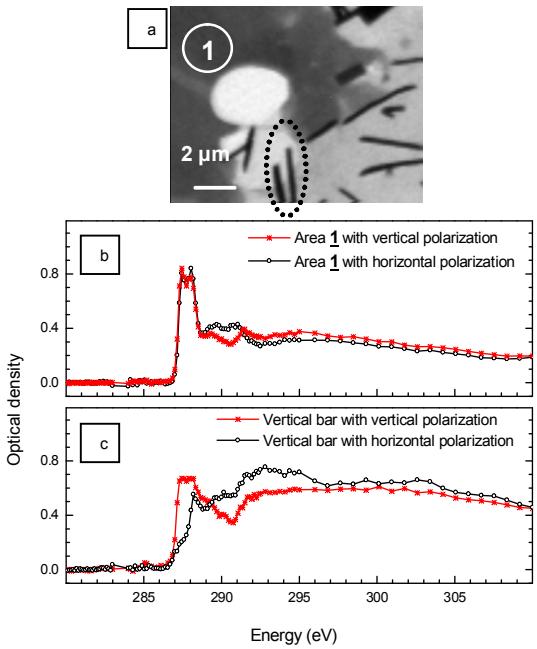

Figure 7. (a) Transmission X-ray image recorded at 288.2 eV with vertical polarization from C36 grown on graphene/Si_3N_4 window at 65 °C (T_{SC} = 10.8 °C). (b, c) corresponding NEXAFS spectra of area 1 (flat region in part a) and the vertical bar recorded with horizontal and vertical polarization.

4. Discussion

4.1 Evolution of Morphology and Orientation with Super-cooling

In comparing the trends in the morphology for the *n*-alkanes of C36, C44, C50 and C60, a pattern of temperature dependent morphologies can be observed. These results are summarized in **Figure 8**. At lower substrate temperature (higher super-cooling), a film of uniform thickness is observed for all *n*-alkanes, with the six-fold symmetry in-plane orientation (three levels of intensity) reflecting the HOPG(0001) substrate symmetry. This morphology is assigned as oriented uniform film, identified as Region A in Figure 8. Layer-by-layer growth appears to dominate, as new layers follow the orientation of the previous layers.

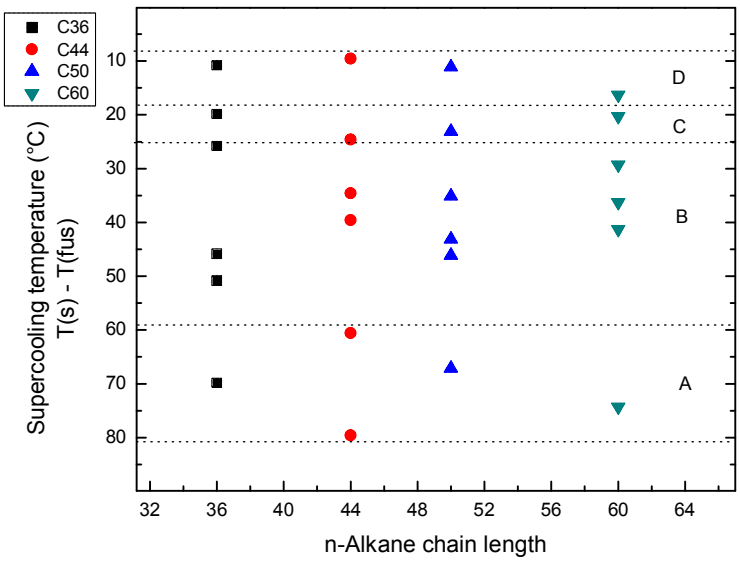

Figure 8. Observation of different surface phases in *n*-alkane thin films grown on HOPG(0001) as a function of supercooling temperature (temperature relative to the melting point): a.) Domains of uniform thickness, oriented by substrate; b.) Bar-shaped domains, reflecting the surface symmetry; c.) Pseudo-rectangular domains; d.) Thin flat film along with scattered pseudo-rectangular domains.

As the super-cooling temperature decreases, bar-like patterns emerge within the flat uniform domains. Figures 1b, 3b and 4b show oriented, high-aspect ratio bar structures that emerge within the oriented domains of uniform thickness. As the super-cooling decreases further, well-ordered bars are separated and clearly illustrate the six-fold symmetry of substrate. This second morphology is identified as oriented bar structures (Region B in Figure 8). The clearest triangular structure is for shorter chains (Figures 1c and 1d for C36), with less order for longer chains (C44: Figures 2c and 2d; C50: Figures 3c and 3d; and C60: Figures 4c and 4d). While the super-cooling index adjusts for differences in chain length, mobility and reptation will become more complex for longer chain lengths, and the formation of oriented bars will have less order.

Increased molecular mobility is required to form bar structures. These results suggest a Strainski-Krastanov growth mechanism at smaller super-cooling temperatures. The observation

of “clusters” of oriented bars (see Figures 1b, 2c, 3b, 4b and 4c) suggest that larger oriented domains of a single orientation are formed first, from which bars emerge, retaining the orientation of the large oriented domains.

At yet higher temperature, a pseudo-rectangular phase is observed in all samples (Region C in Figure 8) which shows no epitaxial order. Since the NEXAFS spectroscopy results show that *n*-alkane molecules in the pseudo-rectangular phase still lie down on the substrate, it can be concluded that the relative strength of the alkane-substrate interaction in region C is comparatively weak, so the *n*-alkane molecules retain in-plane alignment but do not appear to follow the epitaxial orientation of the substrate.

Finally for depositions performed ~10 °C below the melting point, the surface of HOPG(0001) is covered with a continuous thin flat film along with scattered pseudo-rectangular shapes (Region D in Figure 8). NEXAFS results provide the evidence that *n*-alkane molecules have normal orientation in the thin flat film of phase D. This means that in phase D alkane-graphite interaction is too weak to maintain the *n*-alkane molecules in the plane of substrate and *n*-alkane molecules adapt to the thermodynamically stable, entropy driven normal orientation.

In summary, different phases are observed as the relative importance of the oriented alkane-graphite interaction decreases with increased substrate temperature, where the alkane-graphite interaction values are tuned from most significant (phase A) to the lower values (phase D) and the orientation of *n*-alkane thin film varied correspondingly.

In this work, morphologies are observed to vary systematically with the substrate temperature, as controlled with a Peltier heating element. The actual surface temperature might vary due to limited heat conduction of the sample, as the thermal energy of the deposited molecules and the enthalpy of deposition could raise the surface temperature above the regulated

value. However, the use of a similar evaporation rates for all depositions controls these thermal factors. The temperature for the onset of a specific phase is observed vary somewhat from deposition to deposition. However, the evolution of oriented morphologies is consistent, indicating a consistent physical trend. We also note that these phases are metastable states, so there is not a precisely defined phase transition temperature.

4.2. Thermodynamics of the Evolution of Morphology and Orientation

In addition to monitoring the orientation of *n*-alkane molecules grown on HOPG(0001), the morphology changes for laterally orientated *n*-alkane thin films gives insight into the nature of organic epitaxial growth. This study presents new results on how the orientational morphology of *n*-alkane thin films, deposited on HOPG(0001), varies with deposition conditions. Most previous studies of *n*-alkane growth focused on the change in molecular orientation with deposition conditions, from lateral to the most stable normal oriented form. However, the morphology has not been widely explored. Leunissen et al.[3.1] have observed an oriented bar morphology with a six-fold symmetry morphology for C32 deposited on HOPG(0001).[3.1] In this work, we observe oriented uniform films (Region A; Figure 8), oriented bar (Region B; Figure 8), and pseudo-rectangular (Region C; Figure 8), morphologies with a lateral molecular orientation; these are followed by normal orientation (Region D; Figure 8), in films deposited at smaller super-cooling.

Likewise, within oriented uniform films grown at large super-cooling temperatures, the domain size varies with temperature: small domains at higher super-cooling temperature (Figure 2a), and larger domains at reduced super-cooling temperature (Figures 2b). This is attributed to the nucleation of in-plane oriented domains: lower substrate temperatures (higher super-cooling) will show a greater nucleation of oriented domains, which will then grow and expand into each

other; higher deposition temperatures will have a lower nucleation density and larger domains. Fu et al.[3.5] made a similar observation for thin films of C60 on NaCl(001). On the basis of the six-fold symmetry of the *n*-alkane thin films on HOPG(0001), we assume that the oriented domains arise from the epitaxial alignment of *n*-alkane chains oriented along the six-fold symmetry of the HOPG(0001) substrate. With an increased substrate temperature, an oriented bar pattern is observed by optical microscopy, initially as densely packed bars with three level of intensity, then as films with separated bars.

The above mentioned morphology variation can be attributed to the translational as well as rotational mobility of *n*-alkane molecules. The molecular STM and AFM studies[3.26,3.27] have shown that an *n*-alkane monolayers, grown on HOPG(0001), form a lamellar structure with parallel *n*-alkane backbones that are separated by narrow troughs. As the temperature increases, these *n*-alkane monolayers show increased translational motion; also at higher temperatures, *gauche* defects appear instead of an all-*trans* geometry as a result of single bond rotational entropy.[3.28,3.29] This phenomenon is reflected in our morphologies: *n*-alkane chains that are oriented in uniform domains at low substrate temperature, earn translational mobility as the substrate temperature increases and form bars. Bars that initially are densely packed within domains of uniform orientation, start to separate as substrate temperature increases. A further increase in the substrate temperature after this point provides additional kinetic energy to overcome directional epitaxial growth, when pseudo-rectangular shapes are formed. Pseudo-rectangular domains are still in a lateral orientation on the surface but have lost registry with the HOPG(0001) substrate symmetry. Above this temperature, coexisting lateral and normal orientation emerges.

Normal orientation of *n*-alkane at high substrate temperature can be explained by a weaker alkane-graphite interaction. The orientation of a multilayer is determined in the initial stages of growth, when lateral or normally oriented nuclei form according to the balance of the adsorbate kinetic energy and the substrate interaction.[3.4] An increased substrate temperature can change the *n*-alkane conformation from an all-*trans* state, as *gauche* defects increase. These *gauche* defects are thought to displace methylene groups from the substrate,[3.30,3.31] reducing the effective alkane-graphite interaction strength. The reduced interaction strength and "unzipping" from the substrate provides a pathway for the flexible chain to adopt a new, normally oriented equilibrium conformation.

Conclusions

In this work, we have affirmed previous observations and theory that shows that molecular orientation depends on the evaporation conditions (substrate temperature, substrate identity, and evaporation rate) and chain length. Different modes of growth occur, from layer-by-layer growth, to modes that allow for the formation of oriented islands. Uniquely, this work shows a complex series of oriented morphologies that evolve with deposition conditions. NEXAFS spectroscopy and microscopy, along with polarized optical microscopy shows laterally oriented *n*-alkane chains at high T_{SC}, in a range of film morphologies (oriented uniform film; oriented bar, and pseudo-rectangular), and normal oriented *n*-alkane chains for the smallest super-cooling temperature. The *n*-alkane orientation changes from lateral to normal with the decreased degree of super-cooling, T_{SC}. These orientational morphology differences are attributed to differences in molecular mobility versus the relative influence of directional epitaxy on the sample surface during growth, and the role of kinetic trapping of metastable states.

Acknowledgements

SGU is funded by NSERC (Canada). Research described in this paper was performed at the Canadian Light Source, which is supported by the Natural Sciences and Engineering Research Council of Canada, the National Research Council Canada, the Canadian Institutes of Health Research, the Province of Saskatchewan, Western Economic Diversification Canada, and the University of Saskatchewan.

Supporting Information Available

XLDM (X-ray Linear Dichroism Microscopy) study is presented in a graph that shows the polarization dependence of transmission X-ray microscopy of a sample of C60 grown on graphite/TEM-grid at 25 °C (T_{SC} = 74.3 °C). This material is available free of charge via the Internet at http://pubs.acs.org.

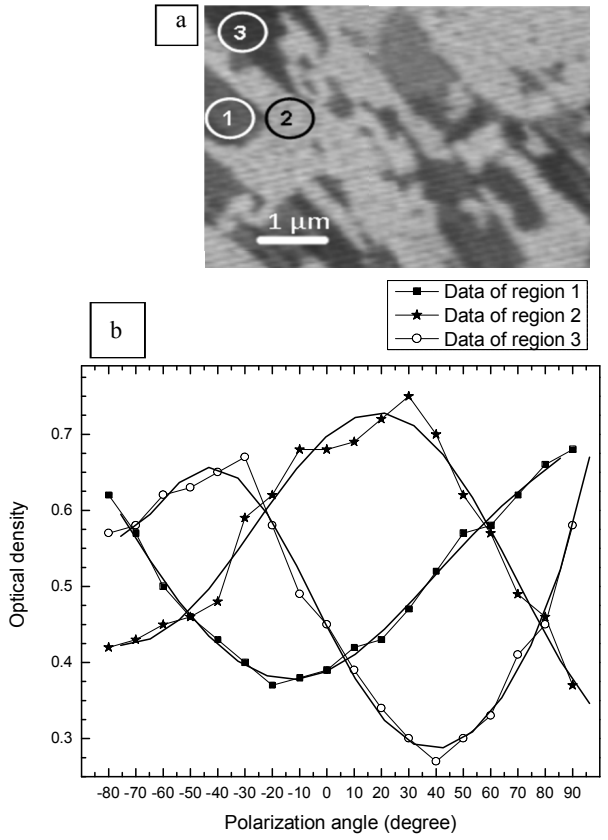

Figure S. a.) Optical density image recorded at 287.5 eV with the polarization of 30° from C60 grown on graphite/TEM-grid at 25 °C (T_{SC} = 74.3 °C); b.) corresponding XLDM data from areas 1,2 and 3 (regions with different contrasts in Figure S.a.); the 6^{th}-order polynomial fits are superimposed on experimental data for three regions.

Appendix

The current paragraph was not included in the published manuscript and is a supplementary result. The process of studying *n*-alkane thin film growth on HOPG(0001) was continued up to the substrate temperature at which normally oriented *n*-alkane forms. To complete this study the substrate temperature was raised above the temperature at which a normally oriented film formed. A new morphology was observed as separate circular shapes. This morphology was seen for all the *n*-alkanes studied in this chapter including C36, C44, C50 and C60. Figure A(a) shows the optical microscope image of 50 nm C60 grown on HOPG(0001) at the substrate temperature of 95 ºC (T_{SC}=4.3 ºC). Figure A(b) presents a transmission X-ray image recorded at 288.2 eV with vertical polarization from a 50 nm film of C36 grown on graphene/Si_3N_4 window at the substrate temperature of 71 ºC (T_{SC}=4.8 ºC). Similar to other morphologies, the orientation of *n*-alkane molecules was studied by acquiring C 1s NEXAFS spectra with the horizontal and vertical polarizations as shown in Figure A(c). Since there is no inversion in the intensity of peaks at 288 eV (C 1s $\rightarrow \sigma^*_{C\text{-}H}$) and 293 eV (C 1s $\rightarrow \sigma^*_{C\text{-}C}$), the higher intensity at 288 eV in both polarizations proves a normally oriented *n*-alkane film. After this stage increasing the substrate temperature results in complete evaporation of *n*-alkane and an *n*-alkane film is not formed.

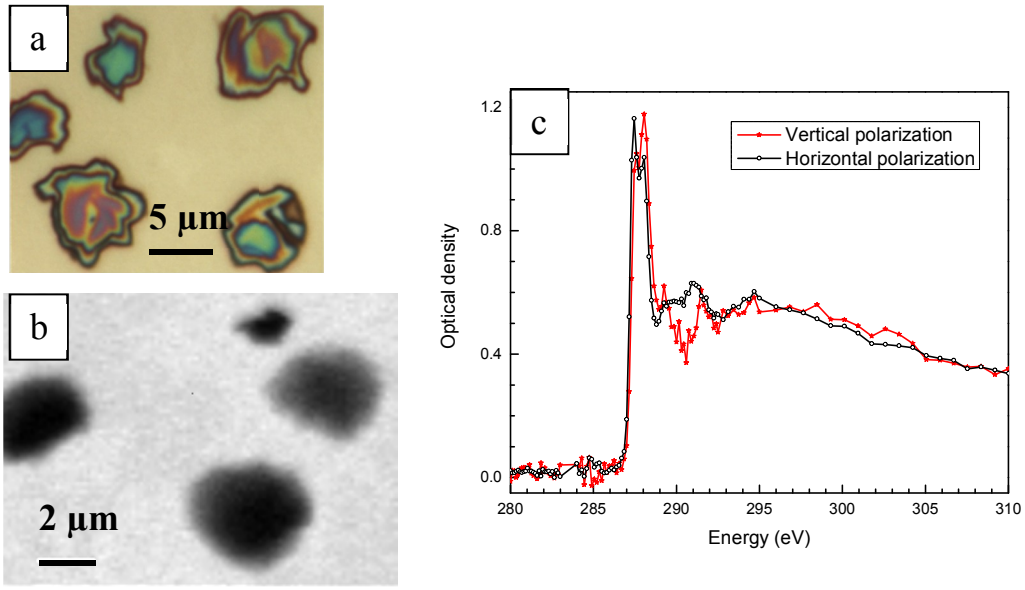

Figure A. a.) Optical microscope image from C60 evaporated on HOPG (0001) at substrate temperature of 95 °C (T_{SC} = 4.3 °C); b.) Transmission X-ray image recorded at 288.2 eV with vertical polarization from C36 grown on graphene/TEM-grid at 71 °C (T_{SC} = 4.8 °C); c.) corresponding NEXAFS spectra of a circular domain recorded with horizontal and vertical polarization.

References

(3.1) Leunissen, M. E.; Graswinckel, W. S.; van Enckevort, W. J. P.; Vlieg, E. Epitaxial nucleation and growth of *n*-alkane crystals on graphite (0001). *Cryst.Growth.Des.* **2004**, *4*, 361.

(3.2) Urquhart, S. G.; Lanke, U. D.; Fu, J. Characterization of molecular orientation in organic nanomaterials by X-ray linear dichroism microscopy. *Int. J. Nanotechnol*. **2008**, *5*, 1138.

(3.3) Nozaki, K.; Saihara, R.; Ishikawa, K.; Yamamoto, T. Structure of normal alkane evaporated films: molecular orientation. *Jpn. J. Appl. Phys.* **2007**, *46*, 761.

(3.4) Kubono, A.; Akiyama, R. Classical nucleation theory applied to molecular orientations in vapor-deposited organic thin films. *J. Appl. Phys*. **2005**, *98*, 093502.

(3.5) Fu, J.; Urquhart, S. G. Effect of chain length and substrate temperature on the growth and morphology of *n*-alkane thin films. *Langmuir* **2007**, *23*, 2615.

(3.6) Fukao, K.; Horiuchi, T.; Matsushige, K. Observation of molecular orientation in evaporated films of *n*-paraffins. *Thin Solid Films* **1989**, *171*, 359.

(3.7) Kubono, A.; Akiyama, R. Orientational mechanism for long-chain organic molecules during physical vapor deposition. *Mol. Cryst. Liq. Cryst*. **2002**, *378*, 167.

(3.8) Matsuzaki, F.; Inaoka, K.; Okada, M.; Sato, K. Molecular-orientation in physical-vapor deposition of long-chain stearic-acid. *J. Cryst. Growth* **1984**, *69*, 231.

(3.9) Mauritz, K. A.; Baer, E.; Hopfinger, A. J. Molecular energetics of the epitaxial crystallization of polyethylene on alkali halide substrates. *J. Polym. Sci., Part B: Polym. Phys.* **1973**, *11*, 2185.

(3.10) Hooks, D. E.; Fritz, T.; Ward, M. D. Epitaxy and molecular organization on solid substrates. *Adv. Mater*. **2001**, *13*, 227.

(3.11) Forrest, S. R.; Burrows, P. E. Growth modes of organic semiconductor thin films using organic molecular beam deposition: epitaxy, van der Waals epitaxy, and quasi-epitaxy. *Supramol.Sci*. **1997**, *4*, 127.

(3.12) Endo, O.; Horikoshi, T.; Katsumata, N.; Otani, K.; Fujishima, T.; Goto, H.; Minami, K.; Akaike, K.; Ozaki, H.; Sumii, R.; Amemiya, K.; Nakamura, M.; Kosugi, N. Incommensurate crystalline phase of *n*-alkane monolayers on graphite (0001). *J. Phys. Chem. C* **2011**, *115*, 5720.

(3.13) Taub, H.; Herwig, K. W.; Matthies, B.; Hansen, F. Y. Neutron diffraction studies of the structure, growth, and melting of intermediate-length *n*-alkane films adsorbed on graphite. *Inorg.Mater*. **1999**, *35*, 996.

(3.14) Groszek, A. J. Selective adsorption at graphite/hydrocarbon interfaces. *Proc. R. Soc. A* **1970**, *314*, 473.

(3.15) Chen, Q.; Yan, H. J.; Yan, C. J.; Pan, G. B.; Wan, L. J.; Wen, G. Y.; Zhang, D. Q. STM investigation of the dependence of alkane and alkane ($C_{18}H_{38}$, $C_{19}H_{40}$) derivatives self-assembly on molecular chemical structure on HOPG surface. *Surf.Sci.* **2008**, *602*, 1256.

(3.16) Yin, S.; Wang, C.; Qiu, X.; Xu, B.; Bai, C. Theoretical study of the effects of intermolecular interactions in self-assembled long-chain alkanes adsorbed on graphite surface. *Surf. Interface Anal*. **2001**, *32*, 248.

(3.17) Diama, A.; Matthies, B.; Herwig, K. W.; Hansen, F. Y.; Criswell, L.; Mo, H.; Bai, M.; Taub, H. Structure and phase transitions of monolayers of intermediate-length *n*-alkanes on graphite studied by neutron diffraction and molecular dynamics simulation. *J Chem Phys* **2009**, *131*, 084707.

(3.18) Pashley, D. W. Epitaxy growth mechanisms. *Mater.Sci. Technol*. **1999**, *15*, 2.

(3.19) Couto, M. S.; Liu, X. Y.; Meekes, H.; Bennema, P. Scanning tunneling microscopy studies on *n*-alkane molecules adsorbed on graphite. *J. Appl. Phys*. **1994**, *75*, 627.

(3.20) Tanaka, K.; Okui, N.; Sakai, T. Molecular orientation behavior of paraffin thin films made by vapor deposition. *Thin Solid Films* **1991**, *196*, 137.

(3.21) Shimizu, H.; Tanigaki, N.; Nakayama, K. Molecular orientation and periodical structure of vacuum-deposited films of long-chain molecules. *Jap.J. Appl. Phys*. **1995**, *34*, L701.

(3.22) Dirand, M.; Bouroukba, M.; Briard, A.-J.; Chevallier, V.; Petitjean, D.; Corriou, J.-P.Temperatures and enthalpies of (solid + solid) and (solid + liquid) transitions of *n*-alkanes. *J. Chem. Thermodyn*. **2002**, *34*, 1255.

(3.23) Kaznatcheev, K. V.; Karunakaran, C.; Lanke, U. D.; Urquhart, S. G.; Obst, M.; Hitchcock, A. P. Soft X-ray spectromicroscopy beamline at the CLS: Commissioning results. *Nucl.Instrum. Methods Phys. Res., Sect. A* **2007**, *582*, 96.

(3.24) Wang, Y.; Zou, Y.; Araki, T.; Luning, J.; Kilcoyne, A. L. D.; Sokolov, J.; Ade, H.; Rafailovich, M. M. Probing the chain and crystal lattice orientation in polyethylene thin films by Near Edge X-ray Absorption Fine Structure (NEXAFS) spectroscopy. *Macromolecules* **2010**, *43*, 8153.

(3.25) Fu, J.; Urquhart, S. G. Linear dichroism in the X-ray absorption spectra of linear *n*-alkanes. *J. Phys. Chem. A* **2005**, *109*, 11724.

(3.26) Taki, S.; Ishida, K.; Okabe, H.; Matsushige, K. Direct observation of the growth process of organic crystals by scanning tunneling microscopy. *J. Cryst. Growth* **1993**, *131*, 13.

(3.27) Magonov, S. N.; Yerina, N. A. High-temperature atomic force microscopy of normal alkane $C_{60}H_{122}$ films on graphite. *Langmuir* **2003**, *19*, 500.

(3.28) Bucher, J.-P.; Roeder, H.; Kern, K. Thermally-induced disorder and conformational defects of alkane monolayers on graphite. *Surf.Sci*. **1993**, *289*, 370.

(3.29) Askadskaya, L.; Rabe, J. P. Anisotropic molecular dynamics in the vicinity of order-disorder transitions in organic monolayers. *Phys. Rev. Lett*. **1992**, *69*, 1395.

(3.30) Gellman, A. J.; Paserba, K. R. Kinetics and mechanism of oligomer desorption from surfaces: *n*-alkanes on graphite. *J. Phys. Chem. B* **2002**, *106*, 13231.

(3.31) Paserba, K. R.; Gellman, A. J. Effects of conformational isomerism on the desorption kinetics of *n*-alkanes from graphite. *J. Chem. Phys*. **2001**, *115*, 6737.

CHAPTER 4: EVALUATION OF DEPOSITION RATE EFFECT ON THE *N*-ALKANE THIN FILMS EPITAXIAL GROWTH ON GRAPHITE

Introduction

An extensive study of morphology and orientation variation of *n*-alkane thin films grown epitaxially on HOPG(0001) at different substrate temperatures was presented in Chapter 3. In the current chapter, the effect of deposition rate as a growth parameter is studied. That was not considered before. In order to have a suitable growth condition for epitaxy, the deposition is performed at very low rates, the extreme of which can be seen in organic molecular beam deposition.[75] Since the lowest possible deposition rate was applied to prepare the samples in Chapter 3, the effect of higher rates on the structure of *n*-alkane films grown on graphite at a constant substrate temperature is examined here. The results and discussion of variable deposition rate at constant substrate temperatures is presented in §4.1. Based on the results of varying deposition rate, a model is postulated in §4.2 to rationalize the formation of bar structure in *n*-alkane thin films. In the last part of this chapter, §4.3, the possibility of changing the orientation of *n*-alkane molecules after growth is examined. It is hypothesized that the metastable bar structure transforms to the stable normal orientation by annealing a thin film of *n*-alkane grown on HOPG(0001) that contains a combination of both orientations. It is assumed that the re-evaporation and re-orientation processes can change the orientation of *n*-alkane film from lateral to the normal during annealing.

4.1 The effect of deposition rate

One of the kinetic parameters of the PVD growth is the deposition rate. This can affect the effective diffusion of atoms/molecules on the surface of substrate. It is known that the effect

of higher deposition rate is similar to lower substrate temperature.[76] At a high deposition rate the deposit molecules do not have enough time to diffuse on the surface before arrival of subsequent molecules from the gas phase. At low substrate temperature the deposit molecules do not have enough kinetic energy to move on the surface and find the most stable sites on the substrate; therefore the landing sites are not necessarily the spots with the lowest free energy. The relative rate of nucleation increases at high supersaturation (high deposition rate and/or low substrate temperature) and results in smaller domain size.[9,76] Amar and Family[77] showed that the domain size (R) is proportional to the ratio of diffusion rate (D) to deposition rate (F), ($R \propto D/F$). It was shown in Chapter 1 (Equation 1.2) that the diffusion rate is directly related to the substrate temperature, ($D \propto exp\ (-1/T)$).[77] Therefore, the domain size is expected to be larger at a higher substrate temperature and a lower deposition rate. The effect of higher substrate temperature in increasing the domain size has been seen before in Chapter 3. Figure 2a and Figure 2b in Chapter 3 show that increasing the substrate temperature from 6 °C to 25 °C for a sample of C44 deposited on HOPG(0001)increases the domain size of an uniform thickness film. This sample was prepared at a low deposition rate of 0.3 ± 0.2 Å/s, which was the lowest achievable deposition rate. In the current chapter, samples of C44 on HOPG(0001) will be grown at varying deposition rates while the substrate temperatures is kept constant at 25 °C, 41 °C, 55 °C and 59 °C. In this section, deposition rates are reported as a range of values (2-5 Å/s, 5-10 Å/s, 10-25 Å/s) and not as distinct values due to the large fluctuation in the values measure by the quartz crystal microbalance.

4.1.1 Results of variable deposition rate

Figure 4.1 shows the morphology of C44 on HOPG(0001) grown at the substrate temperature of 25 °C and different deposition rates. C44 forms a uniform thickness film consisting large domains at the deposition rate of 0.3 Å/s (Figure 4.1a). At the higher deposition rate (5-10 Å/s), observed domains are smaller and some fine features are formed inside the domains (Figure 4.1b).

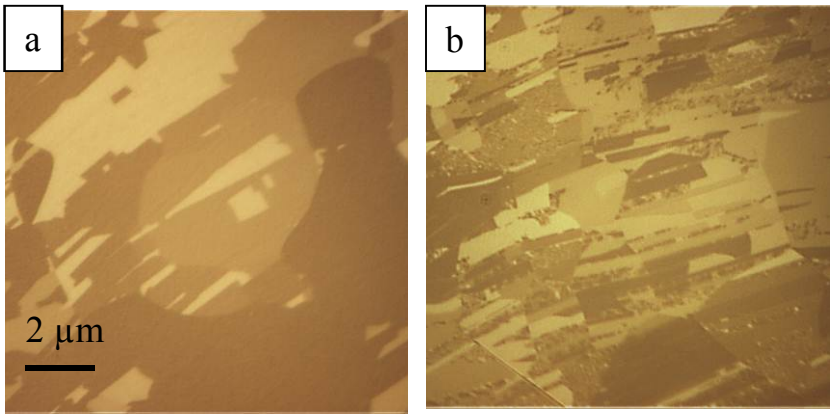

Figure 4.1 Polarized optical microscope images of a.) 50 nm C44 on HOPG(0001), deposition rate <1 Å/s; b.) 100 nm C44 on HOPG(0001), deposition rate=5 to 10 Å/s. Substrate temperature during deposition is 25 °C for images (a) and (b).

Figure 4.2 shows the effect of deposition rate variation when C44 is grown on HOPG(0001) at the substrate temperature of 41 °C. At low deposition rate, (< 1 Å/s) (Figure 4.2a), a pattern of small separate bars is observed. This changes to the structure of narrower and denser bars when the rate is increased to 2-5 Å/s (Figure 4.2b). The bar structure fades away completely at the deposition rate of 5-10 Å/s when a uniform thickness film is formed (Figure 4.2c).

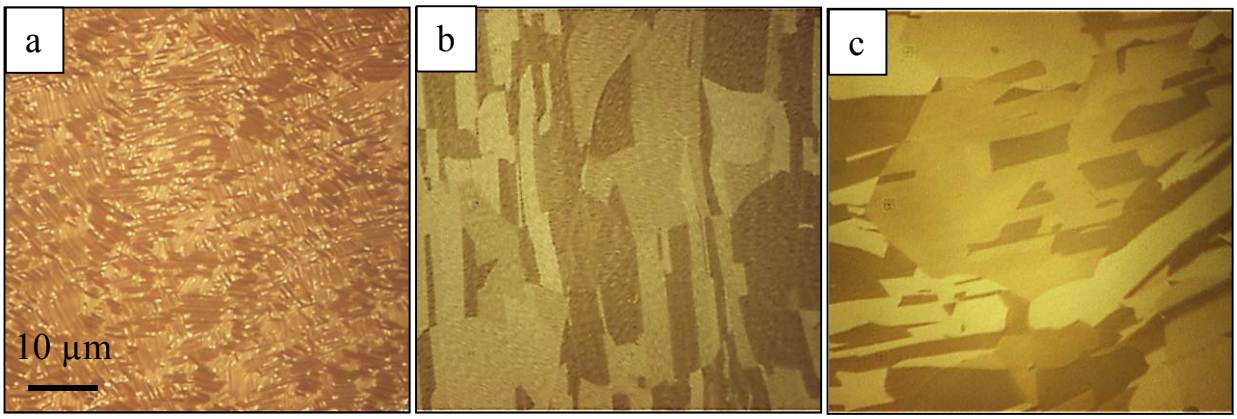

Figure 4.2 Polarized optical microscope images of a.) 50 nm C44 on HOPG(0001), deposition rate < 1 Å /s; b.) 80 nm C44 on HOPG(0001), deposition rate=2 to 5 Å/s; c.) 80 nm C44 on HOPG(0001), deposition rate=5 to 10 Å/s. Substrate temperature is 41 °C for images (a) to (c).

The trend seen in Figure 4.2 is almost repeated in Figure 4.3 in which C44 is grown on HOPG(0001) at the substrate temperature of 55 °C. At low deposition rate, (< 1 Å/s) (Figure 4.3a), the 6-fold symmetric ordered bar structure is more pronounced compared to that in Figure 4.2a. By increasing the deposition rate to 2-5 Å/s (Figure 4.3b) and 5-10 Å/s (Figure 4.3c) bars get denser and narrower but they do not fade away completely.

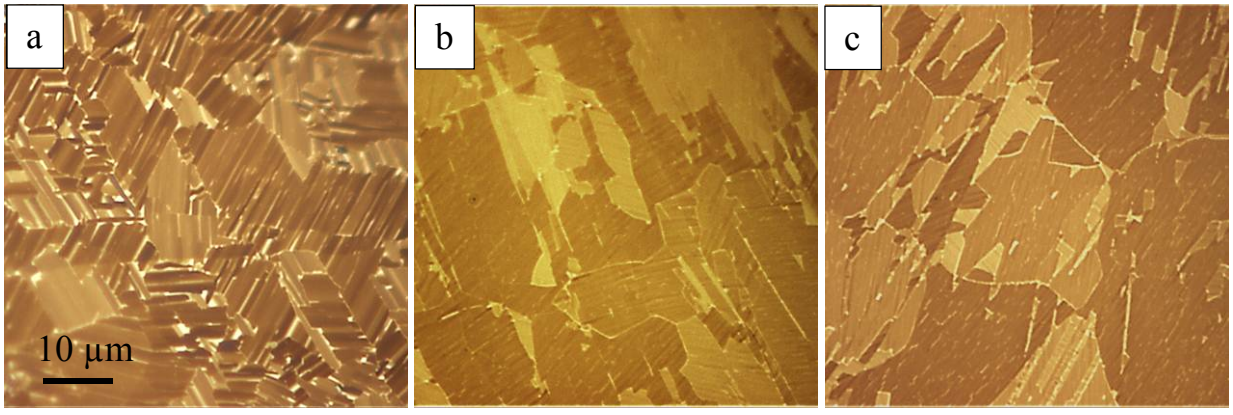

Figure 4.3 Polarized optical microscope images of a.) 50 nm C44 on HOPG(0001), deposition rate < 1 Å/s; b.) 28 nm C44 on HOPG(0001), deposition rate=2 to 5 Å/s; c.) 50 nm C44 on HOPG(0001), deposition rate=5 to 10 Å/s. Substrate temperature is 55 °C for images (a) to (c).

Figure 4.4a shows that C44 grows in the form of pseudo-rectangular disordered film on HOPG(0001) at the substrate temperature of 59 °C. Increasing the deposition rate to 5-10 Å/s (Figure 4.4b) and 10-25 Å/s (Figure 4.4c) makes the disordered features become denser, but no other changes in the structure are observed.

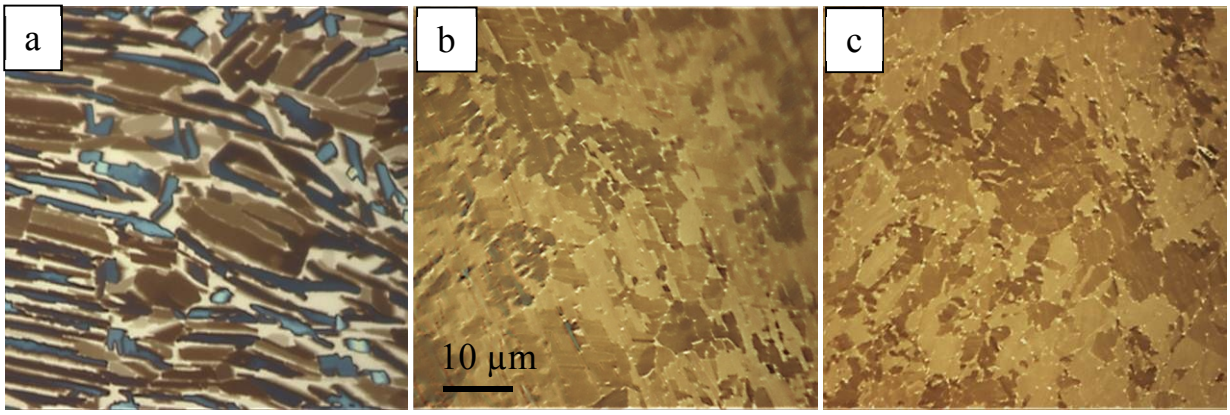

Figure 4.4 Polarized optical microscope images of a.) 50 nm C44 on HOPG(0001) at 61 °C, deposition rate < 1 Å/s; b.) 100 nm C44 on HOPG(0001) at 61 °C, deposition rate = 5 to 10 Å/s; c.) 100 nm C44 on HOPG(0001) at 59 °C, deposition rate =10 to 25 Å/s.

4.1.2 Discussion of results related to the variable deposition rate

The results of varying deposition rate were described in §4.1.1. At each one of Figures 4.1 to 4.4, the deposition rate is varied at a constant substrate temperature for a film of C44 on HOPG(0001). At any single substrate temperatures of 25, 41 and 55 °C, the trend of morphology change with deposition rate is inversely related with that was seen for structure changes of C44 thin film with substrate temperature (Figure 2, Chapter 3).[69] The general trend of morphology change of an *n*-alkane film by substrate temperature includes the following structures: small uniform thickness domains, larger uniform thickness domains, dense and narrow bars, separated and wider bars, pseudo-rectangular domains and normally oriented continuous film.

At the lowest substrate temperature explored (25 °C), as shown in Figure 4.1, a higher deposition rate causes the decrease of the domain size of the uniform thickness film of C44 on HOPG(0001). It is assumed that nucleation density is larger at higher deposition rate. A similar trend was seen by Fu and Urquhart,[63] as an increase in the domain size of C60 thin film on NaCl(001) by increasing the substrate temperature.

At a higher substrate temperature of 41 °C, as shown in Figure 4.2, increasing the deposition rate influences the morphology in a different manner than in Figure 4.1. At this temperature, increasing deposition rate does not simply show changes in the domain size but shows the morphology change of C44 on HOPG(0001). The trend of morphology variation in Figure 4.2 looks as if the substrate temperature has been reduced, because it transforms from wide bars to narrower bars and finally to the uniform thickness film from left to right. Since the morphology is bar structure in Figure 4.2a but uniform thickness film in Figure 4.2c, it can be deduced that at a constant substrate temperature, *n*-alkane molecules need enough time to diffuse on the surface and form the bar structure otherwise the upcoming molecules land on the surface successively and form the uniform thickness structure. Forrest[13] has reported that substrate temperature influences the molecular diffusion along the surface, and the balance between adsorption rate and surface diffusion determines the roughness of the morphology.

Figure 4.3 (substrate temperature is 55 °C) shows a trend similar to Figure 4.2 except that it does not show the uniform thickness morphology even with the deposition rate of 5-10 Å/s.

The morphology variation of C44 on HOPG(0001) with deposition rate at the substrate temperature of 59 °C is presented in Figure 4.4. These results are different from the trend seen in the lower temperature deposition. Figure 4.4 shows these structures are not epitaxial and that C44 forms pseudo-rectangular structure at low deposition rate (Figure 4.4a) and a dense and

disordered structure at the higher deposition rates (Figures 4.4b and 4.4c). Increasing the rate of deposition does not return the morphology back to epitaxial growth conditions with a signature of ordered bar structure as if a lower substrate temperature would do. This result indicates that at the substrate temperature of 59 °C, the alkane-graphite enthalpic forces are not as strong as required for epitaxial growth. It is hypothesized that the weaker interaction is due to *n*-alkane conformational entropy at higher temperature and the deviation from an all-*trans* state. As the number of *n*-alkane segments with gauche conformation increases with substrate temperature, fewer methylene groups interact with HOPG(0001) and consequently epitaxial growth of *n*-alkane on the surface of graphite is lost.

Another phenomenon that can be distinguished by comparing Figures 4.2 to 4.4 is that increasing the deposition rate results in the formation of a denser and smoother structure. It can be concluded that the growth mode is Stranski-Krastanov (layer-plus-island) at a low deposition rate (*n*-alkane forms bar structure), and Frank-van der Merwe (layer-by-layer) at the higher deposition rate (*n*-alkane forms uniform thickness film). It can be generalized such that layer-by-layer growth mode occurs at the higher supersaturation, while the layer-plus-island mode happens at the lower supersaturation. This conclusion is in contrary to the model by Venables et al.[9] in which they suggested that layer-by-layer growth mode happens at low supersaturation due to stronger binding of adsorbate to the substrate and consequently slower re-evaporation. This leads us to conclude that *n*-alkane molecules are hypothetically under lattice strain in the uniform thickness film due to crystallization in a form different than their natural crystalline form (orthorhombic) on HOPG(0001). The strained form of crystallization happens because of energetic gain of epitaxial growth. This hypothesis will be discussed in more details in §4.2.

In each of the Figures 4.1 to 4.4 it is assumed that by keeping the substrate temperature constant, the molecular mobility is also constant. Therefore, it can be concluded that lower deposition rate enables the deposit molecules to grow in the more thermodynamically stable form by providing the time for re-evaporation and re-orientation. Nozaki et al.[76] have investigated the substrate temperature along with deposition rate as two growth parameters. They observed that at a high substrate temperature and low deposition rate, normal orientation (the thermodynamically stable state) is predominant. They also observed that at a low substrate temperature and high deposition rate the *n*-alkane film is formed of a combined structure of normal and lateral orientations (metastable state).

4.2 The origin of bar formation

In the process of transformation from uniform thickness film to the bar structure, re-evaporation and re-orientation are assumed to be the growth parameters that initiate the formation of bar structure at the high substrate temperature or low deposition rate. In addition to the re-evaporation and re-orientation (kinetic parameters), a thermodynamic factor is required to govern the stability of bar structure over the uniform thickness film at low supesatuartion. Two hypotheses are provided for the stability of the bar structure. The first reasoning is attributed to the different crystal structures of *n*-alkane in the uniform thickness film and in the bar structure; and the second reasoning is related to the relative strength of alkane-alkane interactions in <001> and <hk0> directions.

4.2.1 First hypothesis for bar formation

n-Alkane in the bar structures grows in Stranski-Krastanov growth mode which consists one (or few) complete monolayer(s) upon which bar-like islands grow.[78] As mentioned in

Chapter 1 any reason that prevents the first monolayer to grow into a bulk crystal in layer-by-layer mode can govern the island formation. In the current system the lattice parameters of *n*-alkane crystal structure are different between the partially commensurate monolayer and the bulk crystal and potentially can be responsible for the island formation.

n-Alkanes, C_nH_{2n+2}, with *n* (even) ≥ 36 and *n* (odd) crystalize in the centred orthorhombic structure in the bulk as shown in Figure 4.5. The distance between two neighboring molecules on the {101} surface of orthorhombic *n*-alkane crystal is 0.50 nm.[78,79] It can be assumed that *n*-alkanes in the bar-like crystallites are also in orthorhombic structure in which carbon planes of 4 chains are parallel to the surface and the fifth carbon plane in the centre of unit cell is perpendicular to the surface.

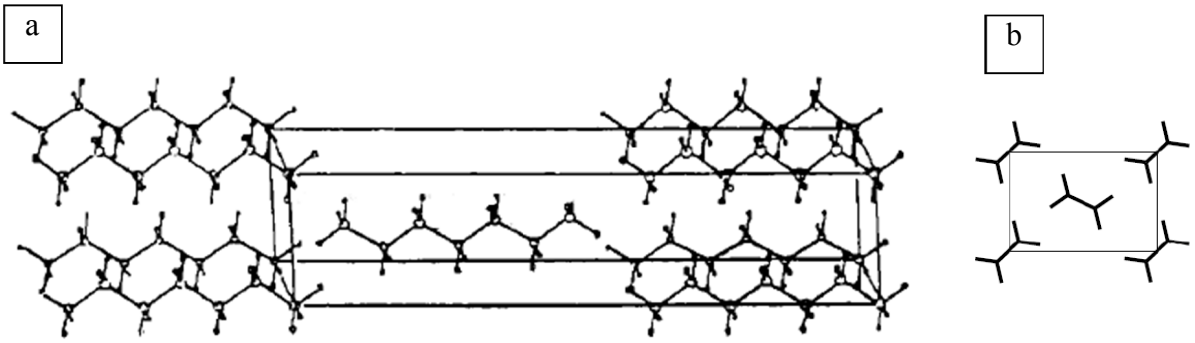

Figure 4.5 a.) Top view of the centred orthorhombic crystal structure of *n*-heptane. Figure adapted from Ref. 80; b.) side view of *n*-alkane centred orthorhombic crystal structure.

Endo et al.[81] have reported that in a monolayer of C36 lying on HOPG(0001) the carbon plane of *n*-alkane molecules changes randomly from flat-on to edge-on and vice versa such that the width of a single molecule on graphite surface varies between 0.426 and 0.630 nm (Figure 4.6).

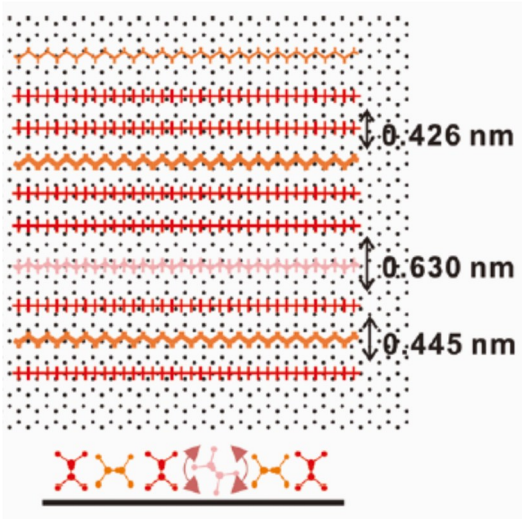

Figure 4.6 Structural model for C36 monolayer on HOPG(0001). Figure reprinted from Ref. 81 with permission.

It can be postulated that the lower number of rotationally displaced molecules (flat-on to edge-on) at low substrate temperatures makes the alkane-graphite enthalpic forces stronger and gives a relatively fixed spacing between neighboring molecules. On the other hand, the diffusion rate is also lower at low temperatures, which leads to the formation of uniform thickness film. It is assumed that the *n*-alkane crystalizes in a structure different from its natural form at the expense of achieving partial commensurism. In contrast, it is assumed that by increasing the substrate temperature, the number of rotated molecules (flat-on to edge-on) increases and makes the growth of a subsequent complete monolayer unfavorable. Higher molecular diffusion should favor the structural transformation from a uniform thickness film to the bar structure film due to formation of thermodynamically stable *n*-alkane crystal in its natural form (orthorhombic crystal). Consistent with this hypothesis, it was reported[3] that if the crystalline structure of a thin organic film is very different from its stable bulk structure; the resultant lattice strain will relaxed early in the growth stages by uncontrolled formation of islands. Likewise, Wetterer et al.[82] reported that the probability of *n*-alkane adsorption on Au(111) is decreased at higher substrate

temperatures due to incomplete accommodation by the surface which emphasizes the role of surface diffusion in the island formation.

In summary, it can be concluded that if the diffusion barrier is overcome, the thermodynamically stable packing of *n*-alkane molecules (natural form of *n*-alkane crystal) is the driving force for bar structure formation.

4.2.2 Second hypothesis for bar formation

Kubono and Okui[83] and Fu and Urquhart[63] reported that in the formation of oriented bars the growth rate along <00l>, which is parallel to the molecular axis, is negligibly small in comparison with those along <hk0> direction, which is perpendicular to the molecular axis.[83] It can be hypothesized that at low substrate temperature (high deposition rate) the growth rates along <001> and <hk0> directions are comparable because there is not enough thermal energy (time) to cause the molecules along <00l> re-evaporate and diffuse to the positions along <hk0> direction. This isotropic growth is in favour of uniform thickness film formation. In contrast, at high substrate temperature (low deposition rate) the re-evaporation and diffusion processes will displace loosely bound molecules (via CH_3-CH_3 end groups) along the <00l> direction from which they join the clusters along the <hk0> direction in which the stronger side-by-side alkane interactions satisfies thermodynamic stability. The higher rate of growth along one direction rationalizes the formation of bar structure, in which *n*-alkane chains are oriented normal to the longitudinal direction of each bar element.

In summary, *n*-alkane uniform thickness film grows at low substrate temperatures due to comparable growth rates in <00l> and <hk0> directions, but bar structure grows at higher substrate temperatures for which the growth rate along the <hk0> direction is much higher than the growth rate along the <00l> direction due to higher re-evaporation and diffusion rates.

4.3 The effect of annealing on the molecular orientation after *n*-alkane film growth

In the previous section, it was hypothesized that re-evaporation and re-orientation of *n*-alkane molecules during growth on HOPG(0001) transforms the structure from a uniform thickness film to oriented bar structure. Likewise, it is hypothesized that *n*-alkane thin film orientation can change from lateral to normal by annealing after the completion of *n*-alkane film growth on HOPG(0001). To test this hypothesis, a sample containing both bar structures and normally oriented domains was chosen. Figure 4.7a is the optical microscope image of a 26 nm C36 film grown on HOPG(0001)/SiO_2/Si (flakes of HOPG were transferred from scotch tape onto Si wafer with 300 nm oxide layer) at 60 ºC. In this image, the morphology of the C36 film is formed of combined orientations of lateral and normal, shown as bar structure and continuous flat domains respectively. Since normal orientation is the thermodynamically stable form, it is expected that the bar structure transforms to the normal orientation by annealing at the temperatures above 65 ºC. This is the temperature at which C36 forms normally oriented film when grow directly on HOPG(0001). (Figure 1e, Chapter 3).

As shown in Figures 4.7b to 4.7d, by annealing the film with the mixed bar and normal structures at temperatures up to 73 ºC, the bar structure has no tendency to transform to the normal orientation. At this point it seems that the thin normally oriented domains are evaporated and the bars are partially melted. Annealing after 78 ºC causes the evaporation of bar structure in a higher rate than the normally oriented domains (Figures 4.7e to 4.7g). In Figure 4.7g there are no more bar structures and only a small portion of normally oriented domains left which evaporate completely at 81 ºC (Figure 4.7h). Kubono et al.[7] also reported that the orientational change of alkanes during annealing occurs for the nuclei that are not larger than four molecules

and as the nuclei grow larger annealing can no longer affect the orientation of *n*-alkane film. This observation is concluded here.

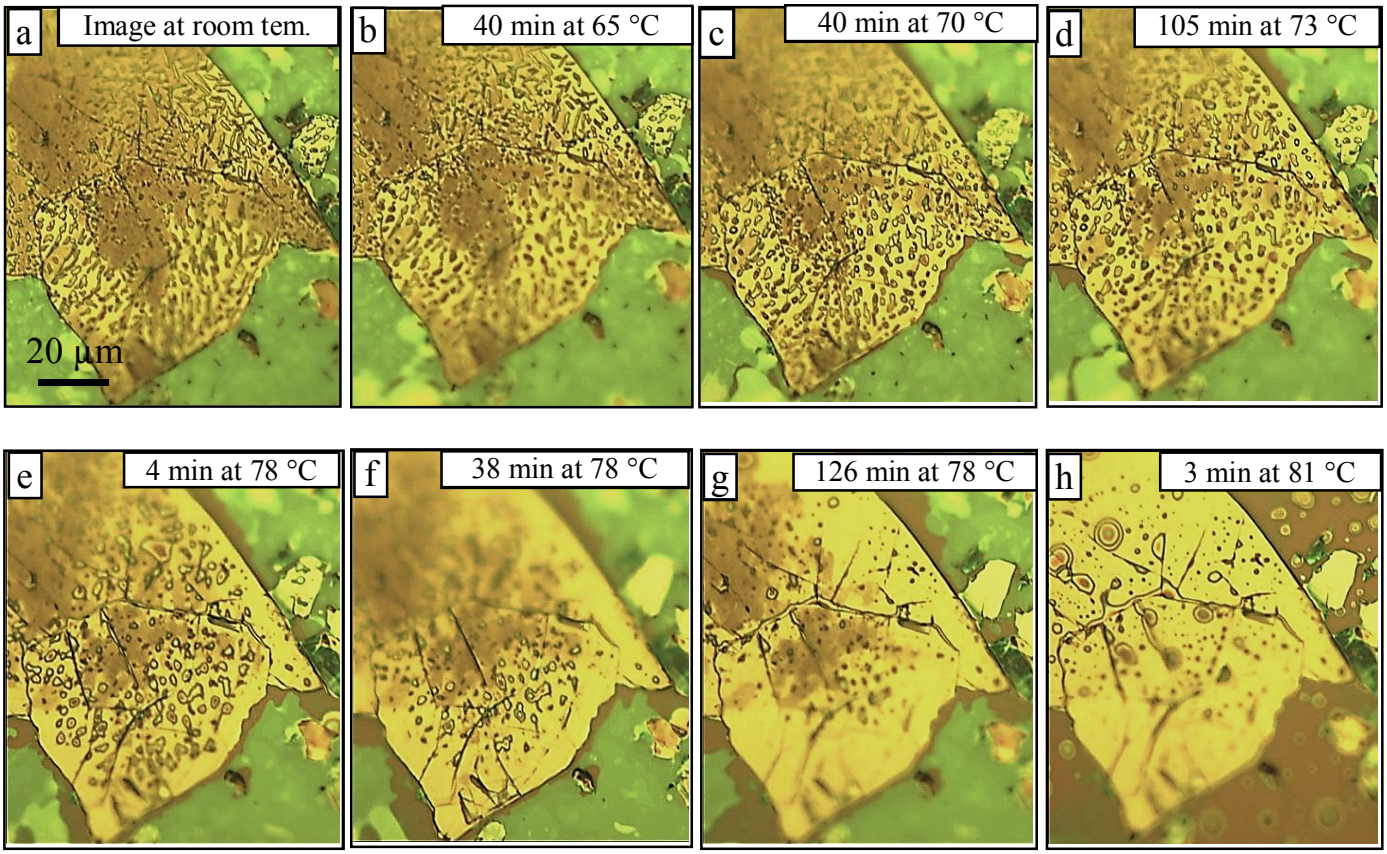

Figure 4.7 Annealing process of 26 nm C36 grown on HOPG(0001)/SiO_2/Si at 60 °C. The optical microscope images (a) to (h) show the trend of annealing at the temperatures of 65 to 81 °C by time.

CHAPTER 5: INDIRECT EPITAXY OF *N*-ALKANE FILMS ON GRAPHITE THROUGH ORGANIC AND METALLIC THIN FILMS

5.1 Why indirect epitaxy?

Any substrate has intrinsic properties that limit the morphology and orientation of films deposited on them. As explained in §1.10.3, a modification of the HOPG(0001) surface is proposed to maintain *n*-alkane epitaxial growth in a larger substrate temperature range. The term of *indirect epitaxy* will be referred to the condition at which *n*-alkane film is grown epitaxially on top of the highly ordered substrates (HOPG(0001) and NaCl(001)) covered with a thin intervening film of different materials. It is generally hypothesized that the middle layer does not apply a preferential structure to the *n*-alkane and acts as a surface modifier. In the current chapter, indirect epitaxy is used to change the *n*-alkane film morphology by altering the surface properties of HOPG(0001) when the molecular mobility of *n*-alkane deposit is too low or too high at the low and high substrate temperatures respectively. As shown in Chapter 3, at lower substrate temperatures epitaxial growth of *n*-alkane occurs in the form of uniform thickness oriented film presumably due to lower molecular mobility. It is intended to investigate the possibility of modifying the surface of HOPG(0001) with an organic thin film that hypothetically improves the molecular mobility of deposit at low substrate temperatures resulting in the formation of the bar-like structures. Also it was shown that epitaxial growth is lost at high substrate temperatures. The surface of HOPG(0001) will be treated with a thin metal film to increase the deposit-substrate interactions so that *n*-alkane grows in the ordered bar structure with epitaxial 6-fold symmetry at higher substrate temperatures.

In §5.2 the surface of HOPG(0001) is treated with a thin film of liquid crystal. It is hypothesized that liquid crystal can act as a lubricant and increase the surface diffusion when *n*-

alkane molecules are deposited at low substrate temperatures. The results of §5.2 will reveal that the liquid crystal forms an ordered template on HOPG(0001), upon which *n*-alkane grows in 6-fold symmetric bar structure. Based on the results obtained in §5.2 another approach is taken in §5.3 to form an ordered bar-like template on HOPG(0001) at low temperatures. In this section the effect of a short *n*-alkane pre-layer on the morphology of subsequent longer *n*-alkane is studied. And finally in §5.4 indirect epitaxy of *n*-alkane films on HOPG(0001) is examined through some metal thin films. It is hypothesized that a metal thin film can improve the strength of alkane-HOPG(0001) van der Waals interactions by providing higher polarizability. It is assumed that stronger attractive forces between the modified substrate and *n*-alkane film can make *n*-alkane grow epitaxially on HOPG(0001) when epitaxy is lost at high substrate temperatures during deposition.

5.2 Epitaxial growth of *n*-alkane on the liquid crystal coated HOPG(0001)

5.2.1 Introduction

As it was seen in Chapter 3, the predominant morphology of *n*-alkane grown at lower substrate temperatures is oriented uniform thickness film with three level of contrast originating from the 6-fold symmetry of HOPG(0001) (Chapter 3, Figures 1a, 2a, 2b, 3a, 4a and 4b). It was seen that at the higher substrate temperatures during deposition, *n*-alkane molecules can form triangular oriented bar structure, which is also a signature of epitaxy on the 6-fold symmetry structure of HOPG(0001).

In this part of study, the substrate temperature will be kept low and the surface mobility will be increased by treating the surface of substrate. A surface treatment that can maintain the high surface mobility of *n*-alkane deposit on the graphite surface can be used to modify the

growth of *n*-alkane. A liquid crystal thin film is known as industrial lubricant and can be a candidate for the treatment of graphite surface. *n*-Alkane molecules have limited translational and rotational mobility on a bare HOPG(0001) surface at low substrate temperatures but are hypothesized to diffuse easily on a liquid crystal coated HOPG(0001). It is also assumed that attractive forces of HOPG(0001) can act through the thin film of liquid crystal to order the *n*-alkane molecules grown on top of the liquid crystal coated HOPG(0001). The liquid crystal that was used to change the alkane-graphite interface was (4-cyano-4`-octyl-biphenyl) (8CB) with the molecular structure of:

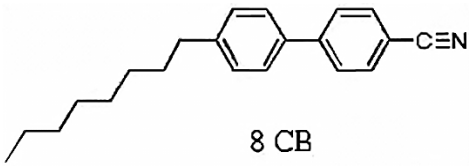

8 CB

Since in this experiment the optimum thickness of liquid crystal film was unknown, a gradient of liquid crystal thickness was made on a square piece of HOPG(0001) (10 x 10 x 2 mm) by putting a small drop of liquid crystal on the HOPG(0001) and diluting it with a drop of ethanol. The results of *n*-alkane epitaxial growth on the liquid crystal coated HOPG(0001) is presented below.

5.2.2 Results and discussion of *n*-alkane epitaxial growth on the liquid crystal coated HOPG(0001)

Growing an *n*-alkane thin film on HOPG(0001) with the varying thickness of liquid crystal coating produces disordered structure in the parts of HOPG(0001) covered with very thin and very thick liquid crystal film (results not shown). There is an optimum thickness of liquid crystal on HOPG(0001), upon which the subsequent *n*-alkane film forms a very ordered 6-fold

symmetric bar structure. Figure 5.1 shows the optical microscope images of *n*-alkanes C36, C44 and C50 on the bare HOPG(0001) and liquid crystal coated HOPG(0001) at the substrate temperatures of 22 °C (Figures 5.1a and 5.1b, T_{SC} =53.8 °C), 30 °C (Figures 5.1c and 5.1d, T_{SC} =55.6 °C) and 46 °C (Figures 5.1e and 5.1f, T_{SC} =46.1 °C) respectively. It is clear that a thin layer of the liquid crystal 8CB changes the uniform thickness oriented morphology of *n*-alkanes to the oriented bars with 6-fold symmetry structures.

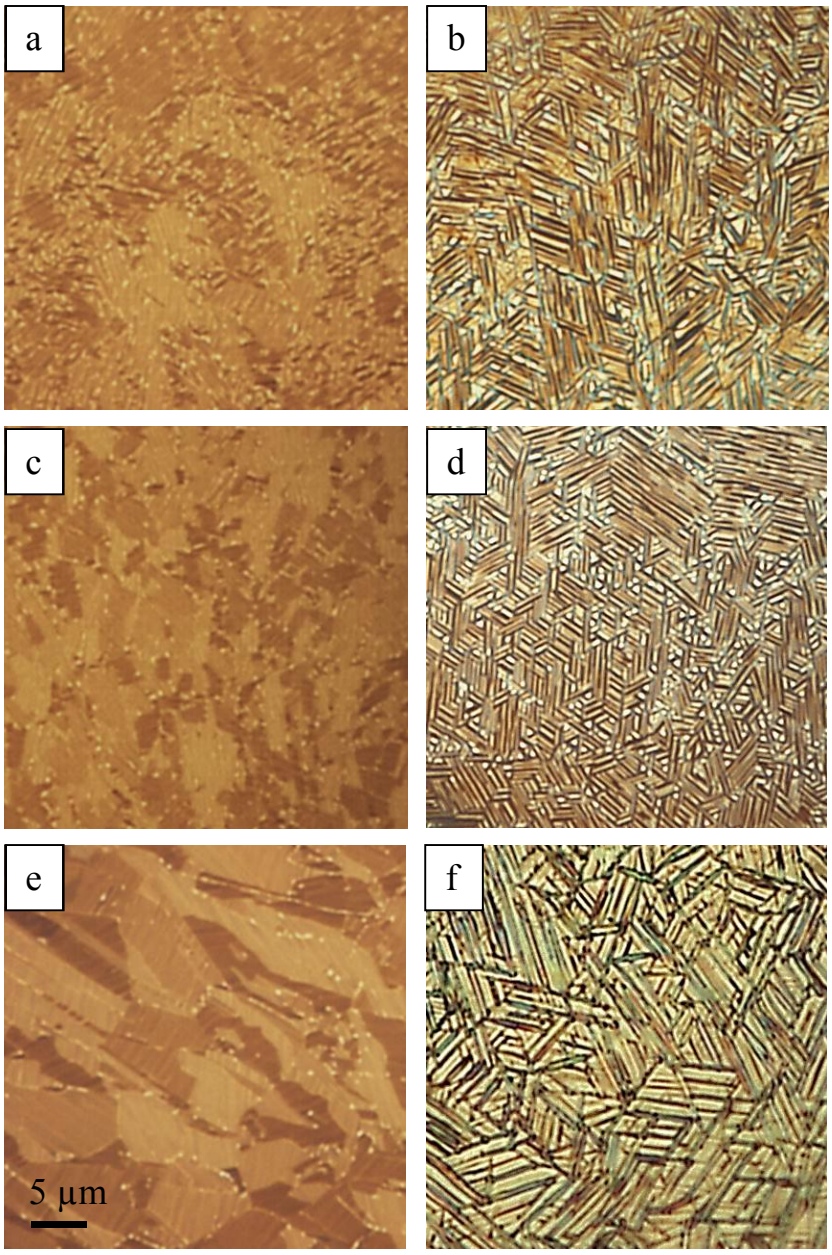

Figure 5.1 Polarized optical microscope images of *n*-alkane grown on the bare HOPG(0001) (left hand side column) and on the liquid crystal coated HOPG(0001) (right hand side column), a.) C36 deposited on bare HOPG(0001) at 22 °C; b.) C36 deposited on LC coated HOPG(0001) at 22 °C; c.) C44 deposited on bare HOPG(0001) at 30 °C; d.) C44 deposited on LC coated HOPG(0001) at 30 °C; e.) C50 deposited on bare HOPG(0001) at 46 °C; f.) C50 deposited on LC coated HOPG(0001) at 46 °C. The thickness of all *n*-alkane films is 50 nm.

In addition to the results shown in Figure 5.1, there is another series of results that modified our understanding towards the role of liquid crystal interlayer in *n*-alkane indirect

epitaxial growth on HOPG(0001). Zuhaib[84] has reported that C40 forms an ordered 6-fold symmetric bar structure on the liquid crystal coated HOPG(0001) at 50 °C (Figure 5.2b). Figure 5.2a shows that C40 forms pseudo-rectangular structure without any order when grown at the substrate temperature of 50 °C on bare HOPG(0001), similar to the results that were presented in Chapter 3.

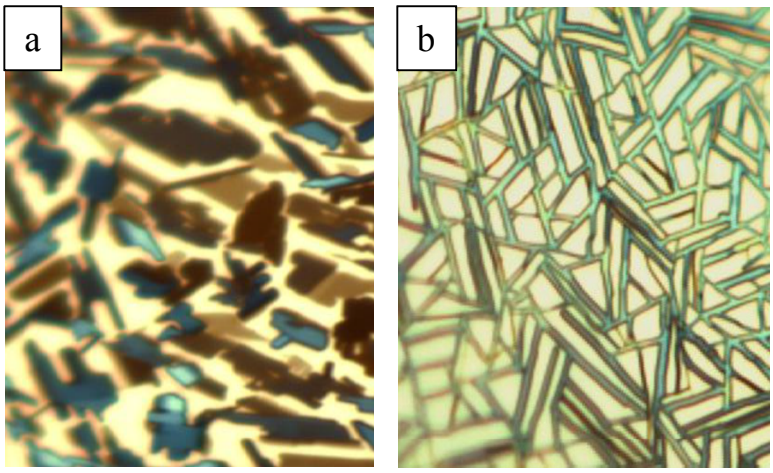

Figure 5.2 a.) 50 nm C40 grown on HOPG(0001); b.) 50 nm C40 grown on the liquid crystal coated HOPG(0001). Both of samples were grown at 50 °C. Figures reprinted from Ref. 84 with permission.

Figures 5.1 and 5.2 show that *n*-alkane forms 6-fold symmetric bar structure on the liquid crystal coated HOPG(0001) at both low and high substrate temperatures during deposition. It can be concluded that liquid crystal is not acting as a lubricant, because molecular mobility at higher substrate temperature should be high enough with the lack of liquid crystal "lubricant". Therefore the higher degree of order of *n*-alkane thin films on HOPG(0001) in the presence of liquid crystal film can be attributed to the formation of an ordered 6-fold symmetric template, upon which the subsequent *n*-alkane growth proceeds. Hickman et al.[85] reported that orientational order of a C40 monolayer can be controlled by deposition of C40 onto a monolayer

of 8CB liquid crystal on HOPG(0001) at the substrate temperature of 36 °C. The mechanism of orientation transfer was described based on the competitive adsorption of *n*-alkane onto the template of liquid crystal on graphite. According to STM results by Hickman et al.[85] this kind of orientation communication between the *n*-alkane and liquid crystal monolayer that results in the displacement of the liquid crystal sacrificial monolayer is called orientation imprinting method. Consistent with the report of Hickman et al.[85] it is suggested that the formation of C44 ordered structures on the liquid crystal coated HOPG(0001) at low and high temperatures also follows the orientation imprinting mechanism.

5.3 Effect of a short *n*-alkane thin film on HOPG(0001) on the morphology of a subsequent longer *n*-alkane film

Introduction

The results and discussion explained in §5.2 suggest that a liquid crystal thin film forms a template on HOPG(0001) and the subsequent *n*-alkane grows on top of the pattern made by the liquid crystal. This result can be extended to the more general system in which a short *n*-alkane is used to form a template on the surface of HOPG(0001) to orient a longer *n*-alkane. Based on the results of Chapter 3, it is expected that at a specific temperature, a shorter *n*-alkane will form oriented bar structure and a longer *n*-alkane will form a uniform thickness oriented film. So similar to liquid crystal, at any substrate temperature, a thin film of a shorter *n*-alkane with ordered bar structure should have the potential to be used as a template to grow longer *n*-alkanes in the bar structure.

As a starting point on this study, C60 was chosen as the long *n*-alkane. C60 forms a uniform thickness film at the substrate temperatures below 58 °C.[69] Any shorter *n*-alkane that

forms ordered bar structure at $T_S < 58$ °C can play the role of a template. C36 forms ordered bar structure in the temperature range of 30-50 °C as shown in Figure 4 in Chapter 3, and potentially can be used to modify the surface of HOPG(0001).

This experiment is performed in two ways, explained in §5.3.1 and §5.3.2. In the first method, the short and long *n*-alkanes are deposited at two separate steps. And in the second method, the long and short *n*-alkanes are mixed before deposition and are deposited in one step. The discussion of results obtained in §5.3.1 and §5.3.2 is presented in §5.3.3.

5.3.1 Results: Effect of a short *n*-alkane pre-layer on the morphology of subsequent longer *n*-alkane on HOPG(0001)

Figure 5.3a presents C60 grown on HOPG(0001) at 40 °C, which a uniform thickness oriented film with three levels of contrast originating from 6-fold symmetry of substrate. In Figure 5.3b, C60 has been grown at 40 °C on the HOPG(0001) covered with a 5 nm film of C36 (C36 was also grown at 40 °C). In this image, C60 forms a coexisting uniform thickness oriented film and oriented bar structure. In an attempt to prepare the most ordered bar structure of C60 in the mentioned conditions, the thickness of 30 nm C36 on HOPG(0001) was found as the minimum thickness required to initiate the growth of C60 in a complete ordered bar structure (Figure 5.3c).

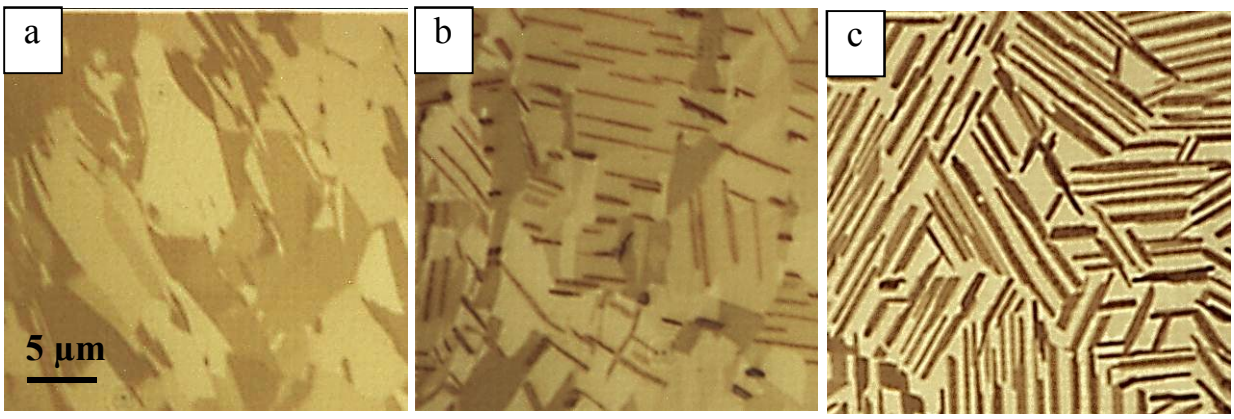

Figure 5.3 Polarized optical microscope images of a.) 50 nm C60 on bare HOPG(0001); b.) 50 nm C60 on (5 nm C36)/HOPG(0001); c.) 60 nm C60 on (30 nm C36)/HOPG(0001). Both C36 and C60 were grown at 40 °C substrate temperature.

This experiment was repeated at the lower substrate temperature of 35 °C. Figure 5.4a presents the same coexisting uniform thickness oriented film and oriented bar structure when C60 is grown on the substrate of (3 nm C36)/HOPG(0001) at 35 °C. As it was expected, applying a thicker film of C36 (10 nm) on HOPG(0001) made the subsequent C60 film grow in an ordered oriented bar structure at 35 °C (Figure 5.4b). Comparing Figures 5.3 and 5.4 implies that at lower substrate temperature a thinner film of short *n*-alkane is required to treat the surface of HOPG(0001) and grow the longer *n*-alkane film in the ordered bar structure (30 nm C36 at 40 °C, 10 nm C36 at 35 °C).

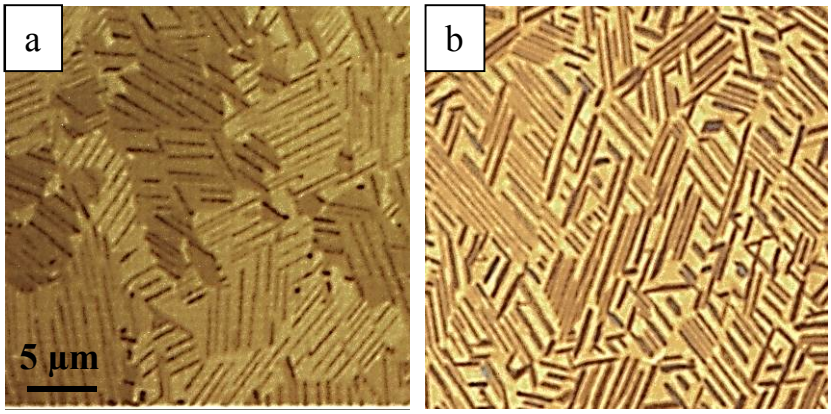

Figure 5.4 Polarized optical microscopy images of a.) 50 nm C60 on (3 nm C36)/HOPG(0001); b.) 50 nm C60 on (10 nm C36)/HOPG(0001). Both C36 and C60 were grown at 35 °C substrate temperature.

5.3.2 Results: Effect of simultaneous deposition of a mixture of short and long *n*-alkanes on HOPG(0001)

In this section, it is intended to premix the short and long *n*-alkanes and evaporate them simultaneously. This method is different from the previous section (§5.3.1) in which the long and short *n*-alkanes were deposited separately in two steps. Keeping the deposition rate as low as possible (~ 0.3 Å/s) ensures a higher vapour pressure for the shorter *n*-alkane. By depositing the short *n*-alkane before the long *n*-alkane at the initial stages of growth, the shorter *n*-alkane can form an ordered template on the HOPG(0001) surface first. By evaporating all the premixed *n*-alkanes placed in the tungsten boat, it can be assumed that the mass fraction of each *n*-alkane in the final film is similar to the initial value placed in the evaporation boat. The results of this study show the dependence of morphology to the mass ratio of two *n*-alkanes in the evaporation boat. Figure 5.5a shows a coexisting structure of the ordered bars and uniform thickness film made from a 3% (w/w) C36, 97% (w/w) C60 mixture. In Figure 5.5b, the mass fraction of the shorter *n*-alkane was increased to 33% (w/w) C36 in order to have more C36 molecules arriving on the surface of HOPG(0001) before C60 and form a stable template. Successfully higher

mass% of C36 in the mixture caused that the growth of C60 proceed in the ordered 6-fold symmetry bar structure.

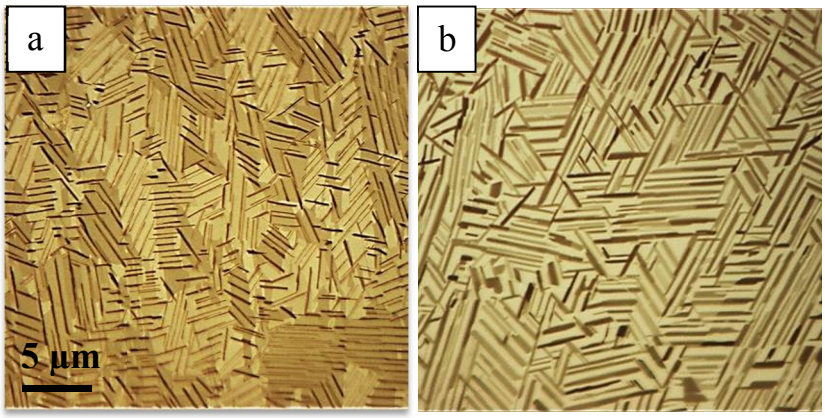

Figure 5.5 Optical microscopy images of a.) (0.1 mg C36) + (2.9 mg C60) deposited simultaneously on HOPG(0001) at 35 °C (C36/C60=3/97 %w/w); b.) (1 mg C36) + (2 mg C60) deposited simultaneously on HOPG(0001) at 35 °C (C36/C60=33/67 %w/w).

5.3.3 Discussion of the results for morphology variation of a long *n*-alkane film grown on HOPG(0001) modified with a thin film of a shorter *n*-alkane

In §5.3.1, the results present a successful morphology change of the long *n*-alkane (C60) by growing it on top of the C36 coated HOPG(0001). In the case that the thickness of C36 film is very low, the coexisting morphology implies that C60 can partially substitute the thin film of C36 and form the structure that it would make in the absence of C36, i.e. a uniform thickness oriented film. However, when C60 is grown on a thicker film of C36/HOPG(0001), it grows preferentially on the pre-formed template of C36 with the oriented bar structure.

In §5.3.2 the goal of forming an ordered template on HOPG(0001) with a short *n*-alkane to change the morphology of the subsequently deposited longer *n*-alkane from uniform thickness oriented film to the oriented bar structure was approached in an alternate way. Opposed to the previous part (§5.3.1), two *n*-alkanes with different chain lengths were not deposited separately

but were mixed together and evaporated simultaneously. Results show a combined morphology of uniform thickness oriented film and oriented bar structure at the small fraction of the shorter *n*-alkane in the mixture (3% w/w C36). It implies that C60 can displace the very thin film of C36 and become adsorbed on the surface of HOPG(0001) because of stronger enthalpic interactions. However, if C36 is a larger mass fraction of the material to be deposited (33% w/w C36), then it forms a robust pre-layer and C60 grows on top the pre-formed oriented bar structured template.

In summary, Figures 5.3, 5.4 and 5.5 suggest that a thin film of a short *n*-alkane (pre-made or in situ) can act as a template to cause a longer *n*-alkane grow in bar structure on HOPG(0001) at low substrate temperatures. Figure 5.6 illustrates the schematic morphology change of a long *n*-alkane when it is evaporated indirectly on the HOPG(0001) modified with a thin film of a shorter *n*-alkane.

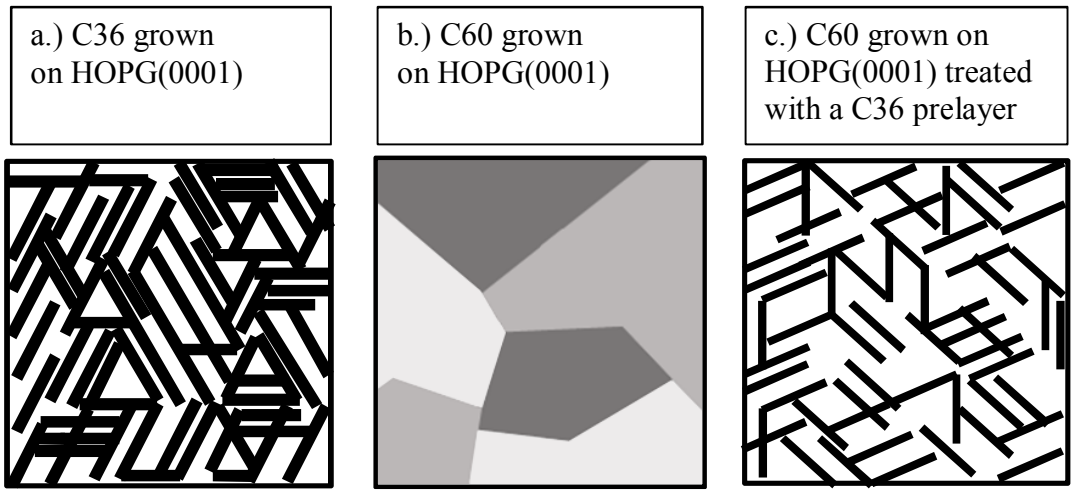

Figure 5.6 Schematic have a HOPG(0001) surface treatment with a C36 thin film that changes the morphology of the subsequently grown C60 film from a uniform thickness film to an oriented bar structure.

Groszek[64] has reported the preferential adsorption of the longer *n*-alkane when he was studying the adsorption heat of C32 from a *n*-heptane solution. His measurements have shown that C32 displaces *n*-heptane molecules from the surface of graphite and lowers the potential energy of adsorption. Alba et al.[86] have worked on the preferential adsorption in a mixture of *n*-alkane and *n*-alcohol. They observed that the longer species of the alkane/alcohol mixture is adsorbed preferentially and if the chain lengths of both components are similar then alcohol is adsorbed preferentially.[86]

5.4 Why use metals for indirect epitaxy?

Metal treatment of HOPG(0001) surface was chosen based on a chance observation described below. One of the objectives sought in Chapter 3 was studying the effect of *n*-alkane chain length on the morphology and orientation of *n*-alkane thin films on the surface of graphite. The morphology of *n*-alkane thin films grown on HOPG(0001) was first studied by optical microscopy; however a X-ray transparent substrate was required to study the orientation of *n*-

alkane molecules on graphite by STXM microscopy. In order to study the samples in the STXM microscope very thin films of graphite (graphene, or 1-10 layers of graphite) were purchased as CVD grown films on the Ni coated Si wafer. To prepare a transparent substrate for STXM microscopy, graphene was transferred from Ni coated Si to Si_3N_4 window by dissolving the Ni layer in a 12 M HCl solution and picking up the floating graphene onto Si_3N_4 window and rinsing it with Millipore water. *n*-Alkane thin films were then deposited on the transparent graphene films. Graphite and graphene were expected to have similar surfaces and apply similar attractive forces to the *n*-alkane thin films grown on top of them. Opposed to what was expected, the morphologies of C28 grown at 25 °C on the 1 mm thick HOPG(0001) and on the transferred graphene were different. The C28 formed a disordered pseudo-rectangular bar structure on HOPG(0001) but an ordered 6-fold symmetric pattern with narrower bars on this graphene sample. It was hypothesized this was due to the presence of Ni contaminant originating from the undissolved film of Ni. This observation motivated us to test the positive influence of the presumed Ni thin film in the formation of ordered *n*-alkane film with a 6-fold symmetric structure.

Other than our observation, there is another reason that makes metals worthwhile to be considered for indirect epitaxy. As mentioned in §1.6, Hosoi et al.[31] reported that C44 grows on a clean metal surface in the flat-on orientation at room temperature due to attractive van der Waals interactions. Therefore the orientation that a clean metallic surface induces in an *n*-alkane thin film is similar to what HOPG(0001) does.

In summary, an experimental observation along with the literature clue for the laterally oriented *n*-alkane films on a metallic surface were the motivations towards the modification of HOPG(0001) surface with metals to drive epitaxial growth of *n*-alkane films at higher substrate

temperatures. In §5.4.1 our unusual observation for the morphology of C28 on HOPG(0001) and graphene is presented. In §5.4.2 the positive effect of the presumed undissolved Ni layer that was left on graphene will be examined in indirect epitaxy of *n*-alkane films on the HOPG(0001) coated with a few different metals thin films.

5.4.1 Initial results for metal contamination on graphene

Figure 5.7 clearly shows different morphologies for two samples of 50 nm C28 deposited on the HOPG(0001) (Figure 5.7a, pseudo-rectangular morphology) and on the graphene with a presumed undissolved Ni layer (Figure 5.7b, narrow ordered bars).

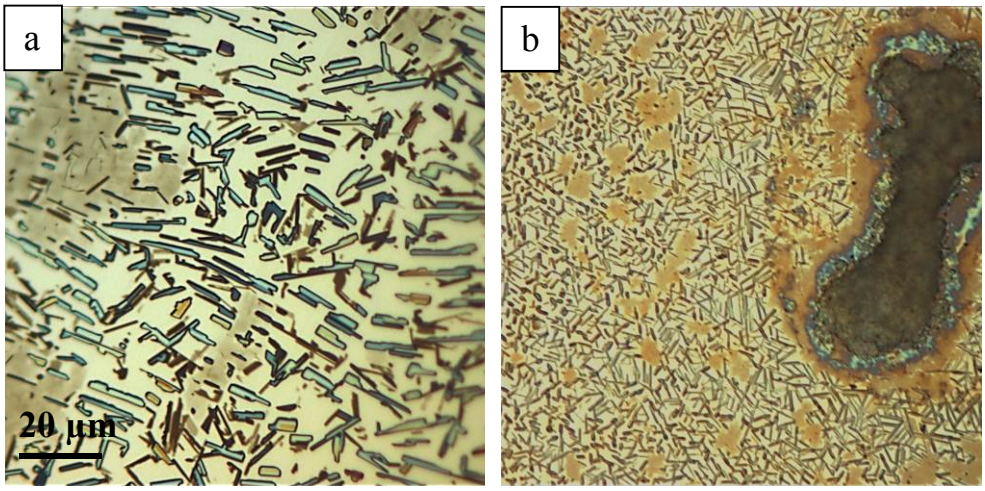

Figure 5.7 Optical microscope images of 50 nm C28 grown at 25 °C substrate temperature on a.) HOPG(0001); b.) graphene transferred from Ni onto Si_3N_4 window containing the presumed undissolved Ni.

In a closer view, Figure 5.8 shows that the C28 film located closer to the presumed Ni contamination on the graphene is more ordered than the regions that are farther from the Ni contamination. This observation led us to perform an investigation about the effect of different

metals thin films grown on graphite to improve the degree of order of the subsequent *n*-alkane thin films.

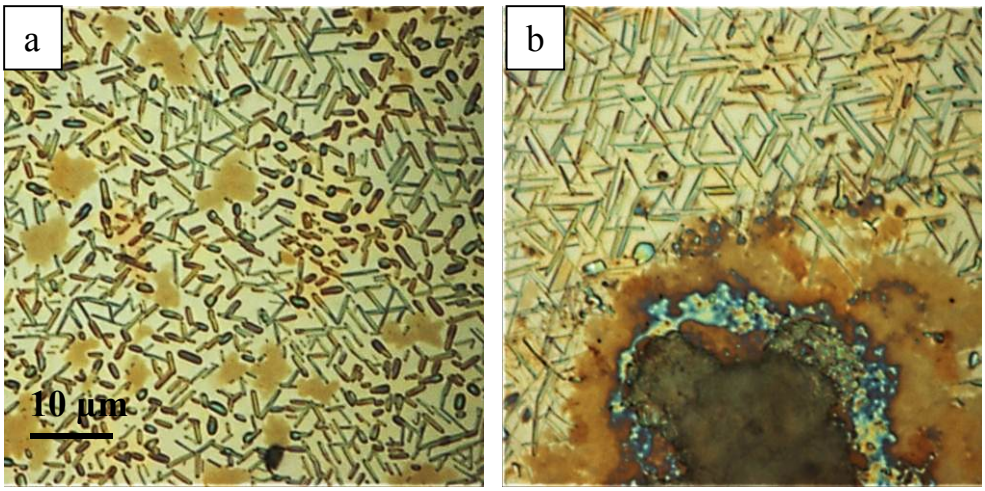

Figure 5.8 Optical microscope images of 50 nm C28 grown at 25 °C substrate temperature on graphene transferred from Ni onto Si_3N_4 window containing the undissolved Ni, a.) C28 film is farther from Ni; b.) C28 film in the immediate vicinity of undissolved Ni.

5.4.2 Investigation of morphology of *n*-alkane thin films grown on the HOPG(0001) coated with different metals

Introduction

As mentioned in §5.4.1 the C28 thin film grown on the graphene containing a presumed undissolved Ni layer shows higher degree of order at 25 °C substrate temperature. It has been postulated that a metal coating on HOPG(0001) provides a stronger van der Waals interactions towards *n*-alkane due to higher polarizability. It is also possible that the *n*-alkane molecules have lower temperature on the metal coated surface due to rapid dissipation of *n*-alkane deposition enthalpy. Therefore, the metals of Au, Cr, Pb, Bi and Se were selected based on their different thermal conductivities as shown in Table 5.1. It is intended to deposit the metallic thin films with variable thicknesses on HOPG(0001) and study the morphology of subsequent *n*-alkane film.

Table 5.1 Thermal conductivity of graphite, NaCl and metals used for indirect epitaxy.

Material	Thermal conductivity (W/m.K)	Hamaker constant (erg x 10^{+13})[87]
Au	315	45.5
Cr	93	-
Pb	34.6	21.4
Bi	7.8	-
HOPG	5.7	47.0
NaCl	5.6	-
Se	0.5	16.2

Results

In this part it will be shown that the presence of some metallic thin films on HOPG(0001) changes the morphology of *n*-alkane deposit. Figures 5.9 and 5.10 illustrate that a thin film of Au and Cr on HOPG(0001) has the largest effect on the order of subsequent C36 film, while a thin film of Pb and Bi on HOPG(0001) has a smaller effect on the degree of order of C36 film as shown in Figures 5.11 and 5.12. Figure 5.13 shows that the presence of a thin film of Se on HOPG(0001) does not improve the order of C36 deposit. Figures 5.9 to 5.12 also illustrate that for each metal, the thickness of the metal coating on HOPG(0001) surface is optimized. The C36 film has a pseudo-rectangular morphology on the bare HOPG(0001) surface and gradually transforms to the ordered 6-fold symmetric bar structure by increasing the thickness of the metal interlayer film.

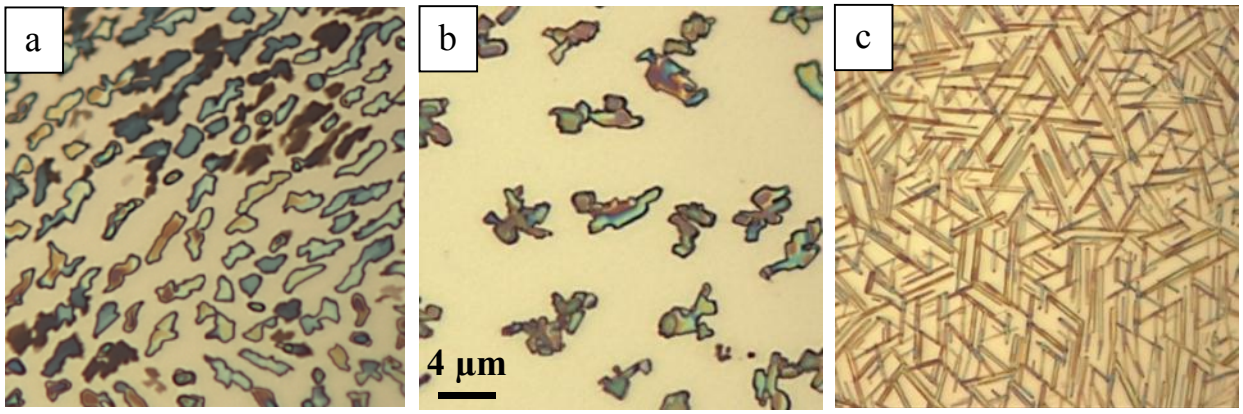

Figure 5.9 Optical microscope images of C36 deposited at 56 °C substrate temperature on the bare and Au coated HOPG(0001), a.) C36 deposited on bare HOPG(0001); b.) C36 deposited on 0.6 nm Au coated HOPG(0001); c.) C36 deposited on 3.7 nm Au coated HOPG(0001).The thickness of C36 in all samples is 50 nm.

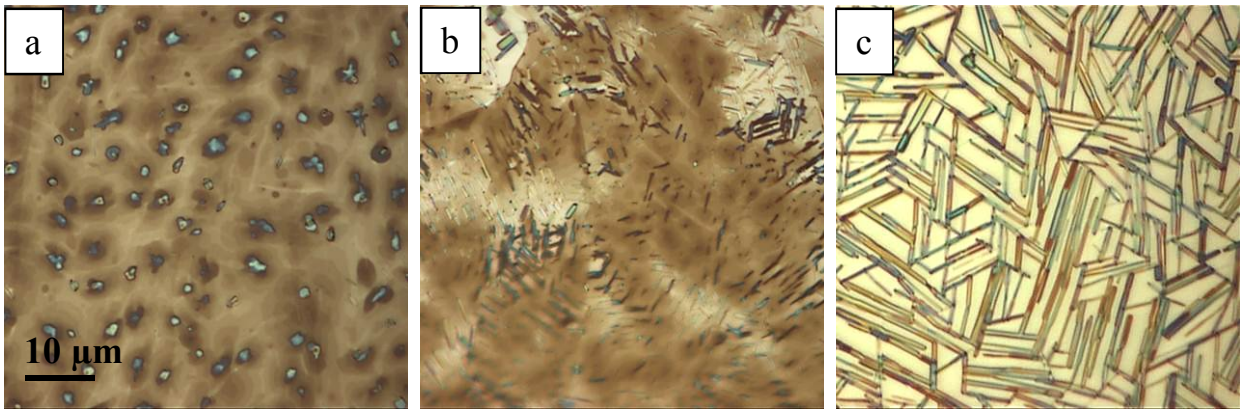

Figure 5.10 Optical microscope images of C36 deposited at 56 °C substrate temperature on the Cr coated HOPG(0001), a.) 1.2 nm Cr on HOPG(0001); b.) 0.8 nm Cr on HOPG(0001); c.) 0.5 nm Cr on HOPG(0001). The thickness of C36 in all samples is 50 nm.

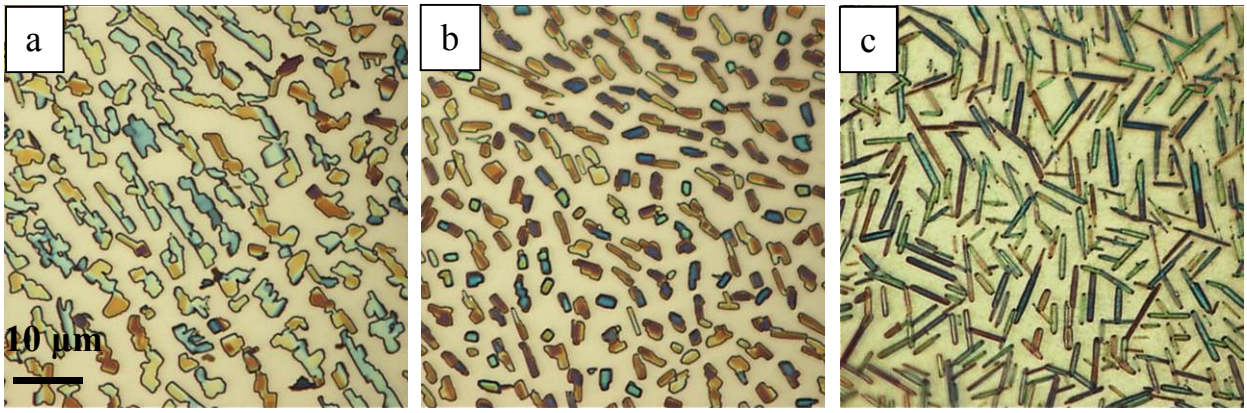

Figure 5.11 Optical microscope images of C36 deposited at 56 °C substrate temperature on the Pb coated HOPG(0001), a.) 0.7 nm Pb on HOPG(0001); b.) 2.7 nm Pb on HOPG(0001); c.) 4.7 nm Pb on HOPG(0001). The thickness of C36 in all samples is 50 nm.

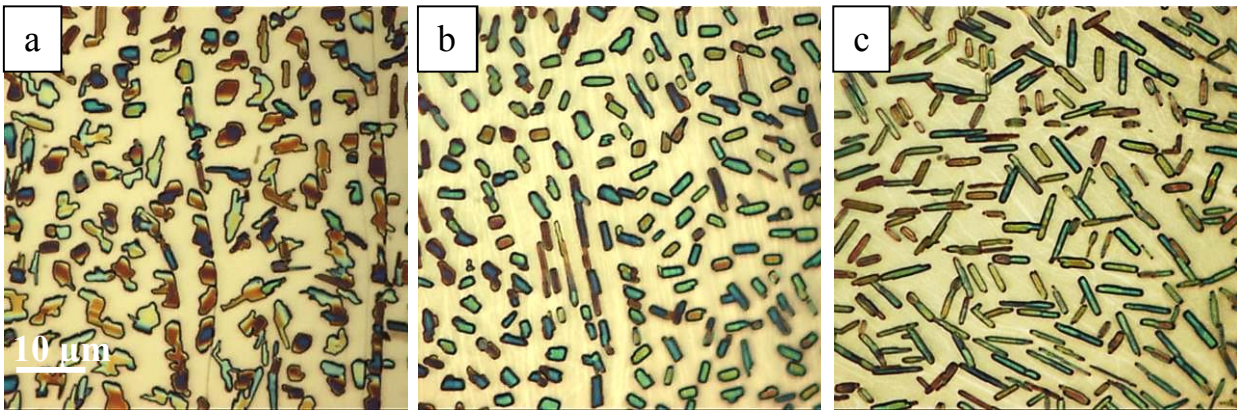

Figure 5.12 Optical microscope images of C36 deposited at 56 °C substrate temperature on the Bi coated HOPG(0001), a.) 0.5 nm Bi on HOPG(0001); b.) 2.5 nm Bi on HOPG(0001); c.) 4.5 nm Bi on HOPG(0001). The thickness of C36 in all samples is 50 nm.

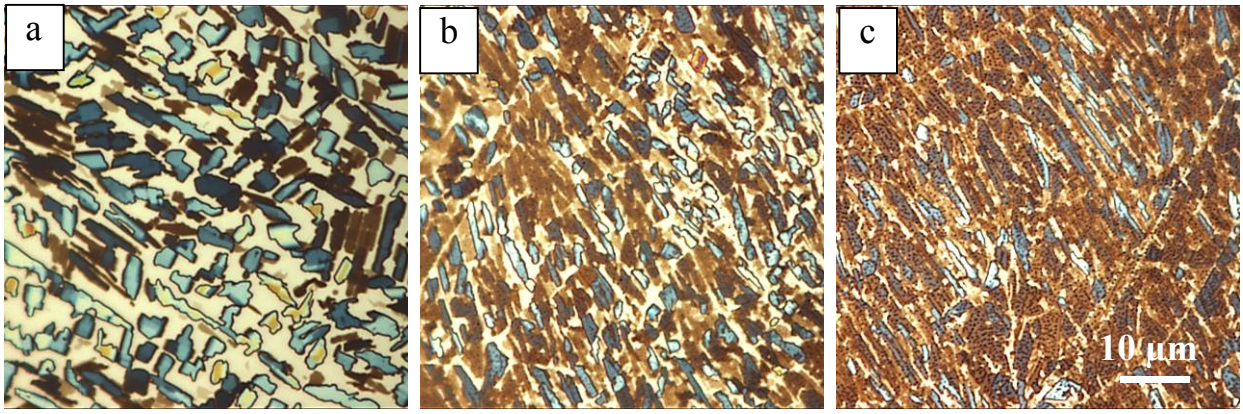

Figure 5.13 Optical microscope images of C36 deposited at 56 °C substrate temperature on the Se coated HOPG(0001), a.) 0.5 nm Se on HOPG(0001); b.) 2.5 nm Se on HOPG(0001); c.) 4.5 nm Se on HOPG(0001). The thickness of C36 in all samples is 50 nm.

Discussion

The results presented in the previous section show that a thin film of Au or Cr on HOPG(0001) can increase the order of C36 film significantly, but a thin film of Pb or Bi on HOPG(0001) increase the order of C36 thin film in a less degree and a thin film of Se on HOPG(0001) does not improve the order of C36 structure. It is hypothesized that the freely moving electron cloud of metals makes it possible to form image-dipole potential of graphite inside the metal coating and transfer the 6-fold symmetry pattern of graphite surface to the *n*-alkane deposit.

The higher order of *n*-alkane deposited on the metal coated HOPG(0001) can be attributed to two factors. First, it can be assumed that indirect interaction of graphite and *n*-alkane film is stronger across the metal film due to higher polarizability of the metals, increasing the strength of the van der Waals interactions. Second, it can be hypothesized that *n*-alkane molecules transfer their deposition enthalpy onto the metal coated HOPG(0001) faster than bare

HOPG(0001) due to the higher thermal conductivity of metals. To approve or reject any of the hypotheses, more theoretical and experimental clues have been sought that are described below.

Equation (5.1)[88,89] presents the van der Waals interaction energy between an adsorbed molecule and a surface (E_{vdw}). E_{vdw} is related to the interaction constant, C (Hamaker constant) and the distance between centres of the adsorbed molecule and surface, r.

$$E_{vdw} = \frac{-C}{r^6} \tag{5.1}$$

By comparing the Hamaker constants of a few materials, one can approximate the strength of van der Waals interaction that each one of them applies towards a specific molecule. The Hamaker constants of some of the metals investigated in this experiment are compared to HOPG(0001) in Table 5.1.The relative values of Hamaker constants of different substrates in Table 5.1 imply that HOPG(0001) on average has a higher Hamaker constant than the rest of metals. Lei et al.[90] have done desorption of a few short *n*-alkanes from HOPG(0001) and the metals of Au, Cu, Pt and Ru. They have observed that the desorption energy of short *n*-alkanes from the graphite surface is higher than all the metals mentioned. Therefore, the attractive forces between *n*-alkane and graphite are stronger than that between *n*-alkane and metals. Consequently, the more ordered structure of an *n*-alkane thin film on the metal coated HOPG(0001) cannot originate from stronger van der Waals interactions. The second hypothesis proposed to justify the higher degree of order of an *n*-alkane thin film on the metal coated HOPG(0001) is discussed below. The data presented in Table 5.1 reveals that the relative magnitudes of thermal conductivities of different metals are consistent with the degree of order of the *n*-alkane films deposited on the HOPG(0001) coated with the corresponding metals. Higher thermal conductivity of the surface of a metal coated HOPG(0001) compared to the bare HOPG(0001) results in the faster dissipation of deposition enthalpy of the *n*-alkane deposit. This

conclusion confirms the previous conclusion in §4.1.2 where it was concluded that the lack of epitaxial growth of *n*-alkane on HOPG(0001) at high substrate temperature is due to higher conformational entropy. It was assumed that larger number of alkane segments with *gauche* conformation facilitates the partial desorption of *n*-alkane chain and ends up with a weaker alkane-HOPG(0001) interaction at high substrate temperatures. Likewise, it can be assumed that faster absorption of deposition enthalpy of *n*-alkane molecules by a metal coated HOPG(0001) increases the possibility of all-*trans* conformation and in-turn increases the strength of alkane-HOPG(0001) interaction.

CHAPTER 6: INDIRECT EPITAXIAL GROWTH OF *N*-ALKANE THROUGH A GOLD THIN FILM

This section investigates the indirect molecular epitaxy of *n*-alkane thin films on Au coated NaCl(001) and HOPG(0001) surfaces. As a complementary study on the indirect epitaxy of *n*-alkane films through metals described in §5.4, this chapter is all devoted to indirect epitaxy of *n*-alkane films through a gold film. A complete series of different gold film thicknesses are examined to investigate the effect of very thin and very thick films of gold on HOPG(0001) on the structure of *n*-alkane deposit. The results also show the successful implementation of *n*-alkane indirect epitaxy on the Au coated substrates of HOPG(0001) and NaCl(001) at elevated substrate temperatures. Observation of 6-fold symmetric pattern for the *n*-alkane grown on Au coated HOPG(0001) and 4-fold symmetry for that on Au coated NaCl is a strong proof of *n*-alkane indirect epitaxy through a thin metal layer. The Au coated substrates govern the *n*-alkane epitaxial growth in the temperatures that *n*-alkane would not form ordered morphology on the bare substrates of HOPG(0001) and NaCl. This work has been submitted for publication and is presented here in its manuscript form.

The author of this thesis developed the concept of indirect epitaxy of *n*-alkane multilayer based on the literature related to inorganic systems, prepared the samples, acquired the optical microscope images and interpreted the new observations. The current document is prepared in a close collaboration with Dr. S. G. Urquhart. The author of this thesis obtained Dr. Urquhart's agreement to present the work in this thesis.

The references of this chapter are presented in the form of *(Chapter No.).(Ref. No.)*.

Indirect Molecular Epitaxy: Deposition of *n*-Alkane Thin Films on Au Coated NaCl(001) and HOPG(0001) Surfaces

Mitra Masnadi and Stephen G. Urquhart[2]

Department of Chemistry, University of Saskatchewan, Saskatoon, SK S7N 5C9, Canada

Abstract

The epitaxial growth of organic molecules can lead to the formation of complex orientated morphologies. In previous work, we studied the kinetic and thermodynamic factors that drive the epitaxial growth of *n*-alkane thin films on HOPG(0001) and NaCl(001) by physical vapor deposition. A wide variety of morphologies are observed as a function of deposition conditions (substrate temperature, *n*-alkane chain length, etc). In the current study we examine how a modified substrate (Au deposited on a HOPG(0001) or NaCl(001) substrate) affects the epitaxial growth of *n*-$C_{36}H_{74}$ (50 nm thick) relative to the uncoated substrates. This "indirect epitaxy", in which the patterned attractive forces of the substrate are transferred through a thin metal film, can tailor the conditions for epitaxial growth. The observation of 4-fold symmetry for *n*-alkane growth on Au/NaCl(001) and 6-fold symmetry for *n*-alkane growth on Au/HOPG(0001) demonstrates indirect epitaxy over a wide range of substrate temperatures during deposition.

[2] Corresponding Author, email: stephen.urquhart@usask.ca

1. Introduction:

Understanding the physical factors that determine the molecular orientation and morphology of organic thin films is important for the rational development of materials based on organic thin films. To this end, we have studied the kinetic and thermodynamic parameters involved in the epitaxial growth of *n*-alkane thin films on a variety of substrates. Physical vapour deposition (PVD) leads to a range of in-plane (lateral) or out-of-plane (normal) orientation, as a function of deposition conditions (substrate temperature, evaporation rate), substrate identity, and substrate symmetry.[6.1-6.3]

NaCl and HOPG substrates are capable of forming oriented organic overlayers through epitaxial growth. When *n*-alkanes are deposited onto NaCl(001) (4-fold symmetric surface) or HOPG(0001) (6-fold symmetric surface), oriented structures are formed with morphologies that reflect these symmetries.[6.1,6.4,6.5] In organic thin films, epitaxial growth occurs when the organic molecules (in this case, *n*-alkane chains) align along energetically favorable directions on the substrate.[6.6,6.7] We have previously studied the morphology of PVD grown thin films of *n*-$C_{36}H_{74}$, *n*-$C_{44}H_{90}$, and *n*-$C_{50}H_{102}$ (50 nm thick) on the surface of HOPG(0001) as a function of substrate temperature.[6.8] A series of characteristic morphologies were observed in this study. Linear dichroism in near edge X-ray absorption fine structure (NEXAFS) spectroscopy recorded in a Scanning Transmission X-ray Microscope (STXM) was used to confirm the molecular orientation in these characteristic morphologies. These studies show that when *n*-alkane thin films are grown on HOPG(0001), the chains adopt a laterial orientation when deposited at low substrate temperature, and a normal orientation when deposited at high substrate temperatures. In addition to the orientation changes with substrate temperature, a range of different morphologies were observed for films with the lateral chain orentation. Uniform thin films with a laterial orientation are observed at low relative substrate temperature, reflecting Frank-van der Merwe

growth.[6.9] At a higher substrate temperature, oriented bar structures reflecting Strainski-Krastanov growth are observed.[6.5,6.7,6.9] Before the on-set of normal chain orientation at higher substrate temperature, a pseudorectangular morphology is observed, in which lateral orientation is observed but the films lack epitaxial registry with the substrate. Similar results were observed by Fu and Urquhart[6.1] in the study of *n*-alkane epitaxial growth on NaCl(001).

As molecular mobility and molecule-substrate interaction strength are some of the variables that affect molecular orientation and order in organic thin films, it is of interest to explore methods to harness these variables for the controlled growth of nanostructured organic thin films. This paper explores *indirect epitaxy*, where a thin metal film (an interlayer) is deposited on top of the HOPG(0001) or NaCl(001) substrates and organic molecules are subsequently deposited on the metal interlayer. This new metal surface has different physical properties that could affect the growth of *n*-alkane thin films. If the metal overlayer is sufficiently thin, the oriented and patterned van der Waals or Coulombic force field of the substrate can be transferred through the intervening thin metal layer. Indirect epitaxy provides an opportunity to combine the directional cues of the substrate with different physical properties from the metal thin film (thermal conductivity, etc).

Distler et al.[6.10] have shown that the "electrically active network structure" of a triglycine sulphate substrate can act through an amorphous selenium thin film and epitaxially orient a subsequently deposited silver chloride thin film. The transfer of substrate forces through the intervening metal film can be justified electrostatically: the surface electric dipole will induce polarization in the metal film, which will in turn guide the epitaxial growth of subsequently deposited thin films.

To examine indirect epitaxy, we have studied the deposition of *n*-alkane overlayer on NaCl(001) or HOPG(0001) substrates, where a variable thickness intervening Au layer is present. *n*-Alkanes are examined as they can form complex, high symmetry epitaxial structures when deposited on NaCl(001) and HOPG(0001).[6.1,6.8] Well-characterized systems are essential for understanding changes in the observed structure with the presence of an intervening layer. To study the indirect epitaxial growth of *n*-alkane on an intervening metal layer, it is necessary to consider two critical questions:

- How does the NaCl(001) or HOPG(0001) substrate affect the deposition and growth of the thin metal film? If the metal grows epitaxially on the substrate surface, this structure could drive the growth of the subsequently deposited *n*-alkane thin film.
- How do *n*-alkane thin films normally grow on the metal film? Is the hypothesized "indirect epitaxy" due to the induced electrostatic cues from the substrate transmitted through the thin metal film, or is this an effect induced by the metal surface? The effect of indirect epitaxy should disappear as the film thickness increases.

In this study, thin Au films are used as the intervening layer for the study of indirect epitaxy. The (111) surface of Au is the thermodynamically most stable surface.[6.11] Au forms films with a well-known structure when deposited on HOPG(0001).[6.12,6.13] When Au is deposited on HOPG substrates, branched structures, grains and terraces are observed depending on growth condition such as substrate temperature, deposition rate and the Au thickness. In some cases, grains are oriented by cleavage steps[6.14,6.15] on the HOPG surface. Blum et al.[6.13] observed branched islands when 5-7 nm of Au is deposited on HOPG(0001) in the temperature range of 60-85 °C, but more Au deposition results in the formation of flat and smooth Au(111) terraces. Klusek et al.[6.12] observed that higher substrate temperature and lower deposition rate results in larger flat

terraces. In the deposition of Au on NaCl(001), it was reported[6.16,6.17] that very thin Au layers (0.2-10 nm) do not grow epitaxially on NaCl at temperatures below 120 °C. These observations will be used to guide the preparation of Au thin films, on NaCl(001) and HOPG(0001) substrates.

The behaviour of *n*-alkanes when deposited on pure Au substrates must also be considered. As indirect epitaxy refers to the transmitted effect of the substrate through a thin metal film, this effect should disappear as the metal thickness increases, and revert to that of a normal Au surface. The attraction forces of *n*-alkanes on NaCl(001) (11.2 kJ / mol.CH_2)[6.4] and *n*-alkane as on Au(111) (~10 kJ / mol.CH_2)[6.18] are similar, so a similar behaviour might be expected. STM studies of *n*-alkane monolayers on Au(111) by Uosaki and Yamada[6.19] showed two-dimensional ordered monolayers of short *n*-alkanes (C_nH_{2n+2}; $n \leq 16$) on Au(111) at room temperature, where the *n*-alkane molecular axis was oriented parallel to the surface. Wöll[6.20] and Kondoh et al.[6.21] used linear dichroism in the Carbon 1s edge NEXAFS spectra of *n*-octane and *n*-hexane monolayers grown on Au(111) surface at 120 K and 110 K respectively, to show in-plane orientation of the *n*-alkane chains.[6.22] In the limit of low coverage, *n*-alkanes will adopt an in-plane orientation on most substrates, including Au, as discussed above. As the coverage increases, the *n*-alkane chains may remain in a metastable in-plane orientation, or reorient to a normal orientation. Nozaki et al.[6.2] show mixed in-plane and normal orientation exists at low substrate temperature during deposition and high evaporation rate (favouring metastable states), while normal orientation is observed at high substrate temperature during deposition and at low evaporation rate (favouring the normal oriented, equilibrium structure). As well, Nozaki et al. observed some cases of "layered" structures: first layers of an *n*-alkane thin film are laterally oriented, and then adopt a normal orientation in subsequent layers.[6.2] Molecular simulations of

Yamamoto et al.[6.23] show that a strongly attractive surfaces will induce in-plane orientation, but that in a multilayer film, top layers can adopt a normal orientation. In the case of Au and HOPG; the absorption strengths are similar, and therefore there should not be a large difference in behaviour.

However, there has been little consideration of the morphology of *n*-alkane thin films on Au. A recent examination of *n*-alkanes on HOPG(0001) shows that the thin film morphology is strongly dependent on deposition conditions.[6.8] Therefore, it will be important to evaluate the morphology of *n*-alkane multilayer films on the Au coated HOPG(0001), from very thin Au to thicker Au films, to examine for preferential structure of *n*-alkane multilayer imposed by Au film.

In this work, the nature of indirect epitaxy on Au/NaCl(001) and Au/HOPG(0001) will be examined. The effect of Au thin films in transmitting and potentially enhancing the spatial and directional cues from the NaCl(001) and HOPG(0001) substrates will be determined by examining the morphology of *n*-alkane thin films grown on these substrates. A comparison of *n*-alkane films grown on Au/NaCl(001) and Au/HOPG(0001) will be used to illustrate how substrate symmetry affects *n*-alkane film morphology. These results will be compared to morphologies of *n*-alkane thin films deposited on thicker Au films, where indirect epitaxial effects will be absent.

2. Experimental:

2.1 Samples and Sample Preparation

Hexatriacontane (*n*-$C_{36}H_{74}$, 98%), Tetratetracontane (*n*-$C_{44}H_{90}$, 99%) and Pentacontane (*n*-$C_{50}H_{102}$, 97%) were purchased from Sigma-Aldrich and used without purification.

The shorthand C36, C44, and C50 will be used in this paper to refer to these *n*-alkanes. NaCl(001), was obtained from International Crystal Labs and Highly Oriented Pyrolytic Graphite (HOPG(0001)) (10 x 10 x 2 mm, ZYH grade, mosaic angle is 3.5° +/- 1.5°) was obtained from NT-MDT. The surface of HOPG(0001) and NaCl(001) were cleaved to prepare a fresh surface for each experiment.

Sample preparation: Thin Au and *n*-alkane thin films were prepared by physical vapour deposition from a resistively heated tungsten boat, at pressures below 10^{-7} torr. During deposition, the temperature of the substrate was controlled with a Peltier thermoelectric module, and its temperature was measured with a thermistor. The nominal film thickness and rate of the deposition were tracked with a quartz crystal microbalance. The evaporation of Au thin films onto HOPG(0001) was performed at a substrate temperature of 65 °C, with the lowest stable deposition rate (~0.2 Å/s), which is suitable for preparing flat and continuous Au layers on HOPG(0001).[6.13] An Atomic Force Microscopy study of Au thin films grown in these conditions show that thinner films (1.7 nm thickness) have branched structures while grains are observed for thicker (4.7 – 8.7 nm) films (see supporting information, Figure S1). The growth of Au on NaCl(001) was performed in similar conditions, as epitaxy is observed at temperatures above 120 °C.[6.16,6.17]

After preparing the double layer substrates (Au/HOPG(0001) and Au/NaCl(001)), thin films of *n*-alkane were deposited at controlled substrate temperatures. The film thickness and rate of the deposition were tracked with a quartz crystal microbalance; a rate of 0.7 ± 0.2 Å/s was used for deposition of *n*-alkane films. These *n*-alkane deposition conditions are based on a recent study of the epitaxial growth of *n*-alkanes on HOPG(0001).[6.8] The *n*-alkane films grown on NaCl(001) (bare and Au coated) were picked up onto Si wafers after dissolving the NaCl

substrate in Millipore water.

2.2. Sample Characterization

The topography of Au thin layer on HOPG(0001) was studied by AFM microscopy (Ultra Objective, SISCANPanel). The AFM tips with reflex coating, from SiS, were used to acquire images in non-contact mode. *n*-Alkane samples were characterized by optical microscopy (Nikon Eclipse ME600, with a Q-Imaging CCD camera). Images were acquired in bright field, and image contrast arises from thickness differences.

3. Results

The nature of indirect epitaxy is revealed by examining the deposition of *n*-alkane thin films on Au/NaCl(001) and Au/HOPG(0001), and comparing this to the growth of *n*-alkane thin films on bare NaCl(001) and HOPG(0001) substrates. To this end, C36 (hexatriacontane, *n*-$C_{36}H_{74}$) was deposited on bare HOPG(0001) and on Au/HOPG(0001) with varying Au thicknesses (0.6 – 20 nm; Au deposited at a substrate temperature of 65 °C). The AFM images of 1.7, 4.7 and 8.7 nm Au film on HOPG(0001) are shown in the supporting information (Figure S1), along with the complete set of C36 results (Figure S2). A subset of these results is included in Figure 1.

A range of morphologies were observed that are similar to those observed in our previous work.[6.1,6.8] The orientation of the *n*-alkane molecules in each of these characteristic morphologies was also determined in these studies.[6.1,6.8,6.22] Fu and Urquhart[6.1] have shown that the linear dichroism in the C 1s $\rightarrow \sigma^*_{C\text{-}C}$ and C 1s $\rightarrow \sigma^*_{C\text{-}H}$ transitions in the NEXAFS spectra of oriented *n*-alkane thin films can be used for a direct measurement of molecular orientation. In a STXM microscope, this linear dichroism can be used to directly determine molecular orientation in

different domains for sample with a complex morphology. Masnadi and Urquhart[6.8] determined the molecular orientation within characteristic morphologies for *n*-alkanes deposited on HOPG(0001), by direct measurement with STXM microscopy and NEXAFS spectroscopy. These oriented morphologies include:

- An *oriented bar morphology* (high aspect ratio bars with six-fold symmetry) that corresponds to structures with an in-plane molecular orientation along the six-fold symmetry of the HOPG(0001) substrate
- A *pseudorectangular structures* that corresponds to in-plane molecular orientation but without epitaxial registration with the substrate lattice
- Disordered morphologies (*normal oriented thin films*) that correspond to domains with a normal molecular orientation[6.8]

Similar observations were made for *n*-alkanes deposited on NaCl(001): oriented high aspect ratio bars correspond to structures with an in-plane molecular orientation along the four-fold symmetry of the NaCl(001) substrate, and disordered morphologies correspond to domains with a normal molecular orientation.[6.1]

The image contrast in Figure 1 originates from different thickness of the *n*-alkane domains. The surface of a relatively thick layer of Au on HOPG(0001) is expected to behave like a the surface of a pure Au sample. For Au layers of 15-20 nm on HOPG(0001), a disordered C36 *n*-alkane deposit morphology is observed (see supporting information, Figure S2). This morphology corresponds to a normal molecular orientation, based on the previous work of Masnadi and Urquhart.[6.8] These results indicate that *n*-alkanes would adopt a normal orientation when deposited on pure Au, in the deposition conditions used. Structures observed in the

deposition of *n*-alkanes on thinner Au layers on HOPG(0001) can be assumed driven by indirect epitaxy through the Au thin film.

When C36 was grown on bare HOPG(0001) (Figure 1a) at a substrate temperature of 56 °C, a disordered pseudorectangular morphology was observed. This morphology corresponds to in-plane alignment, but without epitaxial registry with the HOPG(0001) substrate. When C36 is deposited at nearly the same substrate temperature (55 °C) onto Au/HOPG(0001) (3.7 nm Au deposited at 65 °C) (Figure 1b), the C36 thin film forms an ordered structure, with thin bars showing a 6-fold symmetry. This morphology corresponds to in-plane alignment of the *n*-alkane chains, where the chains are aligned epitaxially with the substrate, and 3-D oriented bars are formed during the growth process. Similar observations were seen for C44 at 61 °C substrate temperature (Figures 1c and 1d) and C50 at a 68-69 °C substrate temperature (Figures 1e and 1f).

To confirm the transfer of attractive forces from the substrate to the *n*-alkane deposit through a thin metal film, this experiment was also applied to the NaCl(001) substrate, which has a 4-fold symmetric surface. Deposition of *n*-alkanes on bare NaCl(001) leads to structures with 4-fold symmetry.[6.1] To be consistent with the proposed indirect epitaxy model, 4-fold symmetric structures are expected to be on the surface of Au/NaCl(001).

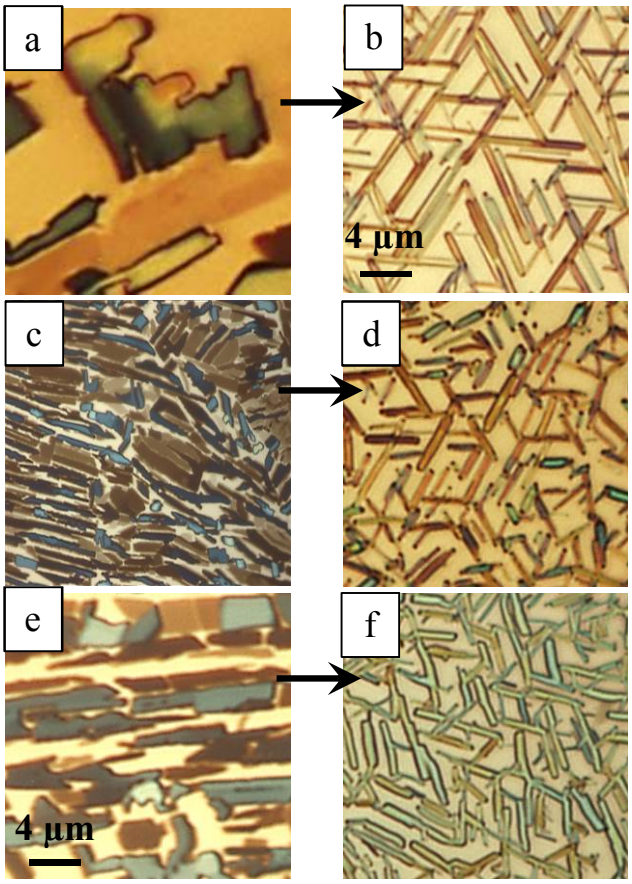

Figure 1. Optical microscopy images of *n*-alkanes deposited on bare HOPG(0001) and Au coated HOPG(0001). a.) C36 deposited on bare HOPG(0001) (C36 deposited at 56 °C substrate temperature); b.) C36 deposited on Au coated HOPG(0001) (3.7 nm Au; C36 deposited at 55 °C substrate temperature); c.) C44 deposited on bare HOPG(0001) (C44 deposited at 61 °C substrate temperature); d.) C44 deposited on Au coated HOPG(0001) (3.8 nm Au; C44 deposited at 61 °C substrate temperature); e.) C50 deposited on bare HOPG(0001) (C50 deposited at 69 °C substrate temperature); f.) C50 deposited on Au coated HOPG(0001) (3.5 nm Au; C50 deposited at 68 °C substrate temperature). All *n*-alkane films are 50 nm thick.

On bare NaCl(001), Fu and Urquhart[6.1] reported that C36 forms a structure with in-plane 4-fold symmetric bars, with some normally oriented domains when deposited at substrate temperature of 22 °C. This morphology changes to all-normally oriented domains for deposition at a substrate temperature of 40 °C.[6.1] In a series of C36 samples grown on NaCl(001) at different substrate temperatures, we observed a combined structure of ordered bars and disordered islands

in a substrate temperature range of 25-50 °C, and a disordered film in the substrate temperature range of 58-70 °C (see supporting information, Figure S3).

When C36 is deposited on Au/NaCl(001) (~ 1-4 nm thick Au layers), the C36 deposit forms evenly ordered 4-fold symmetric bar structures over a wide substrate temperature range (25-70 °C). The results from deposition at two different substrate temperatures are shown in Figure 2. Figures 2a and 2b show that C36 forms ordered bars plus disordered islands on the bare NaCl(001) but an ordered 4-fold symmetry pattern when C36 is deposited on Au/NaCl(001) at 50 °C (3.1 nm Au). Likewise, Figure 2c shows a disordered film of C36 deposited on bare NaCl(001) at 70 °C, but a 4-fold symmetric structure is observed when C36 is deposited on the Au/NaCl(001) at 70 °C (1 nm Au). These results show that the metal layer increases the propensity for epitaxial alignment in substrate temperature conditions where C36 is reported to have a normal orientation by Fu and Urquhart.[6.1]

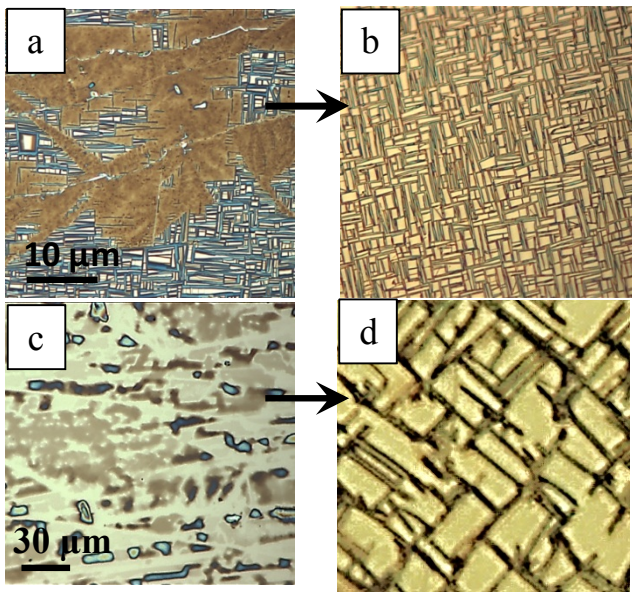

Figure 2. Optical microscopy images of a.) C36 deposited on bare NaCl(001) (at 50 °C substrate temperature); b.) C36 deposited on Au coated NaCl(001) (3.1 nm Au; C36 deposited at 50 °C substrate temperature); c.) C36 deposited on bare NaCl(001) (at 70 °C substrate temperature); d.) C36 deposited on Au coated NaCl(001) (1 nm Au; C36 deposited at 70 °C substrate temperature). All *n*-alkane films are 90 nm thick.

Another aspect of the deposition of *n*-alkane thin films is the rearrangement from in-plane to normal orientation with increased substrate temperature during deposition. Previous results show that C36 starts to form normally oriented structures on HOPG(0001) at substrate temperatures of 65 °C.[6.8] Figure 3 shows the effect of Au in maintaining in-plane orientation of C36 on the Au/HOPG(0001) at even higher substrate temperatures. A C36 film adopts a normal orientation on bare HOPG(0001) at 70 °C (Figure 3a), but forms a bar structure when deposited on Au/HOPG(0001) (3 nm Au). Although the bars do not show strong six-fold symmetry, the morphology is strong evidence of in-plane orientation of C36, and indirect epitaxy at higher deposition temperature.

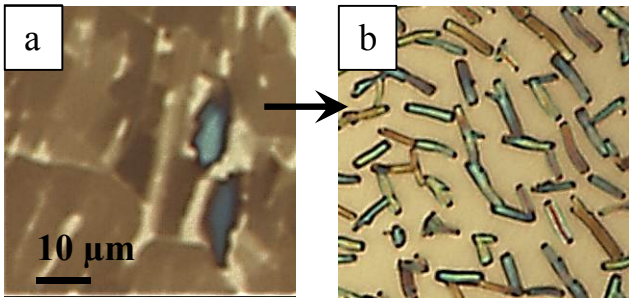

Figure 3. Optical microscopy images of a.) C36 deposited on bare HOPG(0001) (50 nm C36 deposited at 70 °C substrate temperature); b.) C36 deposited on Au coated HOPG(0001) (3 nm Au; 50 nm C36 deposited at 70 °C substrate temperature).

4. Discussion:

The results presented in Figures 1 and 2 demonstrate that epitaxial growth conditions for *n*-alkane thin films persist through a thin metal film. 6-Fold symmetry persists through an Au film deposited on HOPG(0001), and 4-fold symmetry persists through an Au film deposited on NaCl(001). These symmetries reflect the substrate symmetries, so the spatially distinct and oriented van der Waals and polar interactions are transmitted through the metal thin film, causing the *n*-alkane deposit to follow the substrate symmetry.

The transfer of van der Waals forces from the apolar HOPG(0001) through Au and ionic forces from NaCl(001) through Au can be explained by mirror-image potential effect, which is the potential induced by the polarization of metal.[6.24,6.25] Stoneham and Tasker[6.26] reported that a metal plane adjacent to the (100) plane of NaCl forms the lattice of image charges that continue the primary ionic lattice. The preservation of epitaxial growth on Au deposited on an apolar lattice (graphite) suggests that the virtual dipole moment present in the graphite lattice is reflected in the Au layer.

Further, the metal thin film appears to amplify the strength of the epitaxy. In this work, growth conditions on bare substrates and substrates with a thin Au coating were examined. In

otherwise identical deposition conditions, the thin Au film led to greater in-plane alignment, at higher deposition temperatures. This epitaxial morphology, in conditions where normal orientation is otherwise observed, is evidence of strong directional coincidence.

Some researchers have suggested that pinholes in the interlayer are the means by which structural information from the substrate is transmitted to the deposit (see discussion in Shirokoff and Erb).[6.27] Shirokoff and Erb provided evidence to refute the pinhole suggestions: where Au and Ag microspheres were deposited on NaCl and Si substrates with an amorphous silica or carbon interlayer (<20 nm), an epitaxial relationship between the microspheres and the substrate was observed. If pinholes were responsible, then only a few scattered microspheres would show the epitaxial relationship.[6.27,6.28] An analogy can apply to this study: Figure 1b shows a high symmetry structure, with many high aspect ratio bars, with six-fold symmetry. This result must represent the presence of many distributed nucleation sites for the growth of oriented bars; a high density of evenly distributed pinholes would be required for such a high symmetry structure. Pinholes could be present, but this explanation would not support the observed structure.

The origin of the ordered growth at higher substrate temperatures is an unanswered question. It is possible that the enthalpy of *n*-alkane deposition is dispersed more rapidly on the surfaces of Au/HOPG and Au/NaCl during deposition, relative to bare HOPG(0001) and NaCl(001). The thermal conductivity of Au is 317 W/m.K,[6.29] significantly higher than HOPG (~3 W/m.K, between the layers of graphite)[6.30] and NaCl(001) (6.02 W/m.K)[6.31]. The enthalpy of deposition of the *n*-alkane deposit can be more rapidly dispersed by the Au substrate due to its higher thermal conductivity. In contrast, the *n*-alkane deposit on HOPG(0001) or NaCl(001) might maintain its thermal energy and be less strongly bound to the surface and to reorient, leading to disordered in-plane or normally oriented films. If the deposition enthalpy is more

rapidly dissipated on the Au coated surface, kinetically trapped in-plane structures are more likely to be formed. Nozaki et al.[6.2] have reported that the low thermal conductivity and heat capacity of polyimide results in formation of normally oriented *n*-alkane molecules while silicon and glass substrates with a higher thermal conductivity and heat capacity form a coexisting normal and in-plane orientation of an *n*-alkane deposit. As an alternative origin of the ordered growth at higher substrate temperatures, one might invoke a hypothesis that Au thin films form six-fold symmetric structures on HOPG(0001) and four-fold structures on NaCl(001). The evolution of the surface symmetry of Au films on HOPG(0001) and NaCl(001) is beyond the scope of this study. As shown in Figure S2, there is just one optimum thickness of Au film that causes the epitaxial growth of the subsequent *n*-alkane film on the Au coated HOPG(0001) and NaCl(001).

5. Conclusion:

In the current study, indirect epitaxial growth of *n*-alkane thin films has been demonstrated. Here, organic epitaxy is characterized by in-plane alignment of *n*-alkane chains along preferred directions on the NaCl(001) or HOPG(0001) surfaces, from directional coincidence. Directional coincidence is still observed when an *n*-alkane overlayer is deposited on an Au intervening layer on HOPG(0001) and NaCl(001) substrates. In this indirect epitaxy, the patterned attractive forces of the substrates can act indirectly through an Au intervening layer as thick as 4 nm, and drive oriented organic growth. More ordered epitaxial structures are formed by indirect epitaxy, at higher substrate temperatures than on the uncoated substrates. The mirror-image potential effect could transmit the cues for indirect epitaxy through the thin metal film, and the higher thermal conductivity of the Au thin film could be responsible for the unusual temperature dependence leading to higher order.

Acknowledgment:

This research is supported by NSERC (Canada) and the Canadian Foundation for Innovation.

Supporting information

Gold thin films with thicknesses between 0.6 – 20 nm were deposited on HOPG(0001) at a substrate temperature of 65 °C. AFM images of some of these films are presented in Figure S1; these data show that gold has branched islands at 1.7 nm thickness (Figure S1a) and a similar grain pattern at 4.7 and 8.7 nm (Figures S1b and S1c).

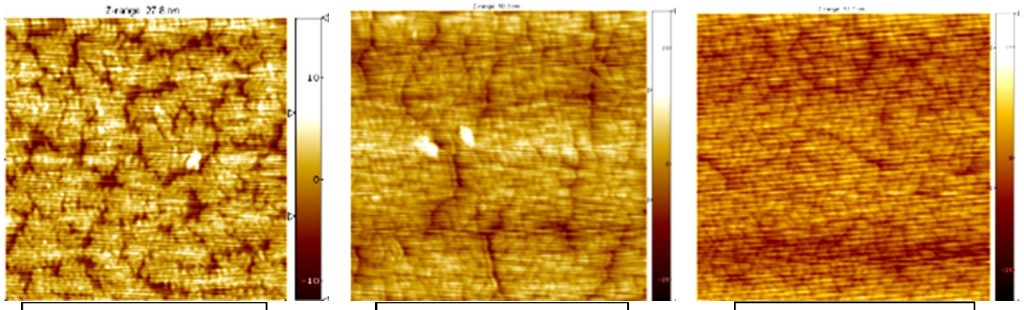

a) 1.7 nm Au on HOPG(0001)

b) 4.7 nm Au on HOPG(0001)

c) 8.7 nm Au on HOPG(0001)

Figure S1. Non-contact mode Atomic Force Microscopy images of the morphology of Au thin film deposited on HOPG(0001) at substrate temperature of 65 °C. Images are squares of 3 µm, 2 µm, and 2 µm from left to right.

C36 deposition on Au coated HOPG(0001), where the Au film is deposited at 65 °C substrate temperature:

The most ordered *n*-alkane structure was observed for a ~4 nm gold overlayer. After this optimum point, increasing the thickness of Au causes the formation of disordered bar structure.

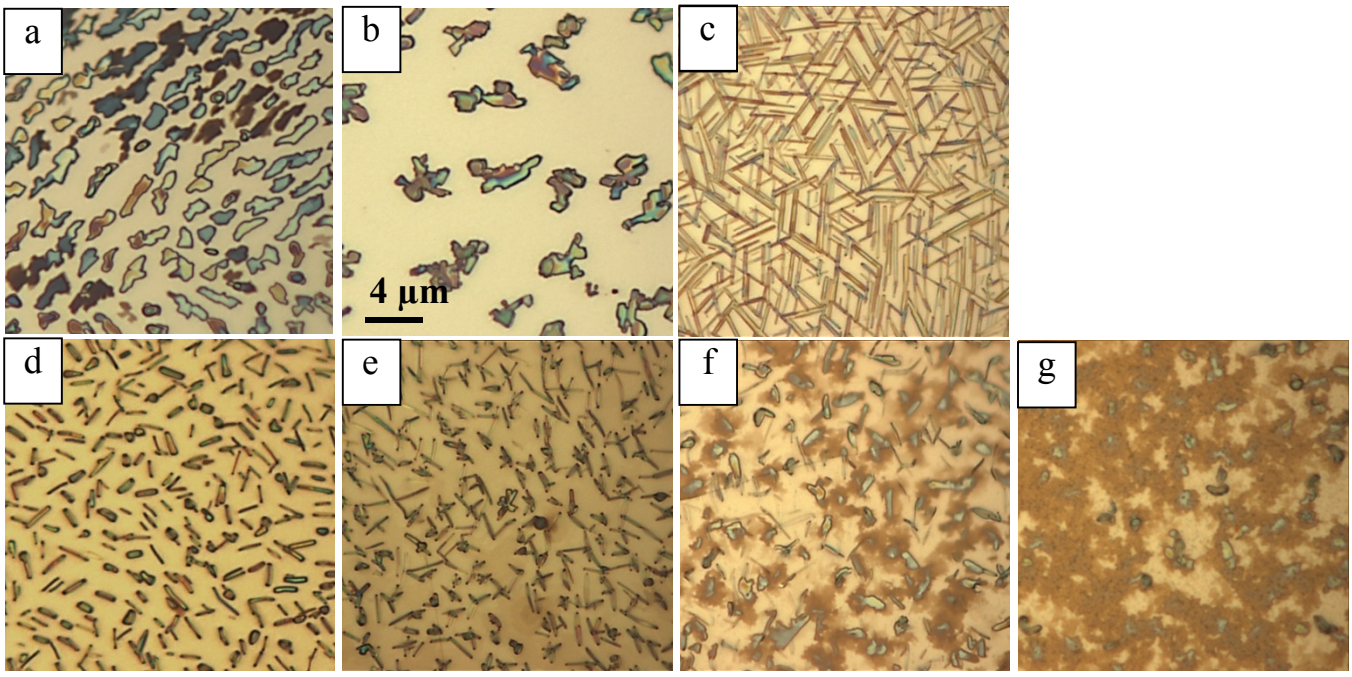

Figure S2. Optical microscope images of an *n*-alkane deposited on bare and Au coated HOPG(0001). a.) C36 deposited on bare HOPG(0001); b.) C36 deposited on 0.6 nm Au coated HOPG(0001); c.) C36 deposited on 3.7 nm Au coated HOPG(0001); d.) C36 deposited on 4.6 nm Au coated HOPG(0001) e.) C36 deposited on 10 nm Au coated HOPG(0001) f.) C36 deposited on 15 nm Au coated HOPG(0001) g.) C36 deposited on 20 nm Au coated HOPG(0001). All *n*-alkane films are 50 nm thick and deposited at 56 °C substrate temperature.

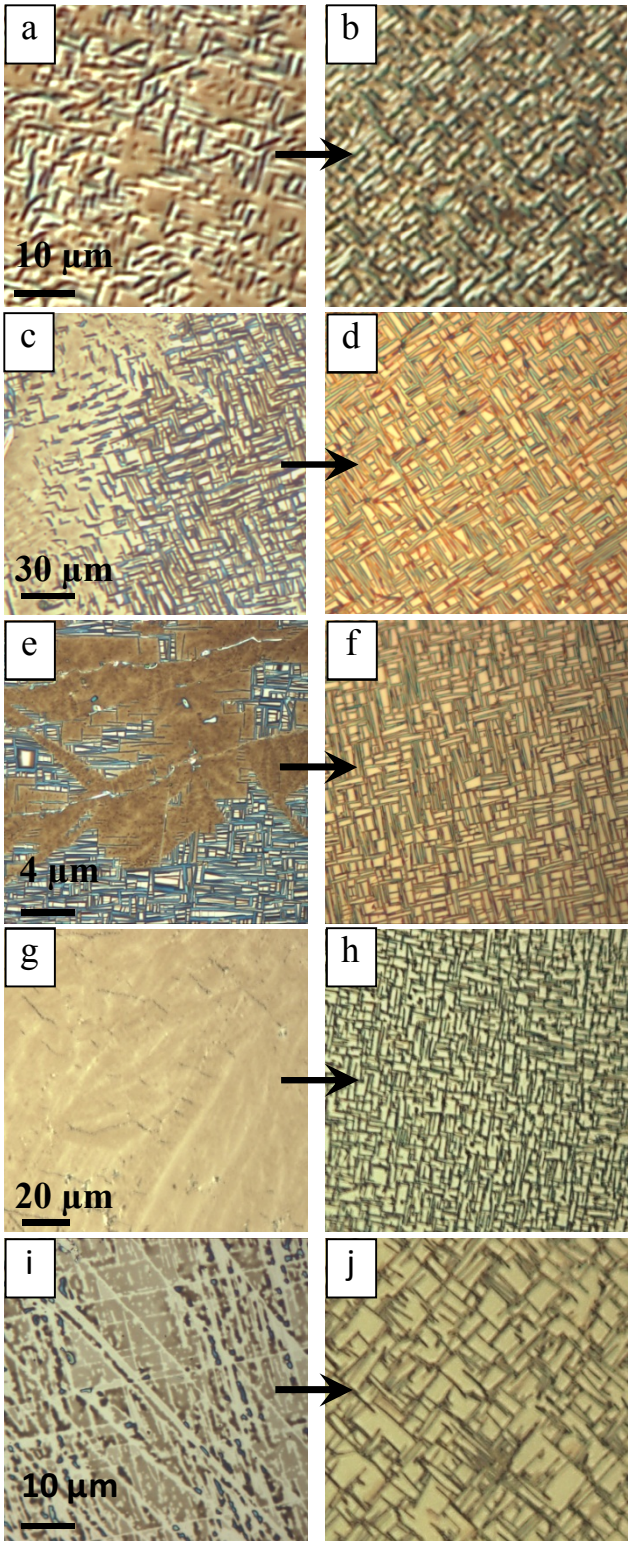

Figure S3. Optical microscope images of an *n*-alkane deposited on bare NaCl(001) and Au coated NaCl(001). a.) C36 deposited on bare NaCl(001) at 25 °C substrate temperature; b.) C36 deposited on Au coated NaCl(001) (2 nm Au; C36 deposited at 25 °C substrate temperature); c.) C36 deposited on bare NaCl(001) at 45 °C substrate temperature; d.) C36 deposited on Au coated NaCl(001) (3.6 nm Au; C36 deposited at 45 °C substrate temperature); e.) C36 deposited on bare NaCl(001) at 50 °C substrate temperature; f.) C36 deposited on Au coated NaCl(001) (3.1 nm Au; C36 deposited at 50 °C substrate temperature); g.) C36 deposited on bare NaCl(001) at 58 °C substrate temperature; h.) C36 deposited on Au coated NaCl(001) (2 nm Au; C36 deposited at 58 °C substrate temperature); i.) C36 deposited on bare NaCl(001) at 70 °C substrate temperature; j.) C36 deposited on Au coated NaCl(001) (1 nm Au; C36 deposited at 70 °C substrate temperature). All *n*-alkane films are 90 nm thick.

References:

(1) Fu, J.; Urquhart, S. G. Effect of chain length and substrate temperature on the growth and morphology of *n*-alkane thin films *Langmuir* **2007**, *23*, 2615.

(2) Nozaki, K.; Saihara, R.; Ishikawa, K.; Yamamoto, T. Structure of normal alkane evaporated films: molecular orientation. *Jpn. J. Appl. Phys.* **2007**, *46*, 761.

(3) Kubono, A.; Yuasa, N.; Shao, H.-L.; Umemoto, S.; Okui, N. Adsorption characteristics of organic long chain molecules during physical vapor deposition. *Appl. Surf. Sci.* **2002**, *193*, 195.

(4) Mauritz, K. A.; Baer, E.; Hopfinger, A. J. Molecular energetics of the epitaxial crystallization of polyethylene on alkali halide substrates. *J. Polym. Sci., Part B: Polym. Phys.* **1973**, *11*, 2185.

(5) Leunissen, M. E.; Graswinckel, W. S.; van Enckevort, W. J. P.; Vlieg, E. Epitaxial nucleation and growth of *n*-alkane crystals on graphite (0001). *Cryst. Growth Des.* **2004**, *4*, 361.

(6) Hooks, D. E.; Fritz, T.; Ward, M. D. Epitaxy and molecular organization on solid substrates. *Adv. Mater.* **2001**, *13*, 227.

(7) Forrest, S. R.; Burrows, P. E. Growth modes of organic semiconductor thin films using organic molecular beam deposition: epitaxy, van der Waals epitaxy, and quasi-epitaxy. *Supramol. Sci.* **1997**, *4*, 127.

(8) Masnadi, M.; Urquhart, S. G. Effect of substrate temperature on the epitaxial growth of oriented *n*-alkane thin films on graphite. *Langmuir* **2012**, *28*, 12493.

(9) Pashley, D. W. Epitaxy growth mechanisms. *Mater. Sci. Technol.* 1999, *15*, 2.

(10) Distler, G. I.; Vlasov, V. P.; Kanevsky, V. M. Orientational and long-range effects in epitaxy. *Thin Solid Films* **1976**, *33*, 287.

(11) Vitos, L.; Ruban, A. V.; Skriver, H. L.; Kollar, J. The surface energy of metals. *Surface Science* **1998**, *411*, 186.

(12) Klusek, Z.; Balcerski, J.; Olejniczak, W.; Kobierski, P. Scanning tunneling spectroscopy investigations of gold films deposited on the (0001) basal plane of highly oriented pyrolitic graphite. *Electron. Technol.* **1998**, *31*, 512.

(13) Blum, B.; Salvarezza, R. C.; Arvia, A. J. Vapor-deposited gold film formation on highly oriented pyrolitic graphite. A transition from pseudo-two-dimensional branched island growth to continuous film formation. *J. Vac. Sci. Technol. B* **1999**, *17*, 2431.

(14) Hammiche, A.; Webb, R. P. Scanning tunneling microscopy observation of the growth evolution of gold films evaporated on highly oriented pyrolitic graphite. *J. Vac. Sci. Technol. B* **1994**, *12*, 1413.

(15) Kuwabara, M.; Smith, D. A.; Clarke, D. R. Observation of gold evaporated on graphite (0001) cleaved surfaces. *J. Appl. Phys.* **1990**, *68*, 6520.

(16) Gottsche, H. Uber die orientierung dunner aufdampfschichten von metallen - eine untersuchung mit elektroneninterferenzen. *Zeitschrift Fur Naturforschung Part a-Astrophysik Physik Und Physikalische Chemie* **1956**, *11*, 55.

(17) Kehoe, R. B. On the texture of evaporated films. *Philos. Mag.* **1957**, *2*, 455.

(18) Wetterer, S. M.; Lavrich, D. J.; Cummings, T.; Bernasek, S. L.; Scoles, G. Energetics and kinetics of the physisorption of hydrocarbons on Au(111). *J. Phys. Chem. B* **1998**, *102*, 9266.

(19) Uosaki, K.; Yamada, R. Formation of two-dimensional crystals of alkanes on the Au(111) surface in neat liquid. *J. Am. Chem. Soc.* **1999**, *121*, 4090.

(20) Wöll, C. Small hydrocarbons on metal surfaces: adsorption-induced changes in electronic and geometric structure as seen by X-ray absorption spectroscopy. *J. Synchrotron Radiat.* **2001**, *8*, 129.

(21) Kondoh, H.; Matsui, F.; Ehara, Y.; Yokoyama, T.; Ohta, T. Surface-monolayer-controlled molecular alignment of short *n*-alkane multilayers. *Langmuir* **2001**, *17*, 8178.

(22) Fu, J.; Urquhart, S. G. Linear dichroism in the X-ray absorption spectra of linear *n*-alkanes. *J. Phys. Chem. A* **2005**, *109*, 11724.

(23) Yamamoto, T.; Nozaki, K.; Yamaguchi, A.; Urakami, N. Molecular simulation of crystallization in *n*-alkane ultrathin films: Effects of film thickness and substrate attraction. *J. Chem. Phys.* **2007**, *127*, 154704.

(24) Hosoi, Y.; Sakurai, Y.; Yamamoto, M.; Ishii, H.; Ouchi, Y.; Seki, K. Structures of a film of the long-chain *n*-alkane *n*-$C_{44}H_{90}$ on a Cu(100) surface. *Surf. Sci.* **2002**, *515*, 157.

(25) Morgenstern Horing, N. J. Van der Waals interaction between adsorbate layer/molecules and substrate. *Int. J. Hi. Spe. Ele. Syst.* **2008**, *18*, 385.

(26) Stoneham, A. M.; Tasker, P. W. Metal-non-metal and other interfaces: the role of image interactions. *J. Phys. C: Solid State Phys.* **1985**, *18*, L543.

(27) Shirokoff, J.; Erb, U. Long-range ordering effects in metal-non-metal interfaces revisited. *Philosophical Magazine A* **1994**, *70*, 1055.

(28) Cahn, R. W. Epitaxy keeps rolling along. *Nature* 1995, *375*, 363.

(29) Kumar, S.; Vradis, G. C. Thermal conductivity of thin metallic films. *J. Heat Transfer* **1994**, *116*, 28.

(30) Klein, C. A.; Holland, M. G. Thermal conductivity of pyrolytic graphite at low temperatures. I. Turbostratic structures. *Phys. Rev.* **1964**, *136*, A575.

(31) Hakansson, B.; Andersson, P. Thermal-conductivity and heat-capacity of solid NaCl and NaI under pressure. *J. Phys. Chem. Solids* **1986**, *47*, 355.

CHAPTER 7: MEASURING THE STRAIN THROUGH X-RAY LINEAR DICHROISM IN AN EPITAXIALLY GROWN INORGANIC THIN FILM

7.1 Introduction

Strained $Si_{1-x}Ge_x$ alloy films are very important in microelectronics industry because of the higher electron mobility as a result of strain. The large lattice mismatch between the crystal structure of Si and Ge (4%) is the origin of strain in these films. Despite the lattice mismatch, Si and Ge form a uniform alloy in all compositions. The degree of strain in a $Si_{1-x}Ge_x$ film depends on the Ge content, film thickness and annealing temperature. The thick and annealed films relaxed from the strain show lower desired effects that are sought in the strained $Si_{1-x}Ge_x$ films. It is necessary to measure the degree of strain in $Si_{1-x}Ge_x$ films to improve the performance of the corresponding electronic devices. Strained SiGe films have been studied by transmission electron microscopy (TEM),[91] X-ray diffraction,[92] and Raman microscopy[93] before. TEM is able to measure the degree of strain via shape transformation. The best spatial resolution of the other techniques does not exceed 100 nm while the new electronic devices made of $Si_{1-x}Ge_x$ films are smaller than 90 nm. Therefore, it is needed to measure the strain of these uniform alloyed films with a higher spatial resolution technique. Synchrotron based X-ray microscopy techniques can provide polarization dependent high spatial resolutions imaging. In this study the strain of $Si_{1-x}Ge_x$ films is measured through linear dichroism in Si 1s NEXAFS spectroscopy.

Si 1s NEXAFS spectrum exhibits a doublet peak at the energy of 1839 - 1844 eV which is attributed to Si 1s→ Si 3p conduction band transition. The relative intensity and position of the polarization dependent doublet peak depends on the Ge content and degree of strain in the Si_xGe_{1-x}films, which form anisotropic final states in Si. The goal of current study is determining the relationship between degree of strain and magnitude of linear dichroism in Si 1s NEXAFS

spectra. It is known that the local symmetry of Si atoms is perturbed from normal tetrahedral environment and Si-Si interatomic spacing is stretched in a $Si_{1-x}Ge_x$ film relative to pure Si crystal. In turn the Si-Si distance is decreased in the orthogonal direction which results in splitting the conduction band under such a spatially anisotropic field.[46,47,94]

The value of linear dichroism can be measured by subtracting the two spectra acquired by vertical and horizontal polarizations. The details of each polarization are provided in the experimental section below. Since the Ge composition differences between samples can change the shape and intensity of peaks in Si 1s NEXAFS spectra, subtracting spectra obtained from two polarizations removes the variations due to different compositions of alloys and isolates the effect of strain.

The magnitude of strain is independently measured by Raman spectroscopy using Equation (7.1)[95]

$$\varepsilon_{SiGe}=\frac{520-\omega_{SS}-70.5X}{830} \qquad (7.1)$$

In Equation (7.1) ω_{ss} is the Si-Si peak position and X is the Ge content. As shown in Figure 7.1, three types of peaks show up in the Raman spectrum of a SiGe alloy corresponding to Si-Si, Si-Ge and Ge-Ge vibrations. Just the Si-Si (~500 cm^{-1}) feature changes significantly by Ge content and fits in Equation (7.1).

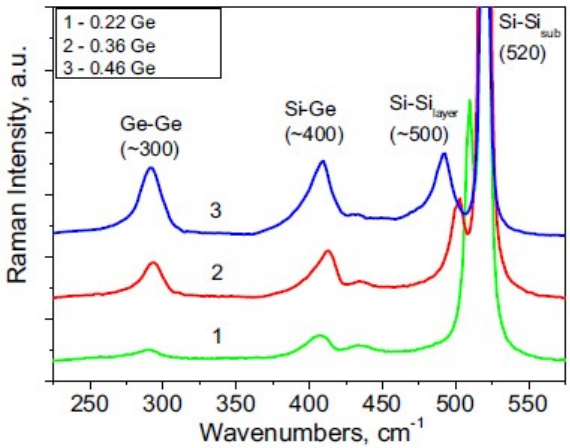

Figure 7.1 Raman spectra for strained $Si_{1-x}Ge_x$ film with different Ge content (x). Figure reprinted from Ref. 95 with permission.

7.2 Experimental section of side project

$Si_{1-x}Ge_x$ alloy films were grown on the commercial (100) oriented Si wafers by molecular-beam epitaxy (MBE) using electron beam evaporators and solid Si and Ge sources at the Institute for Microstructural Sciences National Research Council (NRC-IMS) of Canada. The Si 1s NEXAFS spectra were measured by total electron yield (TEY) method with a sampling depth of 70 nm at the Canadian Light Source, Soft X-ray Microcharacterization Beamline (SXRMB).[96] The X-ray beam was set to strike the sample at a glancing angle of 18°. Each sample was measured with horizontal and vertical polarizations in which the electric field vector was in the sample plane and, almost normal to the surface (18° with respect to the surface normal) respectively.[97] The horizontal and vertical polarizations could be obtained by rotating sample along an axis parallel to the incidence X-ray beam.

In the first series of $Si_{1-x}Ge_x$ samples it was intended to investigate the effect of film thickness in the strain relaxation by measuring linear dichroism in Si 1s NEXAFS spectra. The film thickness was varied between 30 nm and 1μm with a fixed Ge composition (x=0.9). In the

second series of samples the Ge content was variable between 0.5 and 1 while thickness was almost similar (110-320 nm). The native oxide of surface was removed by a short etch (5 s in a 10% HF solution) prior to measurement which results in a lower work function and improves electron yield detection.

Raman spectra from the $Si_{1-x}Ge_x$ films were acquired on the Raman microscope at Saskatchewan Structural Science Centre (SSSC) centre, using the 514.5 nm laser radiation.

7.3 Results

7.3.1 NEXAFS data analysis method

It is expected that the difference between Si 1s NEXAFS spectra acquired with horizontally and vertically polarized beam will be proportional to the degree of strain.[98] Figure 7.2a presents the normalized Si 1s NEXAFS spectra for a $Si_{1-x}Ge_x$ sample (x=0.24) measured at horizontal, *TEY(H)*, and vertical ,*TEY(V)*, polarizations. Obvious differences are found for the spectra at the energy range of 1839-1845 eV (due to the multiple scattering effects that arises ~5 eV above the 1s ionization potential)[47] while the rest of spectrum is overlapping in two polarizations. The differences between TEY(V) and TEY(H) spectra is extracted and called TEY_d. The spectrum of TEY_d contains both positive and negative features (Figure 7.2b). To count all features in linear dichroism, TEY_d is converted to the absolute value scale as shown in Figure 7.2c. The resultant TEY_d spectrum is quantified by calculating the area under the curve through numerical integration (Figure 7.2d) and is called *integrated* TEY_d afterwards and will be correlated to the degree of strain later.

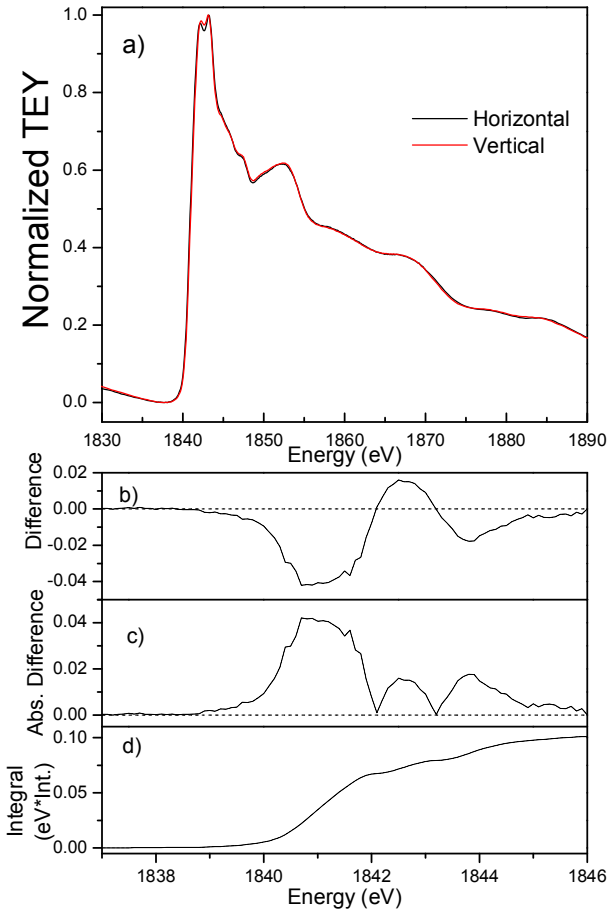

Figure 7.2 a.) Over plot of Si 1s total electron yield spectra acquired by horizontal and vertical polarized X-rays, named as TEY(H) and TEY(V); b.) TEY(V)- TEY(H); c.) |TEY(V)- TEY(H)|; d.) $\int |\mathrm{TEY(V)} - \mathrm{TEY(H)}|$.[97]

7.3.2 Relationship between the degree of Si 1s NEXAFS spectra polarization dependency and the thickness of $Si_{1-x}Ge_x$ alloys on Si(100)

In Figure 7.3a, TEY_d spectra are plotted for alloys with equal compositions ($Si_{0.9}Ge_{0.1}$) and different thicknesses (spectra are offset for clarity), and in Figure 7.3b the corresponding integrated TEY_d data are plotted versus thickness of alloy film. It is clear that the thinnest sample

shows the highest degree of strain which relaxes at higher thicknesses and approaches the background value of 0.01 for pure Si crystal.

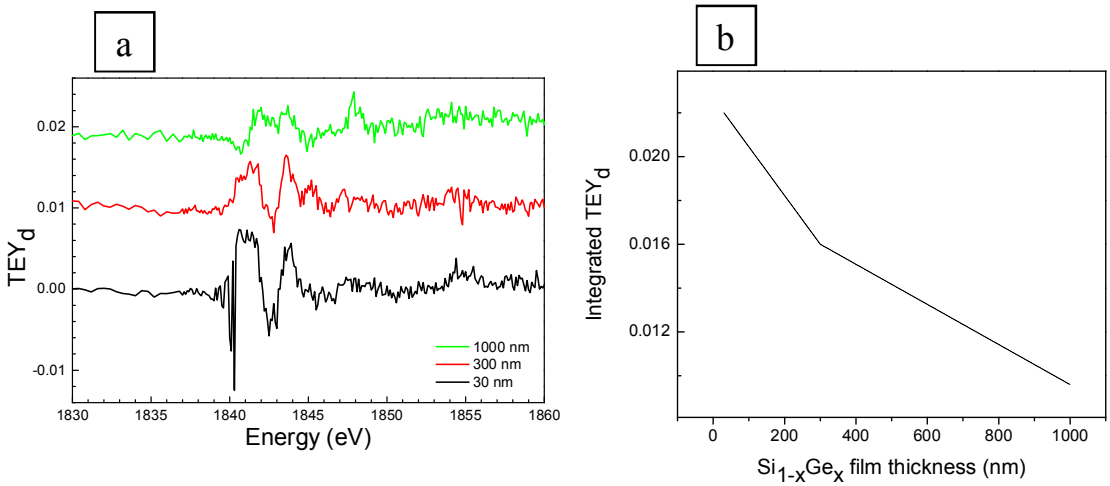

Figure 7.3 a.) Total electron yield spectra difference acquired by horizontal and vertical polarized X-rays, TEY_d (defined as TEY(V)- TEY(H)), at three different thicknesses of $Si_{0.9}Ge_{0.1}$ alloy film on Si(100); b.) integrated TEY_d from part (a) versus thickness of film.

7.3.3 Relationship between the magnitude of linear dichroism in Si 1s NEXAFS spectra and degree of strain of $Si_{1-x}Ge_x$ alloys on Si(100)

Figure 7.4 shows the TEY_d spectra (offset for clarity) of a series of samples with varying Si composition and almost similar thicknesses. It can be seen that the area under the TEY_d spectrum varies with Si content and has an optimum value almost in the alloy of $Si_{0.75}Ge_{0.25}$, which implies the highest degree of strain in this sample. The data in Figure 7.4 are processed further as explained in §7.3.1 and the corresponding linear dichroism value is calculated for each sample.

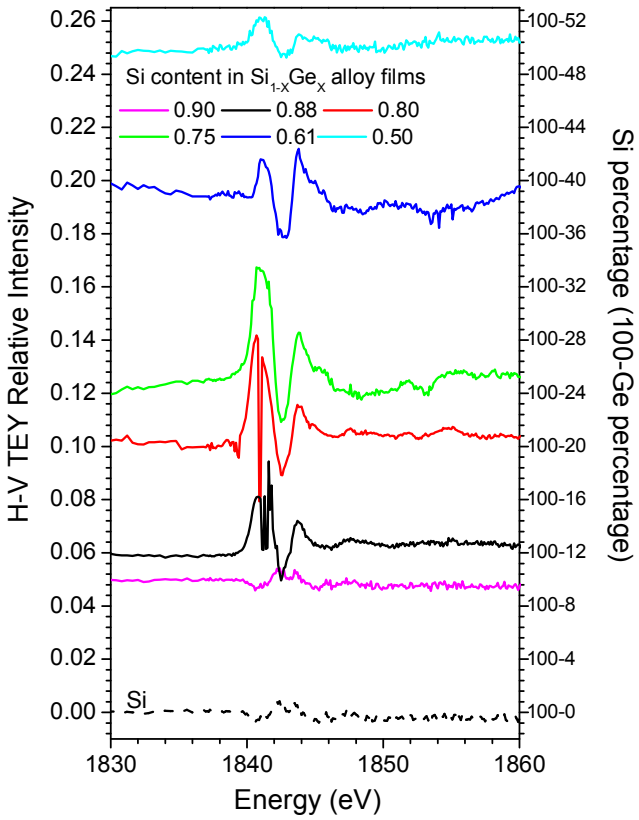

Figure 7.4 TEY_d, total electron yield spectra difference acquired by horizontal and vertical polarized X-rays sorted by the composition of the $Si_{1-x}Ge_x$ alloy.

The corresponding values for degree of strain were calculated by M. Martinson, who determined the position of the Raman peaks by fitting the spectra with an asymmetric Gaussian function.[97] The Si-Si Raman peak position was applied to the Equation 7.1 to calculate degree of strain. As shown in Figure 7.5 there is a linear relationship between magnitude of linear dichroism with the degree of strain in $Si_{1-x}Ge_x$ alloy films grown on Si(100).

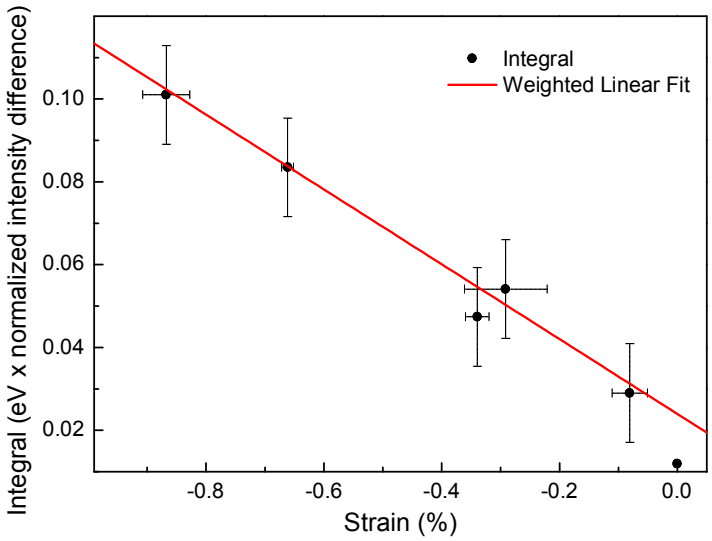

Figure 7.5 Integrated $TEY_{d,}$ (total electron yield difference by horizontal and vertical X-rays) versus degree of strain in $Si_{1-x}Ge_x$ films grown on Si(100).[97]

7.4 Discussion

In Figure 7.3 it was observed that TEY_d decreases with increasing thickness due to strain relaxation. Figure 7.3b shows that the integrated TEY_d drops faster for the thicknesses <300 nm and decrease slower after 300 nm. Bean et. al.[46] have shown that strain in the Si_xGe_{1-x} alloys with $x \leq 0.2$ is independent of thickness in the range of 100-250 nm. It has also been reported[99] that the relaxation of epitaxial strain by thickness is negligible after 100 nm for the alloy $Si_{0.5}Ge_{0.5}$. Our results present a preliminary study due to the limited availability of samples with different thicknesses.

Figure 7.4 presents the TEY_d spectra variation by Si composition in the samples with a small thickness variation (110-320 nm). The area under the absolute TEY_d spectra are calculated and related to the strain values extracted from Raman spectra as shown in Figure 7.5. The data in Figure 7.5 are fitted with a linear function ($y= -9.13x+2.29$, $R^2=0.98$) which can be used further

as a calibration curve to find out the degree of strain for an unknown $Si_{1-x}Ge_x$ sample with measuring its linear dichroism in Si 1s NEXAFS spectra. The measurement of linear dichroism in NEXAFS spectroscopy can be performed with a high spatial resolution microscope such as STXM (resolution < 35 nm) and X-PEEM (resolution < 50 nm) to calculate the degree of strain in nano-scale electronic devices based on $Si_{1-x}Ge_x$ alloy films.

CHAPTER 8: DISCUSSION AND CONCLUSION

This thesis is focused on understanding the determining factors in organic thin films epitaxial growth by monitoring morphology and orientation variations, plus a separate study of strain in semiconductor thin films. After learning the kinetic and thermodynamic factors that guide molecular epitaxial growth, it may then be possible to control the molecular orientation and growth of organic thin films at the same level. In organic molecular devices, these insights could help increase device function by controlling the orientation of interfacial layers. To investigate the determining factors in the epitaxial growth of organic molecules, *n*-alkane thin films were chosen as a model deposit film. *n*-Alkanes are the major part of some organic thin films and the orientation behaviour of alkane part of the larger molecules can be one of the main determining factors in the orientation of the whole molecule. Also the substrate-deposit interaction strength can be tuned easily by altering the *n*-alkane chain length. Epitaxial growth of *n*-alkanes on different substrates was previously studied by Juxia Fu.[57,63]

At the first step, it was intended to control the orientation of *n*-alkane molecules in lateral or normal orientations by surface modification. This could be applied for patterning in the use of arbitrary surfaces. It was hypothesized that self-assembled monolayers (SAM) that interact strongly with *n*-alkane molecules can induce lateral orientation in the *n*-alkane thin films. Two different SAMs were chosen based on the functional groups that could interact with CH_2 groups of an *n*-alkane chain.

The first SAM examined was 11-mercaptoundecanoic acid on gold. It was intended to prepare a normal oriented SAM of 11-mercaptoundecanoic acid on the substrate of gold and then rinse the SAM with an aqueous KOH solution to substitute the acidic hydrogens of the SAM with the K^+ ions. It was assumed that depositing a thin film of *n*-alkane on the modified substrate

can induce lateral orientation via the interaction between CH_2 groups of *n*-alkane and K^+ ions of SAM. The characterization of SAMs with IR spectroscopy was not successful due to interference fringes. Nevertheless, the *n*-alkane samples were prepared on the SAMs and characterized with NEXAFS spectroscopy. The NEXAFS spectra did not show polarization dependence in the C 1s $\rightarrow \sigma^*_{C\text{-}C}$ and C 1s $\rightarrow \sigma^*_{C\text{-}H}$ transitions. The results implied that the *n*-alkane thin film was not grown laterally on the SAM containing K^+ end group, as intended.

The second SAM that was chosen as a substrate to induce lateral orientation to the *n*-alkane thin films was 4-mercaptopyridine. It is known that 4-mercaptopyridine forms lateral and normal oriented SAMs on gold from solutions at different pHs. Therefore, three SAMs of 4-mercaptopyridine were prepared on the gold coated Si wafer from solutions with the pHs of 1, 5 and 10. Then *n*-alkane thin films were deposited on three SAMs of 4-mercaptopyridine which were assumed had different orientations. But none of the *n*-alkane films, deposited on the three different samples of 4-mercaptopyridine SAMs showed polarization dependent NEXAFS spectra. Therefore, the objective of orienting *n*-alkane films laterally was not achieved.

The origin of inability in aligning *n*-alkane films by SAM substrates was not clearly determined. Firstly, it could happen because the SAM samples were not well ordered. The characterization of SAM samples with IR spectroscopy was not successful due to interference fringes and the hydrocarbon contamination of the FTIR optics. Secondly, it was possible that the ordered SAM layers were not able to induce lateral orientation to the *n*-alkane films.

The unsuccessful experiments of aligning *n*-alkane films with SAM samples led us to choose a substrate that was naturally highly ordered. Basic studies of this kind of substrates were started in the group by Juxia Fu. Fu studied the orientation of C36 and C60 on NaCl(001) at different substrate temperatures.[57,63] To complete the epitaxial growth of *n*-alkane films on

highly ordered structures, it was intended to choose a substrate that applies attractive interactions towards *n*-alkane molecules similar to what NaCl(001) does. Based on literature, highly oriented pyrolytic graphite (HOPG(0001)) was chosen as a substrate to study the epitaxial growth of *n*-alkane films in different growth condition.

The research results in Chapters 3 to 6 describe the effect of kinetic and thermodynamic factors in controlling the molecular orientation of *n*-alkane thin films grown epitaxially on HOPG(0001) and NaCl(001). *n*-Alkane thin films were prepared by the physical vapor deposition method due to its ability to control the growth parameters such as substrate temperature and deposition rate. At the first step of characterization, the morphology of *n*-alkane thin films were observed by polarized optical microscopy, and then the corresponding molecular orientations were determined by using linear dichroism in C 1s NEXAFS spectroscopy. The relationship between the morphology and molecular orientation was interpreted by kinetic and thermodynamic parameters that control the growth mode. The results of studying the morphology and orientation of *n*-alkane films grown on HOPG(0001) and NaCl(001) lead to the observation of new morphologies along with their complete orientation analysis. Specifically, it was shown that *n*-alkane molecular orientation depends on the substrate identity, interface nature and deposition conditions such as substrate temperature, and deposition rate. A comprehensive study of epitaxial growth of *n*-alkanes on HOPG(0001) was performed from different aspects. First, the *n*-alkane chain length was varied at constant growth conditions to tune the strength of attractive interactions. Second, tuning the molecular mobility by substrate temperature was varied to probe the molecular diffusion barrier. Third, the deposition rate was tuned to evaluate its role in the epitaxial growth of *n*-alkanes on HOPG(0001). Different modes of growth from

layer-by-layer to layer-plus-island mode were distinguished in a complex series of oriented morphologies that evolved with deposition conditions.

In the first series of experiments presented in Chapter 3, the molecular orientation and morphology of *n*-alkanes of C36, C44, C50 and C60 grown on HOPG(0001) were probed at a wide substrate temperature range during deposition. The substrate temperature during deposition was varied from 6 °C to a temperature 10 degrees below melting point of each *n*-alkane. The combined characterization of the morphology and the molecular orientation of each *n*-alkane film with polarized optical microscopy and X-ray absorption spectroscopy, respectively led to a reliable framework that was extended to similar systems as discussed in Chapters 4 to 6. The results of Chapter 3 are summarized in Figure 8.1. The laterally oriented *n*-alkane chains were obtained at high supercooling temperatures in a series of morphologies shown as phases A (uniform thickness film), B (oriented bars) and C (pseudo-rectangular domains) corresponding to the optical microscope images (a), (b), and (c). The normally oriented *n*-alkane films (Phase D) were obtained for the smaller supercooling temperatures, corresponding to the image (d). These orientational morphology differences were attributed to differences in the relative strength of attractive interactions versus molecular mobility on the surface at any substrate temperature.

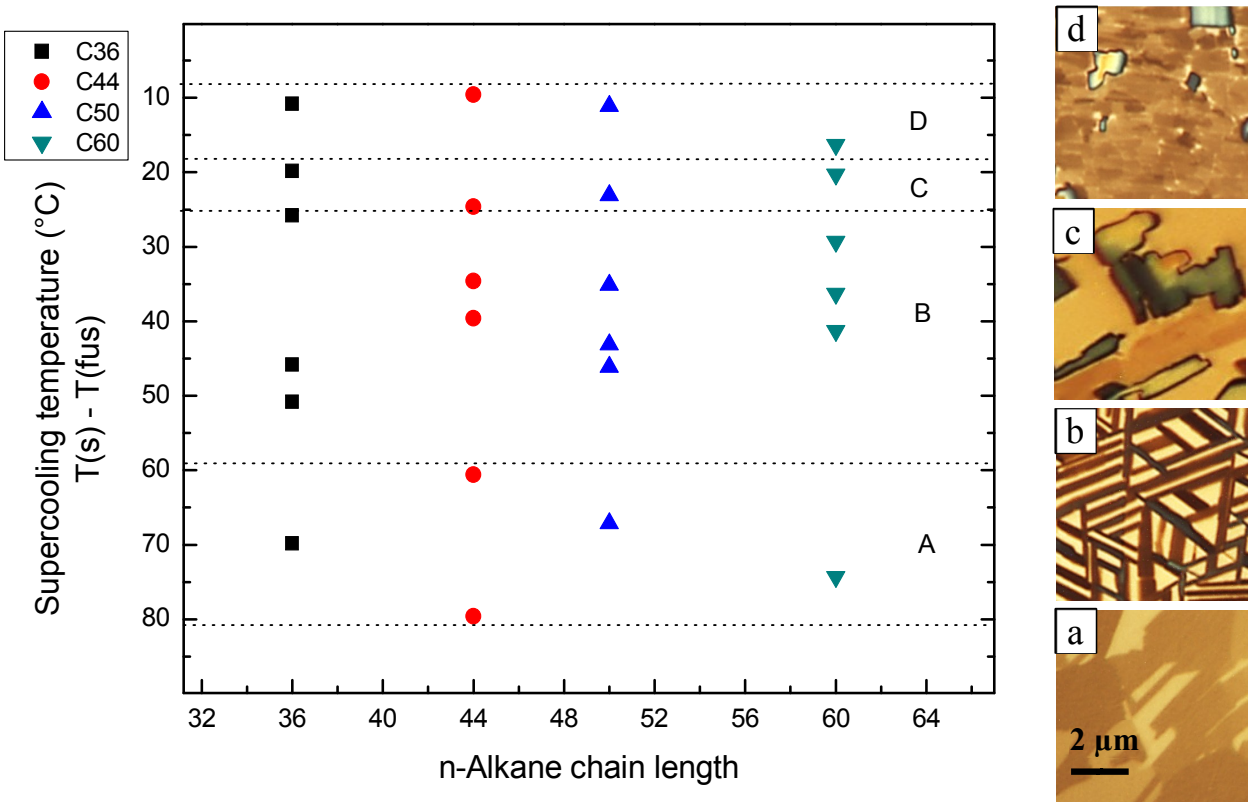

Figure 8.1 Different surface phases in *n*-alkane thin films grown on HOPG(0001) as a function of supercooling temperature (substrate temperature relative to *n*-alkane melting point). Phases *A* to *D* correspond to the sample optical microscope images (a) to (d) from different *n*-alkane films. Phase *A*.) Domains of uniform thickness, oriented by substrate; Phase *B*.) Bar-shaped domains, reflecting the surface symmetry; Phase *C*.) Pseudo-rectangular domains; Phase *D*.) Thin flat film along with scattered pseudo-rectangular domains.

In Chapter 4, deposition rate was investigated as another growth parameter that is tunable in physical vapour deposition growth method. It is known that deposition rate and substrate temperature are associated with supersaturation, which is the determining factor in the formation of kinetically trapped metastable morphologies of the deposit. It was expected that the variation

of the deposition rate could cause morphological variations in the *n*-alkane thin films similar to what was seen for the variable substrate temperature. In summary, it was shown that a higher deposition rate influences the morphologies of *n*-alkane grown epitaxially on HOPG(0001) similar to that observed at a lower substrate temperature; i.e. layer-plus-island mode could change to layer-by-layer growth mode. The important finding of this series of experiments is that higher deposition rate does not influence the morphology of *n*-alkane film similar to the effect of lower substrate temperature for the *n*-alkane film with pseudo-rectangular morphology. As shown in Phase *C* Figure 8.1, the *n*-alkane does not grow epitaxially at high substrate temperatures and forms a laterally oriented disordered morphology. It is hypothesized that in the pseudo-rectangular morphology, the van der Waals interactions between *n*-alkane molecules and HOPG(0001) are just enough to maintain the *n*-alkane molecules in the lateral orientation on the surface of substrate. Therefore, increasing the deposition rate does not make any substantial change in the degree of order of pseudo-rectangular morphology of *n*-alkane and just makes the islands denser.

In Chapter 5, indirect epitaxial growth of *n*-alkane thin films was investigated through an organic thin film. It was shown that a thin film of a liquid crystal or short *n*-alkane on HOPG(0001) can act as a template, upon which a longer *n*-alkane proceeds growing on the ordered pattern of the template. As shown in Figures 8.2 and 8.3, the liquid crystal and short *n*-alkane thin films form a stable template of oriented bar structures with 6-fold symmetric structure on HOPG(0001) at low substrate temperatures, and the subsequently deposited longer *n*-alkane follows the same pattern.

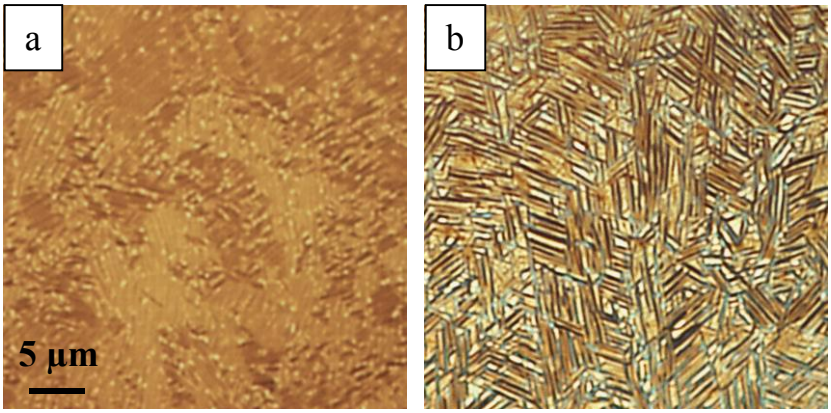

Figure 8.2 a.) C36 deposited on bare HOPG(0001); b.) C36 deposited on liquid crystal coated HOPG(0001). Both samples were prepared at 22 °C substrate temperature.

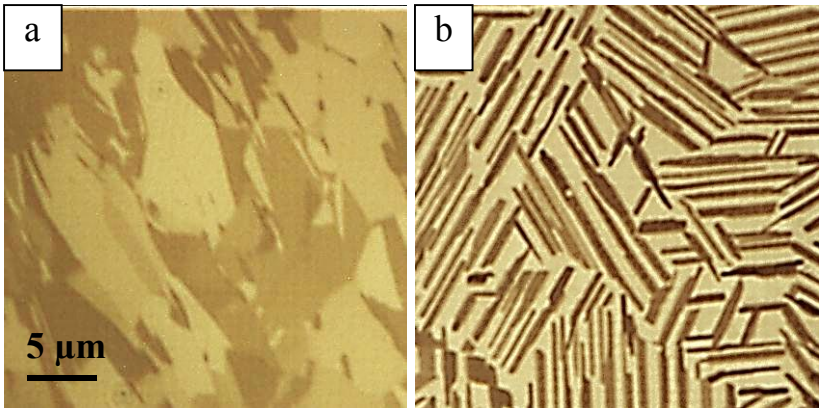

Figure 8.3 a.) C60 on bare HOPG(0001); b.) C60 on (30 nm C36)/HOPG(0001). Both C36 and C60 were grown at 40 °C substrate temperature.

In addition to treating the surface of HOPG(0001) at low substrate temperatures to change the form of *n*-alkane epitaxial growth it was proposed to do another treatment on HOPG(0001) surface to maintain the epitaxial growth at high substrate temperatures. As seen in Figure 8.1, C36 forms pseudo-rectangular disordered morphology when deposited on HOPG(0001) at 56 °C. It was attempted to grow *n*-alkane films on the metal coated HOPG(0001) at high substrate temperatures to form ordered structures. In the second half of

Chapter 5 it was shown that a thin metallic film coated on HOPG(0001), not only transfers the attractive forces of HOPG(0001) to the subsequently deposited *n*-alkane film but also changes the thermal properties of surface. Growing *n*-alkane on a few different metals illustrated that epitaxial growth condition for an *n*-alkane film was maintained at high substrate temperatures when the surface of HOPG(0001) was coated with a thin film of Au (Figure 8.4), Cr, Pb, and Bi. Two metals of Au and Cr have higher thermal conductivities among the group of metals studied for indirect epitaxy and show more ordering effect. It was proposed that faster dissipation of deposition enthalpy by the Au and Cr coated HOPG(0001) resulted in growing of *n*-alkane films epitaxially with 6-fold symmetric structure.

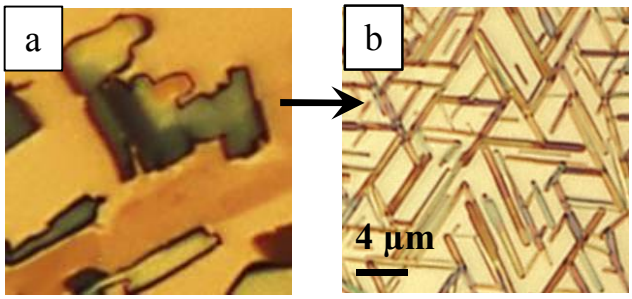

Figure 8.4 a.) C36 deposited on bare HOPG(0001) (C36 deposited at 56 °C substrate temperature); b.) C36 deposited on Au coated HOPG(0001) (3.7 nm Au; C36 deposited at 55 °C substrate temperature).

In Chapter 6, the indirect epitaxial growth of *n*-alkane films through a metallic thin film was focused on gold. In this chapter two goals were sought. First, the effect of metal film thickness on the indirect epitaxial growth of *n*-alkane was investigated by growing C36 on the HOPG(0001) coated with variable thickness of gold film. Second, the indirect epitaxy of *n*-alkane through the metal thin film was proven by obtaining ordered bar structure on a substrate with a different symmetry (NaCl(001), 4-fold symmetry). To this end, the trend of morphology

variation of C36 on the bare NaCl(001) with the substrate temperature was studied first. Previously, Fu and Urquhart[63] have studied the orientation of C36 on NaCl(001) at room temperature and 40 °C substrate temperatures. With the Peltier heater and temperature controller, it was possible to complete the previous study over a larger temperature range with more accurate values. According to the NEXAFS microscopy experiments by Fu,[63] C36 forms a combined morphologies of ordered laterally oriented bar structure plus normally oriented disk like domains at room temperature. A similar trend was obtained in the current study for C36 on NaCl(001) with a more reliably controlled substrate temperature. A combined 4-fold symmetric bar structure plus disordered domains were observed at $25 < T_S < 58$ °C (Figure 8.5a). In the temperature range of 58-70 °C only a thin uniform film (Figure 8.5c) was formed which was presumably made of normally oriented C36 molecules. The interesting achievement of indirect epitaxy through gold was observed for the gold coated NaCl as a substrate for growing a C36 thin film. It was seen that C36 grows epitaxially with 4-fold symmetric structure in the entire temperature range of 25 - 70 °C (Figure8.5) on the gold coated NaCl(001). The positive effect of metal coating in maintaining the epitaxial growth condition was rationalized as follows. The mirror-image potential effect hypothetically plays the role of transmitting the attractive forces of the primitive substrate for indirect epitaxy through the thin metal film. Moreover, the higher thermal conductivity of the metal thin films was suggested to be responsible for the higher degree of order at high substrate temperatures. In summary, it was confirmed that the gold film on HOPG(0001) and NaCl does not not apply a preferential orientation to the *n*-alkane deposit and the 6-fold and 4-fold symmetric structures of *n*-alkane deposited on the gold-coated substrates originates from attractive forces transferred through the metal film.

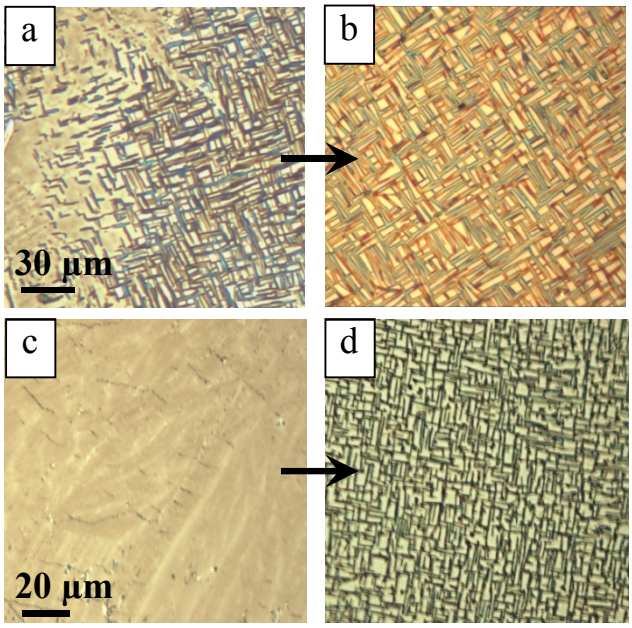

Figure 8.5. a.) C36 deposited on bare NaCl(001) at 45 °C substrate temperature; b.) C36 deposited on Au coated NaCl(001) (3.6 nm Au; C36 deposited at 45 °C substrate temperature); c.) C36 deposited on bare NaCl(001) at 58 °C substrate temperature; d.) C36 deposited on Au coated NaCl(001) (2 nm Au; C36 deposited at 58 °C substrate temperature).

Strain in epitaxially grown $Si_{1-x}Ge_x$ alloy films on Si(100)

Results obtained in the side project were presented in the Chapter 7 in which the degree of strain (measured by Raman spectroscopy) was correlated to the absolute value of linear dichroism in Si 1s NEXAFS spectra of strained $Si_{1-x}Ge_x$ thin films grown epitaxially on the Si(100) substrate. The integrated absolute linear dichroism (integrated TEY_d) in Si 1s NEXAFS spectra from 1839-1845 eV was shown to be related to the degree of strain of $Si_{1-x}Ge_x$ thin films by a linear equation (Figure 8.6). These results can be applied for quantitative strain mapping of semiconductors at the spatial scale of sub-100 nm by linear dichroism measured by X-PEEM or STXM microscopes with the lateral spatial resolutions better than 50 nm.

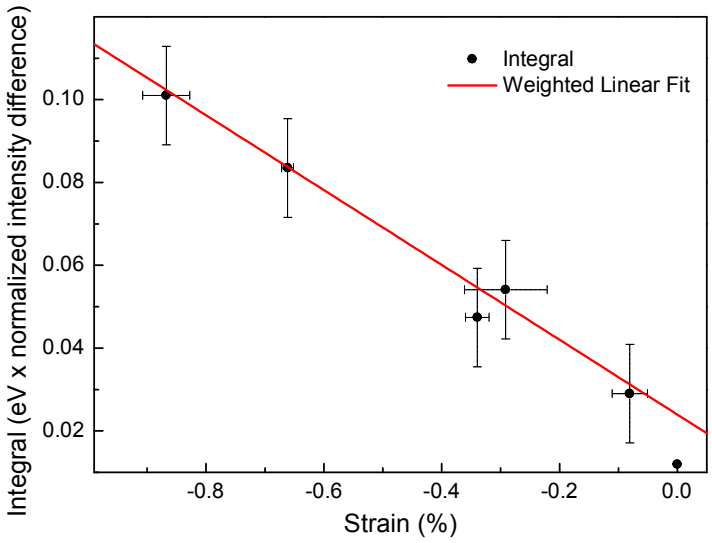

Figure 8.6 Integrated $TEY_{d,}$ (total electron yield difference by horizontal and vertical X-rays) versus degree of strain in $Si_{1-x}Ge_x$ films grown on Si(100).[97]

Comparison of epitaxial growth in the organic and inorganic systems, discussed as the main and side projects, reveals that lattice strain as a common property. As proposed in §4.2.1, strain of an epitaxially grown *n*-alkane film on HOPG(0001) can be relieved during deposition in the form of transformation of the growth mode from layer-by-layer to island-plus-layer to form the bar-like structure. In this process, molecular mobility is an important requirement, because the change in the growth mode happens at higher substrate temperatures, presumably as mobility is required for strain relief. However, in the inorganic $Si_{1-x}Ge_x$ system discussed in §7.3.2, strain is relaxed by defects that grow with increasing thickness in the strained film. Since lattice strain improves the electronic properties of the Si semiconductors, it is necessary to maintain the required strain, by limiting the thickness of the $Si_{1-x}Ge_x$ alloy film.

Main achievements of this project

1.) The morphology and molecular orientation of the *n*-alkane films were characterized to assess the kinetic and thermodynamic factors that determine the orientation of *n*-alkane thin films. Substrate temperature and deposition rate were found as parameters that influence the supersaturation, which in turn determines the molecular orientation. At high supersaturation, three different phases were observed and characterized to have lateral orientations. Among this group, two phases (named oriented uniform thickness film, and oriented bars) were grown epitaxially, and one phase (named pseudo-rectangular domains) was not epitaxial. At the low supersaturation, normally oriented *n*-alkane films were formed. The variations in the orientational morphology were attributed to the balance of molecular mobility and the strength of attractive forces during growth.

2.) Indirect epitaxial growth of *n*-alkane thin films was performed on HOPG(0001) coated with organic thin films as a means to change the morphology of *n*-alkane films from uniform thickness film to the bar structure, by altering the mechanism of growth. Thin films of a liquid crystal and a short *n*-alkane were used to form a template of ordered bar structure at low substrate temperatures. The subsequently deposited longer *n*-alkane proceeded to grow on the premade template.

3.) Another achievement in indirect epitaxy was maintaining epitaxial growth of *n*-alkanes on the metal coated substrates at higher deposition temperatures. Au, Cr, Pb, and Bi coated HOPG(0001) and Au coated NaCl(001) substrates could transfer attractive forces of the primary substrates and improve the degree of order at higher substrate temperatures presumably due to higher thermal conductivity of metal coated substrates.

4.) Finally the degree of strain was correlated to the absolute value of linear dichroism in Si 1s NEXAFS spectra of the strained $Si_{1-x}Ge_x$ thin films grown epitaxially on a Si(100)

substrate. This measurement has a potential of mapping the surface of Si semiconductors in terms of degree of strain by X-ray linear dichroism measurements acquired by high spatial resolution X-PEEM or STXM microscopes.

CHAPTER 9: FUTURE WORK

Introduction

The orientation detection technique used in this project was based on X-ray absorption linear dichroism from the multilayer *n*-alkane films. The normally or laterally oriented *n*-alkane films were characterized after growth. It is of interest to find out the orientation-determining factors during growth. Specifically it is suggested to determine the orientation of the first layer(s) of *n*-alkane in a normally oriented multilayer film as depicted in §9.1.

As discussed in Chapters 5 and 6 a thin metal film hypothetically helps to a faster dissipation of deposition enthalpy which decreases the effective surface temperature and allows the preparation of *n*-alkane films grown epitaxially on HOPG(0001) at high substrate temperatures. Alternatively, it is suggested to increase the deposit-substrate attractive forces to maintain the epitaxial growth at higher substrate temperatures as described in §9.2.

9.1 Evolution of structure and mechanisms during growth

The orientation of the first layer(s) of *n*-alkane during the growth of a normally oriented *n*-alkane multilayer film is still an unanswered question. Martin et al.[100] proposed a model for the normally oriented *n*-alkane films. They suggested that C16 first forms two layers that are laterally oriented on HOPG(0001) and the subsequent layers grow oriented normal to the surface. Also the STM images from *n*-alkane monolayers on gold all show a laterally oriented monolayer while a thicker film of *n*-alkane in the similar condition shows signs of normal orientation. It has been observed that a 50 nm film of C36 hypothetically grows in normal orientation when deposited on a relatively thick Au film (20 nm) at 56 °C (Chapter 6, Figure S2.g).

Based on Martin' model,[100] it is suggested that a longer *n*-alkane that forms a normally oriented film at high substrate temperatures (such as C36 at 65 °C on HOPG(0001)) is grown on top of a (few) laterally oriented monolayer(s) as schematically shown in Figure 9.1.

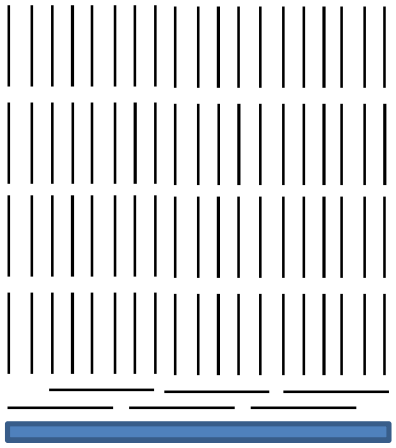

Figure 9.1 Schematic structure of a normally oriented multilayer film of *n*-alkane on HOPG(0001) with two first layers oriented laterally on the surface.

If it is proven that there is a laterally oriented monolayer underneath the normally oriented *n*-alkane films then a more important question should be resolved. It should be investigated what factors make *n*-alkane molecules nucleate normally on the laterally oriented monolayer. Answering to this question can be an important breakthrough towards understanding the determining factors in the orientation of organic thin films. If this question is addressed properly, it may justify the failure of experiments performed to orient the *n*-alkane molecules by deposition on a SAM substrate with a predefined structure (results are presented in Appendix). It is proposed to analyze the orientation of an *n*-alkane monolayer by linear dichroism in NEXAFS spectroscopy measured by TEY or AEY detection techniques.

9.2 Epitaxial growth of *n*-alkane films at high substrate temperatures

It was seen that the morphology of *n*-alkane molecules on HOPG(0001) changes from an epitaxially grown bar structure to disordered pseudo-rectangular domains and finally to the normally oriented film by increasing the substrate temperature during growth. In §9.2.1 it is proposed to form an ordered template of an organic film which is able to lead the subsequent *n*-alkane molecules grow on the premade structure. In §9.2.2 two approaches are proposed to increase the strength of van der Waals interactions between a hydrocarbon film and substrate to maintain the epitaxial growth at higher substrate temperatures.

9.2.1 Indirect epitaxy through an organic thin film

As discussed in §5.4 and Chapter 6, metallic thin films can change the morphology of *n*-alkane films from pseudo-rectangular to the ordered bars at high substrate temperatures. Alternatively, it is proposed to modify the surface of HOPG(0001) with an organic thin film that makes an ordered structure at high substrate temperatures. It is hypothesized that other than varying the chain length it is possible to tune the van der Waals interactions by using the linear equivalent counterparts of *n*-alkanes containing different functional groups. Considering the fact that van der Waals interactions are the major attractive forces in the epitaxial growth of *n*-alkanes on graphite, it is assumed that a fatty acid with a higher polarity may have a stronger interaction with graphite. This can result in the epitaxial growth of the fatty acid and formation of a stable ordered template at high substrate temperatures, when the equivalent *n*-alkane forms a pseudo-rectangular morphology. Alba et al.[86] have reported the preferential adsorption of an alcohol in a mixture of alcohol/alkane with the same chain length. The advantage of this approach is treating the surface of graphite with the fatty acid containing similar chain length to the *n*-alkane. This proposal is supported by some initial results that show corresponding fatty

acid of a short *n*-alkane forms a laterally oriented structure, while the corresponding *n*-alkane is expected to form a normally oriented film. These results are discussed further as follows in below.

Initial results

Figure 9.2 shows the different morphologies of stearic acid ($C_{18}H_{36}O_2$; will be shown as C17COOH) grown on HOPG(0001) at different substrate temperatures. Figure 9.2a presents the morphology of a C17COOH film grown on HOPG(0001) at 25 °C. It is made of 6-fold symmetric bar structure plus a thin film between the bars. The morphology of film turns to big thin and flat domains at 30 °C (Figure 9.2b). It is assumed that stearic acid molecules in the big domains are oriented normal to the surface at 30 °C, which start to evaporate and get thinner at 40 °C as shown in Figure 9.2c.

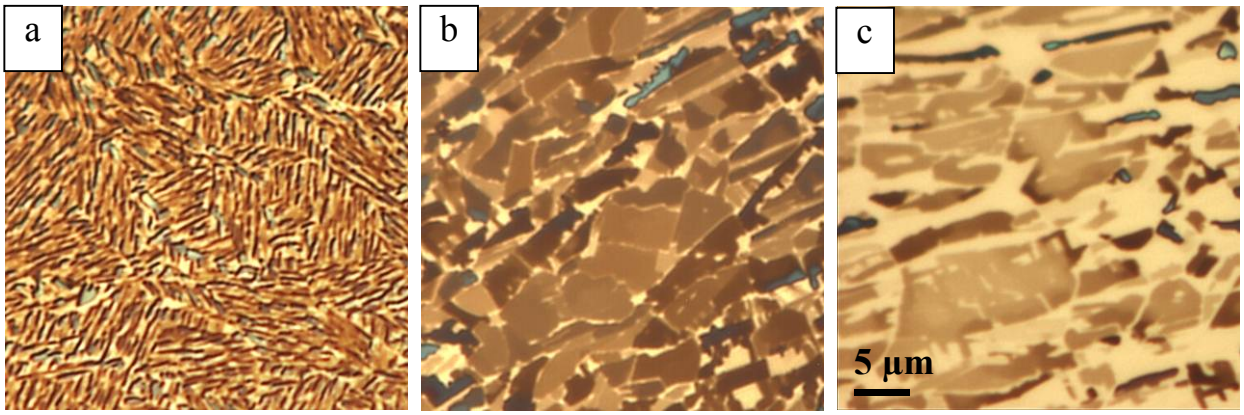

Figure 9.2 Polarized optical microscope images of stearic acid grown on HOPG(0001) at the substrate temperatures of: a.) T_S =25 °C (T_{SC} = 44.5 °C); b.) T_S =30 °C (T_{SC} = 39.5 °C); c.) T_S =40 °C (T_{SC} = 29.5 °C).

Discussion

The presence of bar structure for C17COOH grown on HOPG(0001) at 25 °C suggests a lateral orientation that turns to normal orientation at the substrate temperature of 30 °C, similar to the trend seen for *n*-alkanes on HOPG(0001) in Chapter 3. On the other hand it is expected that C18 forms normally oriented film when it is grown on HOPG(0001) at room temperature referring to the model proposed by Martin et al.[100] Different molecular orientations of C18 and C17COOH on graphite at a similar temperature, 25 °C, imply two conclusions. First, COOH end group interacts with graphite much stronger than a CH_3 end group and causes the stronger van der Waals interaction of a fatty acid than an *n*-alkane with similar chain length. Second, the higher melting point of C17COOH (MP= 69.5 °C) compared to that of C18 (MP=27.5°C) is a measure of molecule-molecule van der Waals interactions and it could imply that the molecule-substrate interactions are comparatively higher for C17COOH too. One can predict the way an unknown linear hydrocarbon behaves on the surface of graphite just by comparing its melting point to those of normal alkanes. In summary, it can be concluded that the polarity of deposited film plays an important role in attractive forces towards HOPG(0001), and an *n*-alkane counterpart compound can be used to form an epitaxially grown template on HOPG(0001) at high substrate temperatures. This template is assumed to lead the growth of the subsequent *n*-alkane to the ordered structure at high substrate temperatures.

9.2.2 New approaches to increase the interaction between a hydrocarbon film and substrate

As suggested in §4.1.2, partial desorption of *n*-alkane chain at high substrate temperatures may decrease the number of interacting CH_2 groups with HOPG(0001) and weaken the total interaction strength. To resolve this issue, it is proposed to increase the strength of attractive van der Waals interactions between deposit and substrate to decrease the partial

desorption and maintain the epitaxial growth condition at higher substrate temperatures. Two plans are suggested as follows in bellow:

Increasing the degree of unsaturation of normal hydrocarbons

It was reported that *n*-alkenes need ~ 4 kJ/mol more energy to desorb from the surface of Cu(100) than the corresponding saturated compounds.[82] It implies that unsaturation increases the van der Waals interactions between a hydrocarbon and substrate. It is intended to investigate the effect of unsaturation in the form of double bonds and aromatic groups in the normal hydrocarbon thin films that hypothetically have stronger interactions with HOPG(0001) and metals. Reinforcing the deposit-substrate interaction can be used to maintain the epitaxial structure and lateral orientation of organic films at higher substrate temperatures.

Using a mixture of metals in indirect epitaxy

It is proposed that using a mixture of metals can increase the *n*-alkanes adsorption energy and improve the indirect epitaxial growth on the HOPG(0001) coated with a thin metallic film at higher substrate temperatures. The starting idea, first introduced by Smirnov et al.,[101] is that alkanes and alkenes are effectively adsorbed on Au+Ni nanoclusters immobilized on an alumina surface. It is known[102,103] that the adsorption ability of gold clusters increase drastically when there is a positive charge on them. Therefore, Lanin et al.[103] related the stronger interaction of paraffins on the mixed Au+Ni systems over the individual gold particles to the presence of a partial positive charge on them. This investigation can be a complementary experiment for the study that was discussed in §5.4 and Chapters 6 regarding the indirect epitaxy through a metallic thin film.

CHAPTER 10: APPENDIX

This chapter presents results that were part of approaches discussed in section 1.10, but did not meet the intended objectives. §A1 is focused on the results obtained for orienting *n*-alkane films on the modified SAM of 11-mercaptoundecanoic acid on gold. In this part, the challenges of characterizing the SAM samples with IR spectroscopy are explained and the IR and NEXAFS data related to the *n*-alkane films deposited on the SAMs are presented. §A2 is devoted to the results of experiments performed to orient the *n*-alkane films on the SAM of 4-mercaptopyridine on gold. This part presents the NEXAFS images and the corresponding spectra of the *n*-alkane films deposited on the SAMs of 4-mercaptopyridine with presumably different orientations on the gold substrate.

A1. Attempts to induce lateral orientation to the *n*-alkane film by depositing on the SAM of 11-mercaptoundecanoic acid (MUA) on gold

It has been predicted by calculations that a lateral oriented *n*-alkane molecule on NaCl(001) interacts strongly with the sodium cations.[60,61] Therefore, it was intended to prepare a normally oriented SAM with K^+ end groups that was hypothesized to cause the subsequently deposited *n*-alkane orient laterally via van der Waals and induced Columbic interactions of CH_2 /K^+.[62] The preparation of SAM samples on the gold substrate was previously discussed in Chapter 2. To characterize the SAM samples on gold, reflective infrared spectra were acquired in single beam mode with a p-polarized beam at an angle of 70° with respect to the surface normal. For each spectrum, 1024 scans were acquired with a resolution of 4 cm^{-1}. The optical density of spectra were calculated by using equation $OD = -\ln(I/I_o)$, in which I_o is the intensity of reflected beam from a clean gold deposited Si wafer.

Figure A1 shows the IR spectra acquired from 11-mercaptoundecanoic acid with different end groups deposited on the gold coated Si substrate. No specific peak corresponding to the 11-mercaptoundecanoic acid layer adsorbed on gold could be distinguished in these three spectra. When the substrate thickness is similar to the wavelength of light, interference fringe might happen. Our attempts to eliminate interference fringes by changing the aperture size and incidence angle and using different substrates such as Si and Si_3N_4 failed. In summary, we could not characterize SAMs on gold because the IR spectra were too noisy and had interference fringes for the thin films.

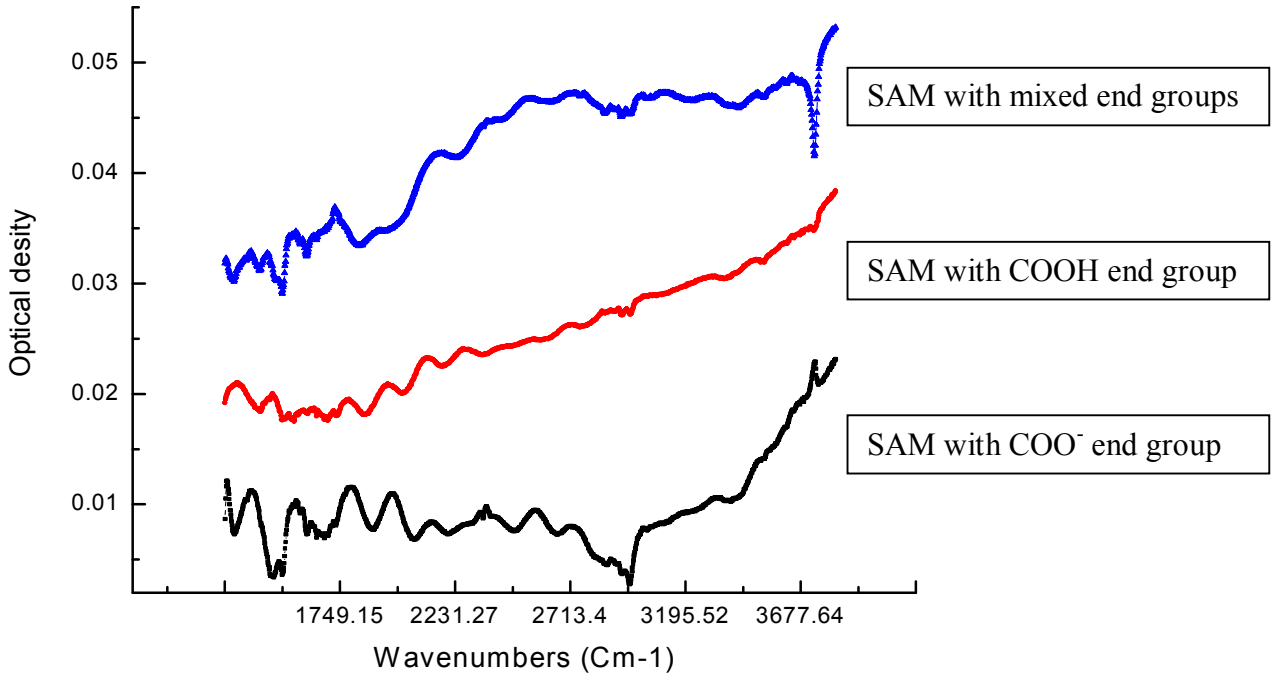

Figure A1 Infrared absorption spectra of 11-mercaptoundecanoic acid SAMs with different end groups on gold substrate.

Despite the inability to characterize the SAM samples, *n*-alkane films were deposited on top of them by the PVD method to see if orientation could be induced nevertheless. The IR spectra acquired from C36 films deposited on 11-mercaptoundecanoic acid samples are shown in Figure A2 in which four similar peaks in the energy range of 2850-2964 cm^{-1} can be seen for all of samples. It is expected that normal and lateral oriented *n*-alkane display IR peaks with different relative heights. Therefore, this result implies the same orientation for *n*-alkane films deposited on 11-mercaptoundecanoic acid SAMs with different presumed end groups. In both Figures A1 and A2 spectra are offset for clarity.

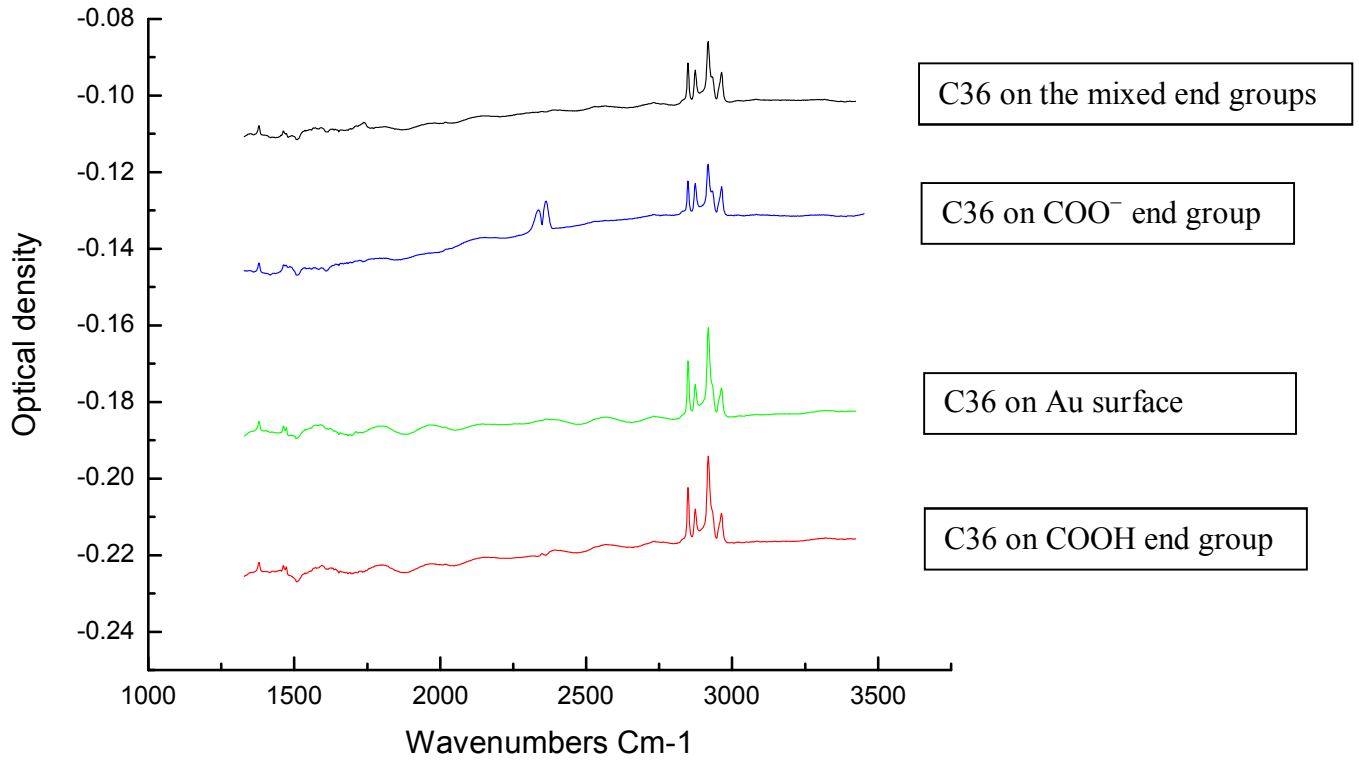

Figure A2 Infrared absorption spectra of C36 on gold and on 11-mercaptoundecanoic acid SAMs with different end groups.

In addition to IR spectroscopy, another characterization technique was applied to determine the orientation of C36 films grown on the 11-mercaptoundecanoic acid SAMs with different end groups. To this end, the C 1s NEXAFS spectra of C36 films grown on the 11-mercaptoundecanoic acid samples on the gold coated Si_3N_4 windows were acquired by the STXM microscope. As shown in Figure A3 all the NEXAFS spectra present a strong peak at 287.7 eV which is assigned to the C 1s $\rightarrow \sigma^*_{C\text{-}H}$ transition. This transition is strong in the normally oriented *n*-alkane molecules.[62] Therefore, the results of IR and NEXAFS spectroscopy consistently show that C36 molecules deposited on the 11-mercaptoundecanoic acid SAMs are oriented normal to the surface.

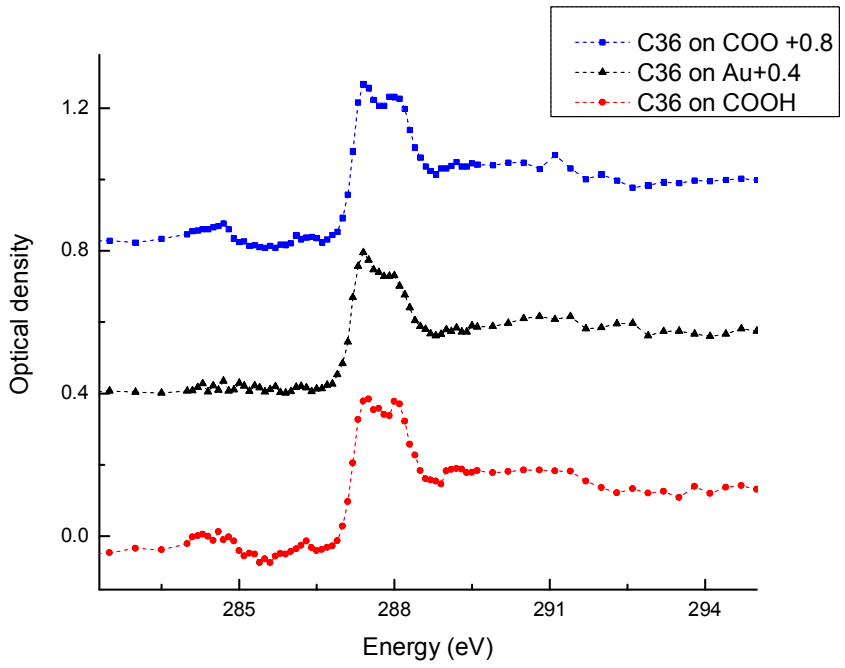

Figure A3 C 1s NEXAFS spectra of C36 deposited on 11-mercaptoundecanoic acid SAMs with COOH and COO^- end groups and C36 on gold.

The present results could imply two conclusions:

1- 11-Mercaptoundecanoic acid SAMs with different end groups were not prepared as hypothesized.

2- 11-Mercaptoundecanoic acid with different end groups is not able to induce different orientations to the subsequent *n*-alkane film.

A2. Approaches to induce lateral orientation to the *n*-alkane film by depositing on the SAM of 4-mercaptopyridine (4MP, C_5H_5NS) on gold

The fact that Kondoh et al.[59] have shown that an aromatic ring has stronger interaction with CH_2 rather than CH_3 makes aromatic compounds a potential choice to align *n*-alkane molecules laterally on the surface. It is required to prepare a laterally oriented aromatic SAM and then deposit the *n*-alkane film on top of it. An aromatic compound which is reported to make a flat lying monolayer on a gold surface is 4-mercaptopyridine. There is a doubt about the pH at which 4-mercaptopyridine lies flat on the gold surface. Some believe that 4-mercaptopyridine forms a disulfide layer in acidic solution (pH=1) in which pyridine ring is parallel to the gold surface.[104,105] Another group have shown that 4-mercaptopyridine can have flat lying orientation on silver in an alkaline solution because of contribution of both sulfur and nitrogen atoms in adsorption on the gold surface (Figure A4, structures VII and VIII).[106]

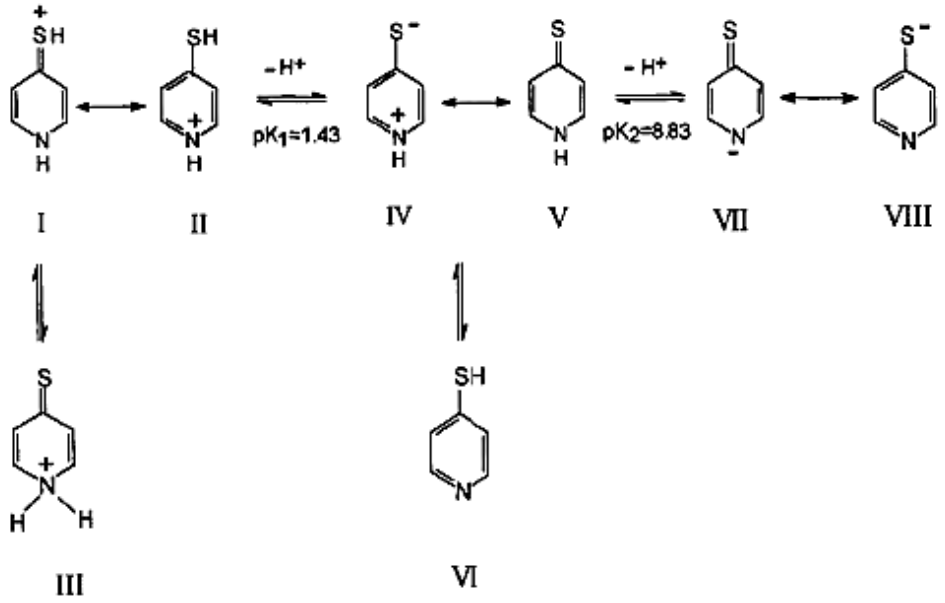

Figure A4 Different structures of 4-mercaptopyridine in the aqueous solutions with different pHs. Figure reprinted from Ref. 106 with permission.

4-Mercaptopyridine SAMs were prepared on the gold coated Si wafer in the aqueous solutions with different pHs as mentioned in Chapter 2. Then 100 nm C36 was deposited at room temperature on 4-mercaptopyridine SAMs prepared at the pHs of 1, 5 and 10. Molecular orientations of C36 films were studied by NEXAFS spectroscopy acquired by STXM.

Although the molecular orientation of 4-mercaptopyridine in the solutions with different pHs was not known, it was hypothesized to get lateral orientation for the C36 film that was deposited on the laterally oriented 4-mercaptopyridine. The STXM microscope images of C36 deposited on 4-mercaptopyridine SAMs prepared at three different pHs are shown in Figure A5. It seems that C36 films do not have any specific order in the images of A5a, A5b and A5c corresponding to the SAMs prepared at the pHs of 1, 5 and 10.

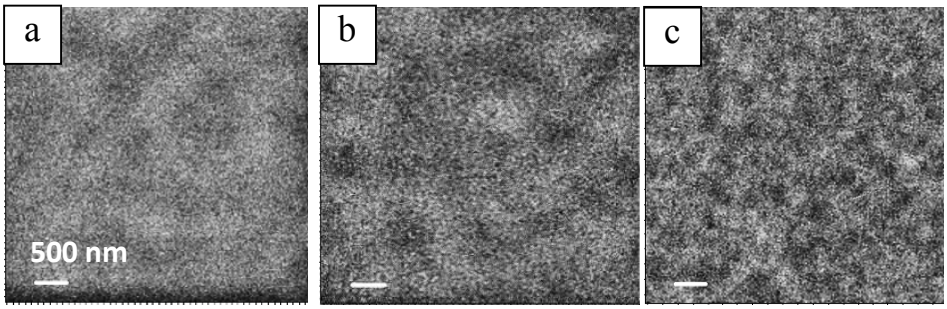

Figure A5 STXM images acquired at 288 eV from C36 deposited on the SAMs of 4-mercaptopyridine on gold prepared at: a.) pH=1; b.) pH=5; c.) pH=10.

The corresponding NEXAFS spectra extracted from dark and light domains of images in Figure A5 are shown in Figures A6; the spectrum from the dark area is offset by 0.1 for clarity.

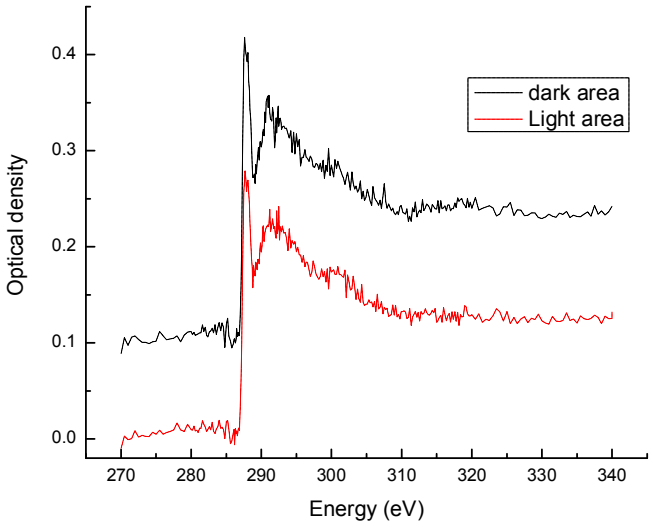

Figure A6 NEXAFS spectra extracted from light and dark areas of Figure A5b. Sample is 60 nm C36 deposited on 4-mercaptopyridine/gold prepared at pH=5.

No considerable difference can be seen between the spectra of light and dark areas. The identical post edge of two regions is an indicative of identical thicknesses of C36 film. The

strong peak at 288 eV indicates normal orientation of C36 molecules in the light and dark regions.

Conclusion

Since we could not identify the molecular orientation of the SAMs of 11-mercaptoundecanoic acid by IR spectroscopy, it cannot be concluded that it was unable to induce lateral orientation to the subsequently deposited *n*-alkane films. At first, the orientation of SAMs of 11-mercaptoundecanoic acid and 4-mercaptopyridine should be determined. Angle dependent NEXAFS spectroscopy from monolayers of 11-mercaptoundecanoic acid and 4-mercaptopyridine acquired by X-PEEM microscope could be used to identify molecular orientations of the SAM samples. After having a clear understanding of SAMs molecular orientation, then it should be investigated if they are able to induce different orientations to the *n*-alkane films deposited on top of them. It is possible that the SAM monolayers presumably oriented laterally on the gold surface cannot induce lateral orientation to the long *n*-alkane multilayers deposited subsequently. As proposed in Chapter 9, future work, it is of great interest to investigate the factors that cause the formation of normally oriented *n*-alkane films on the presumed laterally oriented monolayer(s).

REFERENCES

(1) Uosaki, K.; Yamada, R. Formation of two-dimensional crystals of alkanes on the Au(111) surface in neat liquid. *J. Am. Chem. Soc.* **1999,** *121,* 4090-4091.

(2) Vuillaume, D. Molecular nanoelectronics. *Proc. IEEE* **2010,** *98,* 2111-2123.

(3) Schuerlein, T. J.; Schmidt, A.; Lee, P. A.; Nebesny, K. W.; Armstrong, N. R. Large molecule epitaxy on single-crystal metals, insulators and single-crystal and MBE-grown layered semiconductors. *Jpn. J. Appl. Phys.* **1995,** *34,* 3837-3845.

(4) Ulman, A. An Introduction to Ultrathin Organic Films: *From Langmuir-Blodgett to Self-assembly*, Academic Press: Boston, **1991**.

(5) Kubono, A.; Akiyama, R. Classical nucleation theory applied to molecular orientations in vapor-deposited organic thin films. *J. Appl. Phys.* **2005,** *98,* 093502.

(6) Gerlach, R.; Polanski, G.; Rubahn, H. G. Structural manipulation of ultrathin organic films on metal surfaces: the case of decane thiol/Au(111). *Appl. Phys. A* **1997,** *65,* 375.

(7) Kubono, A.; Akiyama, R. Orientational mechanism for long-chain organic molecules during physical vapor deposition. *Mol. Cryst. Liq. Cryst.* **2002,** *378,* 167-183.

(8) Matsuzaki, F.; Inaoka, K.; Okada, M.; Sato, K. Molecular orientation in physical-vapour deposition of long-chain stearic acid. *J. Cryst. Growth* **1984,** *69,* 231-240.

(9) Venables, J. A.; Spiller, G. D. T.; Hanbücken, M. Nucleation and growth of thin films. *Rep. Prog. Phys.* **1984,** *47,* 399-459.

(10) Yin, S.; Wang, C.; Qiu, X.; Xu, B.; Bai, C. Theoretical study of the effects of intermolecular interactions in self-assembled long-chain alkanes adsorbed on graphite surface. *Surf. Interface Anal.* **2001,** *32,* 248-252.

(11) Hooks, D. E.; Fritz, T.; Ward, M. D. Epitaxy and molecular organization on solid substrates. *Adv. Mater.* **2001,** *13,* 227-241.

(12) Strohmaier, R.; Ludwig, C.; Petersen, J.; Gompf, B.; Eisenmenger, W. STM investigations of C_6Br_6 on HOPG and MoS_2. *Surf. Sci.* **1994,** *318,* L1181-L1185.

(13) Forrest, S. R. Ultrathin organic films grown by organic molecular beam deposition and related techniques. *Chem. Rev.* **1997,** *97,* 1793-1896.

(14) Sloat, C. A.; Menzies, A. W. C. Phenomena due to forces at crystal faces as studied by mutual orientation. *J. Phys. Chem.* **1930,** *35,* 2005-2021.

(15) Cisternas, E. A.; Corrales, T. P.; del Campo, V.; Soza, P. A.; Volkmann, U. G.; Bai, M.; Taub, H.; Hansen, F. Y. Crystalline-to-plastic phase transitions in molecularly thin *n*-dotriacontane films adsorbed on solid surfaces. *J. Chem. Phys.* **2009,** *131,* 114705.

(16) del Campo, V.; Cisternas, E.; Taub, H.; Vergara, I.; Corrales, T.; Soza, P.; Volkmann, U. G.; Bai, M.; Wang, S.-K.; Hansen, F. Y.; Mo, H.; Ehrlich, S. N. Structure and growth of vapor-deposited *n*-dotriacontane films studied by X-ray reflectivity. *Langmuir* **2009,** *25,* 12962-12967.

(17) Minea, T. M.; Point, S.; Gohier, A.; Granier, A.; Godon, C.; Alvarez, F. Single chamber PVD/PECVD process for in situ control of the catalyst activity on carbon nanotubes growth. *Surf. Coat. Technol.* **2005,** *200,* 1101-1105.

(18) Tamada, M.; Koshikawa, H.; Omichi, H. Real-time in-situ observation of PVD of N-vinylcarbazole with FTIR-RAS. *Thin Solid Films* **1997,** *293,* 113-116.

(19) Pound, G. M.; Simnad, M. T.; Yang, L. Heterogeneous nucleation of crystals from vapor. *J. Chem. Phys.* **1954,** *22,* 1215-1219.

(20) Smith, D. L. Deposition: *Thin-film deposition principles and practice*, McGraw-Hill, Inc.: Boston, **1995**, 129-130.

(21) Ruiz, R.; Choudhary, D.; Nickel, B.; Toccoli, T.; Chang, K. C.; Mayer, A. C.; Clancy, P.; Blakely, J. M.; Headrick, R. L.; Iannotta, S.; Malliaras, G. G. Pentacene thin film growth. *Chem. Mater.* **2004,** *16,* 4497-4508.

(22) Tanaka, K.; Okui, N.; Sakai, T. Molecular orientation behavior of paraffin thin films made by vapor deposition. *Thin Solid Films* **1991,** *196,* 137-145.

(23) Ueda, Y.; Ashida, M. The structure of n-hexatriacontane film vacuum-deposited on alkali halide crystals and its transformation by heat treatment. *J. Electron Microsc.* **1980,** *29,* 38-44.

(24) Fukao, K.; Kawamoto, H.; Horiuchi, T.; Matsushige, K. Annealing effects on molecular-orientation in evaporated-films of n-paraffins. *Thin Solid Films* **1991,** *197,* 157-167.

(25) Distler, G. I. Orientational and long-range effects in epitaxy. *Thin Solid Films* **1976,** *33,* 287-300.

(26) Shirokoff, J.; Erb, U. Long-range ordering effects in metal-non-metal interface revisited. *Philos. Mag. A* **1994,** *70,* 1055-1066.

(27) Cahn, R. W. Epitaxy keeps rolling along. *Nature* **1995,** *375,* 363-364.

(28) Yang, J. *Prog. Nat. Sci.* **1995,** *5,* 246-249.

(29) Firment, L. E.; Somorjai, G. A. Low-energy electron-diffraction study of surface of thin crystals and monolayers of normal paraffins and cyclohexane on Ag(111) crystal-surface. *J. Chem. Phys.* **1978,** *69,* 3940-3952.

(30) Yamamoto, M.; Sakurai, Y.; Hosoi, Y.; Ishii, H.; Kajikawa, K.; Ouchi, Y.; Seki, K. Softened CH stretching vibration of a long-chain *n*-alkane, *n*-$C_{44}H_{90}$, physisorbed on a Ag(111)

Surface: An infrared reflection absorption spectroscopic study. *J. Phys. Chem. B* **2000,** *104,* 7370-7376.

(31) Hosoi, Y.; Sakurai, Y.; Yamamoto, M.; Ishii, H.; Ouchi, Y.; Seki, K. Structures of a film of the long-chain n-alkane n-$C_{44}H_{90}$ on a Cu(100) surface. *Surf. Sci.* **2002,** *515,* 157-174.

(32) Firment, L. E.; Somorjai, G. A. Surface-structures of normal paraffins and cyclohexane monolayers and thin crystals grown on (111) crystal-face of platinum-low-energy electron-diffraction study. *J. Chem. Phys.* **1977,** *66,* 2901-2913.

(33) Seki, K.; Hashimoto, S.; Sato, N.; Harada, Y.; Ishii, K.; Inokuchi, H.; Kanbe, J. Vacuum UV photoelectron-spectroscopy of hexatriacontane (*n*-$C_{36}H_{74}$) polycrystal-model compound of polyethylene. *J. Chem. Phys.* **1977,** *66,* 3644-3649.

(34) Seki, K.; Ueno, N.; Karlsson, U. O.; Engelhardt, R.; Koch, E. E. Valence bands of oriented finite linear-chain molecular-solids as model compounds of polyethylene studied by angle-resolved photoemission *Chem. Phys.* **1986,** *105,* 247-265.

(35) Fosser, K. A.; Nuzzo, R. G.; Bagus, P. S.; Wöll, C. The origin of soft vibrational modes of alkanes adsorbed on Cu: An experimental and theoretical investigation. *J. Chem. Phys.* **2003,** *118,* 5115-5131.

(36) Ostrom, H.; Triguero, L.; Weiss, K.; Ogasawara, H.; Garnier, M. G.; Nordlund, D.; Nyberg, M.; Pettersson, L. G. M.; Nilsson, A. Orbital rehybridization in *n*-octane adsorbed on Cu(110). *J. Chem. Phys.* **2003,** *118,* 3782-3789.

(37) Pichugina, D. A.; Lanin, S. N.; Kovaleva, N. V.; Lanina, K. S.; Shestakov, A. F.; Kuz'menko, N. E. Effect of the structure and charge of Au_{10} clusters on adsorption of hydrocarbons. *Russ. Chem. Bull.* **2010,** *59,* 2039-2046.

(38) Ishii, H.; Seki, K. *Conjugated Polymer and Molecular Interfaces* CRC Press, New York, **2002**, p. 293.

(39) Bertel, E. The interaction of rare gases with transition metal surfaces. *Surf. Sci.* **1996,** *367,* L61-L65.

(40) Hill, I. G.; Rajagopal, A.; Kahn, A.; Hu, Y. Molecular level alignment at organic semiconductor-metal interfaces. *Appl. Phys. Lett.* **1998,** *73,* 662-664.

(41) Bagus, P. S.; Staemmler, V.; Woll, C. Exchangelike effects for closed-shell adsorbates: Interface dipole and work function. *Phys. Rev. Lett.* **2002,** *89,* 4.

(42) Brunner, K. Si/Ge nanostructures. *Rep. Prog. Phys.* **2002,** *65,* 27-72.

(43) Shiraki, Y.; Sakai, A. Fabrication technology of SiGe hetero-structures and their properties. *Surf. Sci. Rep.* **2005,** *59,* 153-207.

(44) Bublik, V. T.; Gorelik, S. S.; Zaitsev, A. A.; Polyakov, A. Y. Diffuse X-ray determination of energy of mixing and elastic-constants of Ge-Si solid-solutions. *Phys. Status Solidi b* **1974,** *66,* 427-432.

(45) Aubry, J. C.; Tyliszczak, T.; Hitchcock, A. P.; Baribeau, J. M.; Jackman, T. E. First-shell bond lengths in Si_xGe_{1-x} crystalline alloys. *Phys. Rev. B* **1999,** *59,* 12872-12883.

(46) Bean, J. C.; Feldman, L. C.; Fiory, A. T.; Nakahara, S.; Robinson, I. K. Ge_xSi_{1-X} /Si strained-layer superlattice grown by molecular beam epitaxy. *J. Vac. Sci. Technol. A* **1984,** *2,* 436-440.

(47) Hitchcock A.P., T. T., Aebi P.,; Xiong J.Z., S. T. K., Baines K.M., Mueller K.A.,; Feng X.H., C. J. M., Yang B.X.,; Lu Z.H., B. J.-M., Jackman T.E. Si K-edge and Ge K-edge X-ray absorption spectroscopy of the Si/Ge interface in $[(Si)_m(Ge)_n]_p$ atomic layer superlattices. *Surf. Sci.* **1993,** *291,* 349-369.

(48) Weng, X. D.; Rez, P.; Sankey, O. F. Pseudo-atomic-orbital band theory applied to electron-energy-loss near-edge structures. *Phys. Rev. B* **1989,** *40,* 5694-5704.

(49) Papaconstantopolos, D. A. *Handbook of the band structures of elemental solids*, Springer, New York, **1986**.

(50) Wende, H. Recent advances in x-ray absorption spectroscopy. *Rep. Prog. Phys.* **2004,** *67,* 2105-2181.

(51) Stöhr, J. *NEXAFS Spectroscopy*, Springer-Verlag, New York, **1996**.

(52) Turro, N. J.; Ramamurthy, V.; Scaiano, J. C. *Principles of Molecular Photochemistry: An Introduction*, University Science books, **2009,** p.190.

(53) Urquhart, S. G.; Lanke, U. D.; Fu, J. Characterisation of molecular orientation in organic nanomaterials by X-ray linear dichroism microscopy *Int. J. Nanotechnol.* **2008,** *5,* 1138-1170.

(54) Stöhr, J.; Outka, D. A.; Baberschke, K.; Arvanitis, D.; Horsley, J. A. Identification of C-H resonances in the K-shell excitation-spectra of gas-phase, chemisorbed, and polymeric hydrocarbons. *Phys. Rev. B.* **1987,** *36,* 2976-2979.

(55) Hahner, G. Near edge X-ray absorption fine structure spectroscopy as a tool to probe electronic and structural properties of thin organic films and liquids. *Chem. Soc. Rev.* **2006,** *35,* 1244-1255.

(56) Kinzler, M.; Schertel, A.; Hahner, G.; Wöll, Ch.; Grunze, M.; Albrecht, H.; Holzhuter, G.; Gerber, Th. Structure of mono- and multilayer Langmuir-Blodgett films from Cd arachidate and Ca arachidate. *J. Chem. Phys.* **1994,** *100,* 7722-7735.

(57) Fu, J.; Urquhart, S. G. Linear dichroism in the X-ray absorption spectra of linear *n*-alkanes. *J. Phys. Chem. A* **2005,** *109,* 11724-11732.

(58) Weiss, K.; Ostrom, H.; Triguero, L.; Ogasawara, H.; Garnier, M. G.; Pettersson, L. G. M.; Nilsson, A. XPS and XAS investigation of condensed and adsorbed n-octane on a Cu(110) surface. *J. Electron Spectrosc. Relat. Phenom.* **2003,** *128,* 179-191.

(59) Kondoh, H.; Matsui, F.; Ehara, Y.; Yokoyama, T.; Ohta, T. Surface-monolayer-controlled molecular alignment of short *n*-alkane multilayers. *Langmuir* **2001,** *17,* 8178-8183.

(60) Mauritz K. A.; Baer E.; J., H. A. Molecular energies of the epitaxial crystallization of polyethylene on alkali halide substrates. *J. Polym. Sci.: Polym. Phys.* **1973,** *11,* 2185-2197.

(61) Mauritz, K. A.; Baer, E.; Hopfinger, A. J. Epitaxial crystallization of macromolecules. *J. Polym. Sci., Part D* **1978,** *13,* 1-61.

(62) Fu, J. Linear dichroism in the NEXAFS spectroscopy of *n*-alkane thin films. PhD Thesis, University of Saskatchewan, Saskatoon, **2006**.

(63) Fu, J.; Urquhart, S. G. Effect of chain length and substrate temperature on the growth and morphology of *n*-alkane thin films. *Langmuir* **2007,** *23,* 2615-2622.

(64) Groszek, A. J. Selective adsorption at graphite/hydrocarbon interfaces. *Proc. Roy. Soc. Lond. A*. **1970,** *314,* 473-498.

(65) Couto, M. S.; Liu, X. Y.; Meekes, H.; Bennema, P. Scanning tunneling microscopy studies on n-alkane molecules adsorbed on graphite. *J. Appl. Phys.* **1994,** *75,* 627.

(66) Rosendahl, S. M.; Burgess, I. J. Electrochemical and infrared spectroscopy studies of 4-mercaptobenzoic acid SAMs on gold surfaces. *Electrochim. Acta* **2008,** *53,* 6759-6767.

(67) Reed, M. A.; Tour, J. M. Computing with molecules. *Sci. Am.* **2000,** *282,* 86-93.

(68) Willey, T. M.; Vance, A. L.; vanBuuren, T.; Bostedt, C.; Nelson, A. J.; Terminello, L. J.; Fadley, C. S. Chemically transformable configurations of mercaptohexadecanoic acid self-assembled monolayers adsorbed on Au(111). *Langmuir* **2004,** *20,* 2746-2752.

(69) Masnadi, M.; Urquhart, S. G. Effect of substrate temperature on the epitaxial growth of oriented *n*-alkane thin films on graphite. *Langmuir* **2012,** *28,* 12493-12501.

(70) Kino, G. S.; Corle, T. R. *Confocal Scanning Optical Microscopy and Related Imaging Systems*, Academic Press, **1996**.

(71) *The Theory of Birefringence*, Application note #014, Cambridge Polymer Group, Inc. **2004**, www.campoly.com/application_notes.html

(72) Warwick, T.; Ade, H.; Hitchcock, A. P.; Padmore, H.; Rightor, E. G.; Tonner, B. P. Soft X-ray spectromicroscopy development for materials science at the Advanced Light Source. *J. Electron. Spectrosc. Relat. Phenom.* **1997,** *84,* 85-98.

(73) Hitchcock, A. P.; Koprinarov, I.; Tyliszczak, T.; Rightor, E. G.; Mitchell, G. E.; Dineen, M. T.; Hayes, F.; Lidy, W.; Priester, R. D.; Urquhart, S. G.; Smith, A. P.; Ade, H. Optimization of scanning transmission X-ray microscopy for the identification and quantitation of reinforcing particles in polyurethanes. *Ultramicroscopy* **2001,** *88,* 33-49.

(74) Attwood, D. *Soft X-ray and Extreme Ultraviolet Radiation, Principles and Applications*, Cambrige University Press: New York, **1999**, p171.

(75) Schreiber, F. Organic molecular beam deposition: growth studies beyond the first monolayer. *physica status solidi (a)* **2004,** *201,* 1037-1054.

(76) Nozaki, K.; Saihara, R.; Ishikawa, K.; Yamamoto, T. Structure of normal alkane evaporated films: molecular orientation. *Jpn. J. Appl. Phys.* **2007,** *46,* 761-769.

(77) Amar, J. G.; Family, F. Critical cluster-size - island morphology and size distribution in submonolayer epitaxial-growth. *Phys. Rev. Let.* **1995,** *74,* 2066-2069.

(78) Leunissen, M. E.; Graswinckel, W. S.; van Enckevort, W. J. P.; Vlieg, E. Epitaxial nucleation and growth of *n*-alkane crystals on graphite (0001). *Cryst. Growth Des.* **2004,** *4,* 361-367.

(79) Hastie, G. P.; Johnstone, J.; Roberts, K. J.; Fischer, D. Examination of the structure and melting behaviour of thin film *n*-alkanes using ultra-soft polarised near-edge X-ray absorption spectroscopy. *J. Chem. Soc., Faraday Trans.* **1996,** *92,* 783-789.

(80) Lii, J. H.; Allinger, N. L. Molecular mechanics. The MM3 force field for hydrocarbons. 3. The van der Waals' potentials and crystal data for aliphatic and aromatic hydrocarbons. *J. Am. Chem. Soc.* **1989,** *111,* 8576-8582.

(81) Endo, O.; Horikoshi, T.; Katsumata, N.; Otani, K.; Fujishima, T.; Goto, H.; Minami, K.; Akaike, K.; Ozaki, H.; Sumii, R.; Amemiya, K.; Nakamura, M.; Kosugi, N. Incommensurate crystalline phase of *n*-alkane monolayers on graphite (0001). *J. Phys. Chem. C* **2011,** *115,* 5720-5725.

(82) Wetterer, S. M.; Lavrich, D. J.; Cummings, T.; Bernasek, S. L.; Scoles, G. Energetics and kinetics of the physisorption of hydrocarbons on Au(111). *J. Phys. Chem. B* **1998,** *102,* 9266-9275.

(83) Kubono, A.; Okui, N. Polymer thin-films prepared by vapor-deposition. *Prog. Polym. Sci.* **1994,** *19,* 389-438.

(84) Zuhaib, A. Methods to induce a preferred molecular alignment in the epitaxial growth of *n*-alkane thin films. M.Sc. Thesis, University of Saskatchewan, Saskatoon, **2012**.

(85) Hickman, S.; Hamilton, A.; Patrick, D. L. Controlling molecular alignment in an organic monolayer with a sacrificial liquid crystal template. *Surf. Sci.* **2003,** *537,* 113-122.

(86) Alba, M. D.; Castro, M. A.; Clarke, S. M.; Medina, S.; Messe, L.; Millan, C. Application of the solid state NMR to the study of the alcohol/alkane mixtures adsorption onto graphite. *Solid State Nucl. Magn. Reson.* **2011,** *40,* 138-143.

(87) Visser, J. On Hamaker constants: A comparison between Hamaker constants and Lifshitz- van der Waals constants. *Adv. Colloid Interface Sci.* **1972,** *3,* 331-363.

(88) Maurer, S.; Mersmann, A.; Peukert, W. A new model to predict adsorption equilibria on the basis of Hamaker constants of solids: *Adsorption Science and Technology*, World Scientific Publ Co Pte Ltd: Singapore, **2000**, 421-425.

(89) Su, D. R.; Shiau, Y. H. Power law interaction between adatom and surface in Thomas Jellium model. *Chin. J. Phys.* **1991,** *29,* 367-383.

(90) Lei, R. Z.; Gellman, A. J.; Koel, B. E. Desorption energies of linear and cyclic alkanes on surfaces: anomalous scaling with length. *Surf. Sci.* **2004,** *554,* 125-140.

(91) Liu, C. P.; Gibson, J. M.; Cahill, D. G.; Kamins, T. I.; Basile, D. P.; Williams, R. S. Strain evolution in coherent Ge/Si islands. *Phys. Rev. Let.* **2000,** *84,* 1958-1961.

(92) Robinson, I.; Harder, R. Coherent X-ray diffraction imaging of strain at the nanoscale. *Nat. Mater.* **2009,** *8,* 291-298.

(93) Hayazawa, N.; Motohashi, M.; Saito, Y.; Kawata, S. Highly sensitive strain detection in strained silicon by surface-enhanced Raman spectroscopy. *Appl. Phys. Lett.* **2005,** *86,* 263114.

(94) Woicik, J. C.; List, R. S.; Pate, B. B.; Pianetta, P. Splitting of the white line 1s absorption-edge in crystalline Si, SiGe, and dilute SiGe. *Solid State Commun.* **1988,** *65,* 685-688.

(95) Perova, T. S.; Wasyluk, J.; Lyutovich, K.; Kasper, E.; Oehme, M.; Rode, K.; Waldron, A. Composition and strain in thin $Si_{1-x}Ge_x$ virtual substrates measured by micro-Raman spectroscopy and x-ray diffraction. *J. Appl. Phys.* **2011,** *109,* 033502-033511.

(96) Kasrai, M.; Lennard, W. N.; Brunner, R. W.; Bancroft, G. M.; Bardwell, J. A.; Tan, K. H. Sampling depth of total electron and fluorescence measurements in Si L- and K-edge absorption spectroscopy. *Appl. Surf. Sci.* **1996,** *99,* 303-312.

(97) Cao, W.; Masnadi, M.; Eger, S.; Martinson, M.; Xiao, Q.-F.; Hu, Y.-F.; Baribeau, J.-M.; Woicik, J. C.; Hitchcock, A. P.; Urquhart, S. G. Quantification of strain through linear dichroism in the Si 1s edge X-ray absorption spectra of strained $Si_{1-x}Ge_x$ thin films. *Appl. Surf. Sci.* **2013,** *265,* 358-362.

(98) Hitchcock, A. P.; Tyliszczak, T.; Aebi, P. Polarization dependence of the Si K-edge X-ray absorption spectra of Si-Ge atomic layer superlattices. *Surf. Sci.* **1994,** *301,* 260-272.

(99) Brian, W. D.; Jeffrey, Y. T. Relaxation of strained-layer semiconductor structures via plastic flow. *Appl. Phys. Lett.* **1987,** *51,* 1325-1327.

(100) Martin, D. S.; Weightman, P.; Gauntlett, J. T. The adsorption of n-hexadecane onto highly oriented pyrolytic graphite studied by atomic force microscopy. *Surf. Sci.* **1998,** *398,* 308-317.

(101) Smirnov, V. V.; Lanin, S. N.; Vasil'kov, A. Y.; Nikolaev, S. A.; Murav'eva, G. P.; Tyurina, L. A.; Vlasenko, E. V. Adsorption and catalytic conversion of hydrocarbons on nanosized gold particles immobilized on alumina. *Russ. Chem. Bull.* **2005,** *54,* 2286-2289.

(102) Stakheev, A. Y.; Kustov, L. M. Effects of the support on the morphology and electronic properties of supported metal clusters: modern concepts and progress in 1990s. *Appl. Catal., A* **1999,** *188,* 3-35.

(103) Lanin, S. N.; Pichugina, D. A.; Shestakov, A. F.; Smirnov, V. V.; Nikolaev, S. A.; Lanina, K. S.; Vasil'kov, A. Y.; Zung, F. T.; Beletskaya, A. V. Hydrocarbon adsorption on gold clusters: Experiment and quantum chemical modeling. *Russ. J. Phys. Chem.* **2010,** *84,* 2133-2142.

(104) Wan, L.-J.; Noda, H.; Hara, Y.; Osawa, M. Effect of solution pH on the structure of a 4-mercaptopyridine monolayer self-assembled on Au(111). *J. Electroanal. Chem.* **2000,** *489,* 68-75.

(105) Wan, L. J.; Hara, Y.; Noda, H.; Osawa, M. Dimerization of sulfur headgroups in 4-mercaptopyridine self-assembled monolayers on Au(111) studied by scanning tunneling microscopy. *J. Phys. Chem. B* **1998,** *102,* 5943-5946.

(106) Jung, H. S.; Kim, M. S. Raman spectroscopic investigation of the adsorption of 4-mercaptopyridine on a silver-sol surface. *J. Mol. Struct.* **1997,** *407,* 139-147.